8-2010

Hairy Particles: Polymer Brush-Supported Organocatalysts and Asymmetric Mixed Homopolymer Brushes

Xiaoming Jiang
xjiang4@utk.edu

To the Graduate Council:

I am submitting herewith a dissertation written by Xiaoming Jiang entitled "Hairy Particles: Polymer Brush-Supported Organocatalysts and Asymmetric Mixed Homopolymer Brushes." I have examined the final electronic copy of this dissertation for form and content and recommend that it be accepted in partial fulfillment of the requirements for the degree of Doctor of Philosophy, with a major in Chemistry.

Bin Zhao, Major Professor

We have read this dissertation and recommend its acceptance:

Jimmy Mays, John Bartmess, Wei He

Accepted for the Council:
Dixie L. Thompson

Vice Provost and Dean of the Graduate School

(Original signatures are on file with official student records.)

To the Graduate Council:

I am submitting herewith a dissertation written by Xiaoming Jiang entitled "Hairy Particles: Polymer Brush-Supported Organocatalysts and Asymmetric Mixed Homopolymer Brushes". I have examined the final electronic copy of this dissertation for form and content and recommend that it be accepted in partial fulfillment of the requirements for the degree of Doctor of Philosophy, with a major in Chemistry.

Bin Zhao, Major Professor

We have read this dissertation
and recommend its acceptance:

Jimmy Mays

John Bartmess

Wei He

Accepted for the Council:

Carolyn Hodges

Vice Provost and Dean of the Graduate School

Hairy Particles: Polymer Brush-Supported Organocatalysts and Asymmetric Mixed Homopolymer Brushes

A Dissertation

Presented for the

Doctor of Philosophy Degree

The University of Tennessee, Knoxville

Xiaoming Jiang

August 2010

Acknowledgments

I would like to thank my advisor, Professor Bin Zhao, for his invaluable guidance and advice, patience, encouragement, and support through my graduate studies at the University of Tennessee. I would like to express my appreciation for his being an ideal professional and scholarly role model.

I also thank Professors Jimmy Mays, John Bartmess, and Wei He for serving on my committee and reviewing my work.

I would like to express my gratitude to colleagues and coworkers in our research group during the past five years: Dr. Dejin Li, Xueguang Jiang, Jonathan Horton, Thomas O'Lenick, Jeremiah Woodcock, and Naixiong Jin, for their collaboration, encouragement, discussion, and assistance.

I would also like to thank Professor Christopher Y. Li, Dr. Bingbing Wang, and Dr. Bin Li of Drexel University, Professor Lei Zhu and Mr. Ganji Zhong of Case Western Reserve University, Professor Timothy P. Lodge and Dr. Robert Hafner of University of Minnesota, and Tom Malmgren of University of Tennessee for their help.

Finally, I would like to express my thanks to my parents, my sister, and especially my wife for their love, care, and support.

Abstract

This dissertation presents the synthesis and studies of polymer brush-supported organocatalysts and asymmetric mixed homopolymer brushes grafted on particles. The brushes were synthesized from initiator-functionalized particles by surface-initiated "living" radical polymerizations.

Polymer brush-supported organocatalysts were designed to combine the advantages of both soluble polymer- (high activity) and crosslinked insoluble polymer-supported catalysts (recyclability). Chapter 1 describes the synthesis of a polymer brush-supported 4-*N,N*-dialkylaminopyridine (DAAP) catalyst from initiator-functionalized latex particles by surface-initiated nitroxide-mediated radical polymerization (NMRP). The hairy particles efficiently catalyzed the acylation of secondary alcohols and Baylis-Hillman reaction and were recycled ≥ six times with no or negligible decrease in the reaction yield. Chapter 2 presents the synthesis of a thermosensitive polymer brush-supported DAAP by surface-initiated atom transfer radical polymerization (ATRP) from silica particles with addition of a free initiator. Both hairy particles and the free copolymer formed from the free initiator were used as catalysts for hydrolysis of nitrophenyl acetate at various temperatures. Below the lower critical solution temperature (LCST), the activity of hairy particles was very close to that of the free copolymer. LCST transitions exerted different effects on the reactions catalyzed by hairy particles and the free copolymer.

Chapters 3 and 4 present the studies of the effects of chain length disparity and grafting density on phase morphology of mixed brushes grafted on silica particles. A series of mixed poly(*tert*-butyl acrylate) (P*t*BA)/polystyrene (PS) brushes with a fixed P*t*BA

molecular weight and various PS molecular weights were grown from silica particles functionalized with a monochlorosilane-terminated asymmetric difunctional initiator (Y-initiator) by sequential ATRP and NMRP. The total grafting densities of these brushes were 0.6 – 0.7 chains/nm^2. The morphology of mixed brushes evolved from isolated PS nanodomains, to short PS cylinders, to a nearly bicontinuous nanostructure, and a two-layered nanostructure with the change of chain length disparity of two homopolymers. To study the grafting density effect, a set of high density asymmetric mixed brushes with total grafting densities of 0.9 – 1.2 chains/nm^2 was prepared from triethoxysilane-terminated Y-initiator-functionalized silica particles. The feature sizes of the patterns formed from high density mixed brushes were much smaller than those of lower density mixed brushes.

Content

List of Figures

List of Tables

List of Schemes

Chapter 1. Hairy Particle-Supported 4-*N*,*N*-Dialkylaminopyridine: An Efficient and Recyclable Nucleophilic Organocatalyst

Abstract

This chapter presents the synthesis of polymer brush-supported 4-*N,N*-dialkylaminopyridine catalyst for acylation of sterically hindered alcohols and Baylis-Hillman reaction. Random copolymer brushes of styrene and 4-*N*-(4-vinylbenzyl)oxyethyl-*N*-methylaminopyridine were grown from initiator-functionalized core-shell crosslinked polystyrene particles by surface-initiated nitroxide-mediated radical polymerization. ^{1}H NMR spectroscopy study confirmed the presence of polymer brushes on the particles. The hairy particles were found to be an efficient catalyst for acylation of secondary alcohols at room temperature at a catalyst loading of 5 mol %, and were recycled 8 times with yields ≥ 97 %. The polymer brush-supported catalyst was also efficient in catalyzing Baylis-Hillman reaction of 4-nitrobenzaldehyde and methyl vinyl ketone in THF at 60 ^{o}C at a loading of 17.4 mol %. The catalyst was recycled six times with the yields ≥ 90 %.

1.1 Introduction

4-*N,N*-Dimethylaminopyridine (DMAP) and related compounds are widely used as efficient nucleophilic catalysts for many important organic reactions including acylation of sterically hindered alcohols, silylation, and the Baylis-Hillman reaction.[1] The widespread applications of DMAP in organic synthesis have been considered to contribute to the establishment of organocatalysis as a useful synthetic tool.[2a] Due to the economic consideration and environmental concern, supported catalysts[2] have received growing interest in recent years as they can be recovered and recycled. A number of strategies have been used to immobilize 4-*N,N*-dialkylaminopyridine (DAAP) on various supports including inorganic materials,[3a,3b] linear soluble polymers,[3c-3i] dendrimers and dendritic polymers,[3j,3k] multiarm star copolymers,[3l] and crosslinked insoluble polymers.[3m-3t] Because of their versatility, polymers have been widely used to prepare supported organocatalysts.[2a-c] In general, the linear soluble polymer-supported catalysts exhibit high catalytic activities that can be comparable to those of non-supported small molecule catalysts because of the homogeneity in the reactions. However, separation of the catalysts tends to be difficult. To achieve facile recovery, Bergbreiter and coworkers, for example, developed soluble polymer-supported DAAP catalysts by the use of thermosensitive polymers or thermomorphic systems.[3f,3g] On the other hand, crosslinked polymer-supported catalysts can be easily separated (e.g., by centrifugation or filtering), but it has been generally observed that the catalytic activities are lower than those of non-supported and linear soluble polymer-supported catalysts, likely because the reaction rates are limited by intraparticle diffusion of reactants from the bulk solution to the active sites within the

beads.[2b] To combine the advantages of crosslinked polymers with the catalytic activity of homogeneous catalysts, McQuade et al. recently developed "soluble" heterogeneous catalysts by encapsulating linear soluble polystyrene (PS)-bound DAAP catalysts inside porous microcapsules.[3h,3i] The catalysts were very efficient in catalyzing acylation of secondary alcohols and were recyclable.

One strategy to develop supported organocatalysts that has not been extensively explored but potentially could combine the advantages of both soluble polymer- and crosslinked polymer-supported organocatalysts is the use of polymer brushes as support. Polymer brushes are an assembly of macromolecular chains densely grafted by one end via a covalent bond on a surface.[4] Unlike covalently immobilized small molecules which are completely fixed on the substrate, polymer brushes are a dynamic system possessing a certain degree of mobility, which can be "seen" from ^{1}H NMR spectra of polymer brush-grafted silica particles.[5] Therefore, if an organic catalyst is incorporated into the grafted polymer chains, this immobilized catalyst would resemble linear soluble polymer-supported catalysts. On the other hand, the substrate for polymer brushes can be particles, porous materials, etc., allowing facile recovery and the reuse of the catalyst. Moreover, if polymer brushes are grafted on the particles (i.e., hairy particles), dangling polymer chains can improve the dispersibility of particles in the reaction media, further enhancing the catalytic activity.

Herein we present the synthesis of a hairy particle-supported DAAP catalyst. Random copolymer brushes of styrene (St) and 4-*N*-(4-vinylbenzyl)oxyethyl-*N*-methylaminopyridine (VEMAP)[3l] were grown from initiator-functionalized core-shell polymeric particles (initiator

particles) by surface-initiated polymerization[6] (Scheme 1.1). These hairy particles were found to efficiently catalyze the acylation of secondary alcohols and Baylis-Hillman reaction, and were recyclable. It should be noted here that Challa and coworkers reported the preparation of grafted polymers that contained 4-*N*-(4-vinylbenzyl)- *N*-methylaminopyridine on 12 and 50 nm silica nanoparticles and the use of tethered polymers as ligand to complex with copper (II) ion for oxidative coupling of 2,6-disubstituted phenol.[7a] In this *organometallic catalytic system*, one copper (II) ion coordinates with four pyridine groups,[7a,7b] which may reside on different polymer chains rather than one individual chain. In contrast, the present work describes the use of individual, dangling polymer chains in polymer brushes as support for an *organocatalyst*. It should also be noted here that Ballauf et al. used hairy particles as support for catalytic metal nanoparticles.[7c]

1.2 Experimental Section

1.2.1 Materials

Styrene (Aldrich, 99 %) was distilled over calcium hydride under vacuum and stored in a refrigerator prior to use. Divinylbenzene (Aldrich, technical grade, 55%, mixture of isomers) was passed through a basic alumina column to remove inhibitor and stored in a refrigerator. 2,2,6,6,-Tetramethyl-1-piperidinyloxy (TEMPO, 98%), di-*tert*-butyl peroxide (99%), sodium borohydride (98+%), 4-cyanopyridine (98%), 2-vinylpyridine (97%), 2-(methylamino)ethanol (99%), NaH (60% dispersion in mineral oil), vinylbenzyl chloride (90%), *N,N*-dimethylformamide (extra dry, with molecular sieves), 4-nitrobenzaldehyde (99%), acetic anhydride (p.a.), and sodium dodecyl sulfate were

Scheme 1.1. Synthesis of Hairy Particle-Supported 4-*N,N*-Dialkylaminopyridine

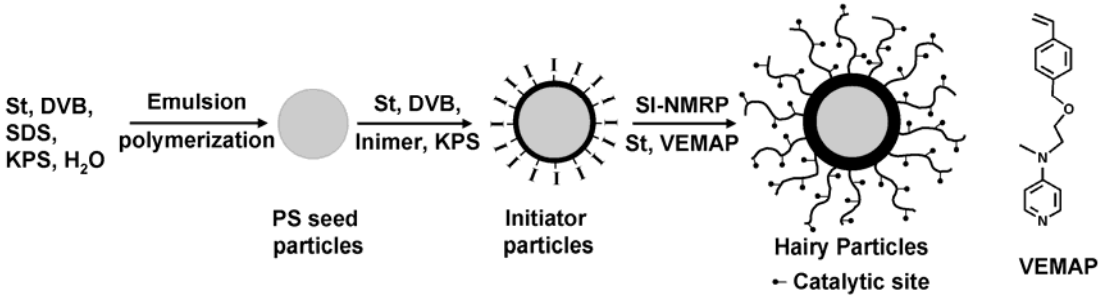

purchased from Fisher Scientific/Acros and were used as received. Diethylene glycol, (*S,S*)-(+)-*N,N*′-bis(3,5-di-*tert*-butylsalicylidene)-1,2-cyclohexanediaminomanganese(III) chloride (Jacobsen's catalyst), potassium persulfate (99+%), (±)-1-(1-naphthyl)ethanol (≥ 99%), (±)-1-phenylethanol (98%), and 3-buten-2-one (methyl vinyl ketone, 99%) were obtained from Aldrich and used as received. 1-Phenyl-1-(2′,2′,6′,6′-tetramethyl-1′-piperidinyloxy)-2-benzoyloxyethane was synthesized according to a literature procedure.[8] All other chemicals were obtained from either Fisher or Aldrich and used without further purification.

1.2.2 Characterization

The ^{1}H NMR spectra were recorded on a Varian Mercury 300 NMR spectrometer or a Bruker AC 250 spectrometer and the residual solvent proton signal was used as the internal standard. ^{13}C NMR (75 MHz) spectra were recorded on a Varian Mercury 300 NMR spectrometer and the residual solvent proton signal was used as the internal standard. Mass spectroscopy was performed at the Mass Spectrometry Center of the Department of Chemistry at the University of Tennessee at Knoxville using a PE Sciex QSTAR XL triple quadrupole time-of-flight (QTOF) mass spectrometer (Concord, Ontario, Canada) with an electrospray ionization source. Transmission electron microscopy experiments were conducted on a JEOL 2000FX TEM with an accelerating voltage of 120 kV. The TEM samples were prepared by drop casting the particle dispersions on carbon-coated copper grids. Size exclusion chromatography (SEC) was carried out at room temperature using PL-GPC 50 plus (an integrated GPC/SEC system from Polymer Laboratories, Inc) with a refractive index detector, one PSS GRAL guard column (50 × 8 mm, 10 micron particles,

Polymer Standards Service-USA, Inc.), and two PSS GRAL linear columns (each 300 × 8 mm, 10 micron, Polymer Standards Service-USA, Inc.). The data were processed using Cirrus^{TM} GPC/SEC software (Polymer Laboratories). *N,N*-Dimethylformamide (DMF) was used as the carrier solvent at a flow rate of 1.0 mL/min. Standard monodisperse polystyrenes (Polymer Laboratories) were used for calibration.

1.2.3 Synthesis of 1-(4-(2-(2-(4-Vinylbenzyloxy)ethoxy)ethoxy)methyl)-phenyl-1-(2′,2′,6′,6′-tetramethyl-1′-piperidinyloxy)ethane (Inimer). The inimer was prepared via a procedure shown in Scheme 1.2. 1-(4-Chloromethyl)phenyl-1-(2′,2′,6′,6′-tetramethyl-1′-piperidinyloxy)ethane (**1**) was synthesized according to a procedure in the literature.[9] ^{1}H NMR ($CDCl_3$): δ (ppm) 0.66, 1.02, 1.15, 1.28 (s, 12H, 4 C*H*$_3$), 1.37 – 1.48 (m, 6H, 3C*H*$_2$), 1.46 (d, 3H, C*H*$_3$CH), 4.57 (s, 2H, C*H*$_2$Cl), 4.78 (q, 1H, CH_3C*H*), 7.28 – 7.34 (m, 4H, aromatic *H*). ^{13}C NMR ($CDCl_3$): δ (ppm) 17.18, 20.30, 23.55, 34.17, 34.44, 40.30, 46.25, 59.65, 82.71, 126.87, 128.31, 135.82, 146.15.

Diethylene glycol (34.69 g, 0.327 mol) was dissolved in dry THF (60 mL) in a 250 mL three-necked flask, followed by addition of NaH (60 % in mineral oil, 1.96 g, 49.0 mmol). After the mixture turned clear, a solution of 4-vinylbenzyl chloride (5.02 g, 29.6 mmol) in dry THF (20 mL) was added in a dropwise fashion. The flask was then placed in a 70 ^{o}C oil bath and the mixture was stirred overnight. After removal of the solvent, the residue was partitioned between water and methylene chloride. The organic phase was separated and the aqueous layer was extracted with methylene chloride (50 mL × 3). The organic phases were combined and dried over anhydrous Na_2SO_4. The solvent was removed by a rotavapor, and purification by silica gel column chromatography with ethyl acetate as eluent afforded

Scheme 1.2. Synthesis of the Inimer

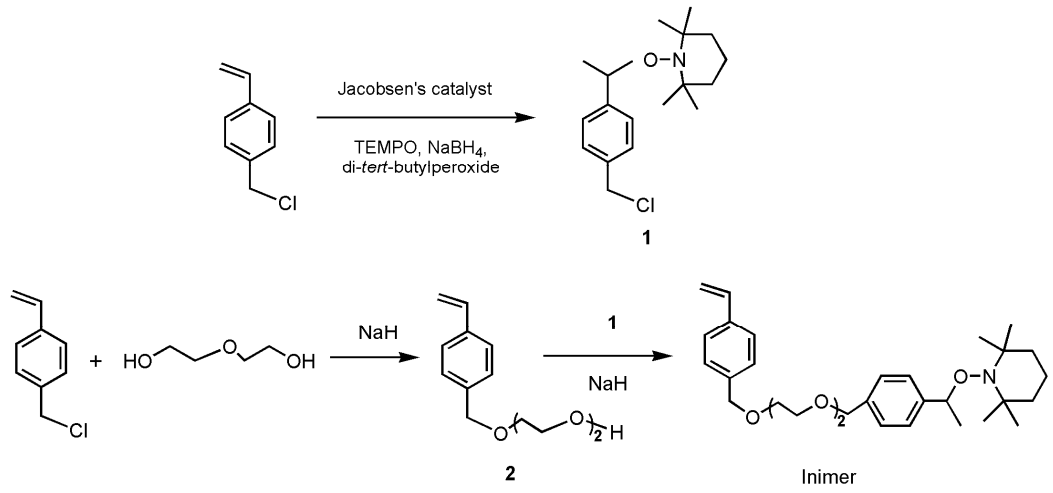

compound **2**, 2-(2-(4-vinylbenzyloxy)ethoxy)ethanol (6.32 g, yield: 96.3 %). ^{1}H NMR ($CDCl_3$): δ (ppm) 2.76 (s, 1H, O*H*), 3.55-3.71 (m, 8H, CH_2CH_2OCH_2CH_2), 4.52 (s, 2H, PhCH_2O), 5.21 (d, 1H, C*H*H=CH), 5.71 (d, 1H, CH*H*=CH), 6.68 (q, 1H, CHH=C*H*), 7.27 (d, 2H, aromatic), 7.36 (d, 2H, aromatic H). ^{13}C NMR ($CDCl_3$): 61.62, 69.27, 70.31, 72.40, 72.87, 113.75, 126.14, 127.89, 136.37, 136.95, 137.45. Mass spectroscopy (ES+) m/z 245.1 ($[M + Na]^+$).

Dry THF (15 mL) and compound **2** (1.082 g, 4.87 mmol) were added into a flask, followed by addition of NaH (60 % in mineral oil, 0.205 g, 5.13 mmol). After the mixture turned clear, a solution of **1** (0.752 g, 2.43 mmol) in THF (8 mL) was added in a dropwise fashion into the flask. The reaction mixture was stirred at 70 ^{o}C overnight. After removal of the solvent, the residue was partitioned between water and methylene chloride. The organic layer was separated and the aqueous layer was extracted with methylene chloride (40 mL × 3). The organic extracts were combined and dried over anhydrous Na_2SO_4. The solvent was removed by a rotavapor, and purification by silica gel column chromatography using ethyl acetate/hexanes (v/v, 2:1) as eluent gave the desired product inimer (0.385 g, yield: 32.0 %). ^{1}H NMR ($CDCl_3$): δ (ppm) 0.66, 1.01, 1.15, 1.28 (s, 12H, 4CH_3), 1.36-1.46 (m, 6H, 3CH_2), 1.45 (d, 3H, CH_3CH), 3.61-3.70 (m, 8H, CH_2CH_2OCH_2CH_2), 4.55, 4.56 (s, 4H, 2PhCH_2O), 4.76 (q, 1H, CH_3CH), 5.23 (d, 1H, C*H*H=CH), 5.74 (d, 1H, CH*H*=CH), 6.70 (q, 1H, CHH=C*H*), 7.26-7.39 (m, 8H, aromatic *H*). ^{13}C NMR ($CDCl_3$): δ (ppm) 17.15, 20.28, 23.59, 34.15, 34.42, 40.25, 59.58, 69.31, 69.33, 70.63, 70.65, 72.90, 73.14, 82.82, 113.69, 126.15, 126.50, 127.50, 127.90, 136.47, 136.54, 136.86, 137.82, 145.18; mass spectroscopy (ES+) m/z 496.2 ($[M + H]^+$).

1.2.4 Synthesis of 4-*N*-(4-Vinylbenzyl)oxyethyl-*N*-methylaminopyridine (VEMAP). 4-(*N*-methyl-*N*-(2-hydroxyethyl)amino)pyridine was prepared according to a literature procedure.[3o] ^{1}H NMR ($CDCl_3$): δ (ppm) 8.12 (d, 2H, NC*H*CH), 6.50 (d, 2H, NCHC*H*C), 3.82 (t, 2H, NC$H_2$$CH_2$), 3.52 (t, 2H, NCH_2CH_2), 3.02 (s, 3H, CH_3), 2.34 (s, broad, 1H, O*H*). ^{13}C NMR ($CDCl_3$): δ (ppm) 149.25, 137.07, 106.68, 59.71, 53.57, 38.24.

4-(*N*-methyl-*N*-(2-hydroxyethyl)amino)pyridine (2.102 g, 13.8 mol) was dissolved in *N,N*-dimethylformamide (DMF, 25 mL) in a 100 mL three-necked flask, followed by addition of sodium hydride (60 % dispersion in oil, 0.906 g, 22.7 mmol) under nitrogen atmosphere. After the mixture was stirred at room temperature for 1.5 h, a solution of 4-vinylbenzyl chloride (2.712 g, 16.0 mmol) in DMF (10 mL) was added in a dropwise fashion into the flask. The reaction mixture was stirred at room temperature overnight. After removal of DMF under vacuum, the residue was partitioned between methylene chloride and water. The organic layer was separated and the aqueous phase was extracted with methylene chloride three times. The combined organic extracts were dried over anhydrous Na_2SO_4. After removal of the solvents, purification by silica gel column chromatography using methanol/ethyl acetate (v/v, 2:1) as eluent gave the desired product VEMAP (1.862 g, yield: 50.4 %). ^{1}H NMR ($CDCl_3$): δ (ppm) 8.15 (d, 2H, NC*H*CH), 7.31 (d, 2H, CH_2CCHCH), 7.17 (d, 2H, CH_2CCHCH), 6.64 (q, 1H, CH_2CH), 6.42 (d, 2H, NCHC*H*C), 5.68 (d, 1H, C*H*H=CH), 5.18 (d, 1H, CH*H*=CH), 4.41 (s, 2H, CCH_2O), 3.56 (t, 2H CH_2CH_2N), 3.48 (t, 2H, OCH_2CH_2N), 2.92 (s, 3H, NCH_3). ^{13}C NMR ($CDCl_3$): δ (ppm) 153.16, 149.54, 137.33, 136.79, 136.20, 127.43, 125.99, 113.65, 106.36, 72.75, 67.06, 50.90, 37.93. MS (ES+) m/z 268.8 ($[M + H]^+$).

1.2.5 Preparation of Polystyrene Seed Particles. Polystyrene seed particles were prepared by emulsion polymerization. A typical procedure is described below. Styrene (3.06 g, 29.4 mmol), divinylbenzene (0.157 g, 0.663 mmol), distilled water (60 mL), and sodium dodecyl sulfate (0.0627 g, 0.22 mmol) were added into a 250 mL three-necked flask, and were stirred vigorously with a magnetic stir bar at room temperature. Potassium persulfate (KPS, 31.3 mg, 0.116 mmol) was added into the flask. The mixture was bubbled with N_2 for 40 min. The flask was then placed in a 60 ^{o}C oil bath. After 16 h, the flask was removed from the oil bath and cooled to room temperature. A portion of the obtained particle dispersion (15 mL) was used directly for the synthesis of initiator-functionalized core-shell PS particles by seeded emulsion polymerization.

1.2.6 Preparation of Initiator-Functionalized Core-Shell Particles. Styrene (0.206 g, 1.98 mmol), inimer (0.160 g, 0.323 mmol), and divinylbenzene (18.4 mg, 0.078 mmol) were mixed in a 100 mL three-necked flask, followed by addition of a portion of the obtained PS seed particles (15 mL) and potassium persulfate (4.0 mg, 0.015 mmol). The mixture was stirred with a magnetic bar and bubbled with nitrogen for 30 min. The flask was then placed in a 60 ^{o}C oil bath. After 15 h, the flask was removed from the oil bath. The particles were isolated by centrifugation (Eppendorf 5804, 11000 rpm, 60 min) and redispersed in methanol. After being separated by centrifugation (11000 rpm, 20 min), the particles were dispersed in THF by sonication (Fisher Ultrasonic Cleaner Model FS6) and the total volume of the dispersion was adjusted to 100 mL. The concentration of the initiator-incorporated core-shell PS particles in THF was determined by gravimetric analysis. 0.690 g of initiator-functionalized PS particles was obtained. The initiator

particles were stored in THF.

1.2.7 Synthesis of Poly(styrene-*co*-VEMAP) Brushes from Initiator Particles by Surface-Initiated Nitroxide-Mediated Radical Polymerization. A portion of the dispersion of initiator particles in THF (20 mL) was used to synthesize hairy particles. The initiator particles were separated by centrifugation (11000 rpm, 25 min) and were dried with a stream of N_2. The particles (138 mg) were then dispersed in dry DMF (5.029 g) in a Teflon tube by sonication. The dispersion was transferred into a 100 mL three-necked flask that contained VEMAP (0.883 g, 3.29 mmol), styrene (2.302 g, 22.1 mmol), and 1-phenyl-1-(2′,2′,6′,6′-tetramethyl-1′-piperidinyloxy)-2-benzoyloxyethane (PTEMPO, 18.3 mg, 0.048 mmol). The reaction mixture was then sonicated in an ultrasonic bath for 5 min while stirring. Three freeze-pump-thaw cycles were applied to degas the polymerization mixture. The flask was then placed in a 120 ^{o}C oil bath. After the polymerization proceeded for 40.3 h, the flask was removed from the oil bath and cooled to room temperature. The conversion of monomers, determined by ^{1}H NMR spectroscopy analysis, was 55.0 %. The mixture was diluted with THF, and the particles were separated by centrifugation (11000 rpm, 20 min). The free random copolymer of styrene and VEMAP in the supernatant liquid that was formed from the free initiator in the solution was collected and purified by precipitation in hexanes and diethyl ether. The molecular weights and composition of the free polymer were measured by SEC and ^{1}H NMR spectroscopy analysis. The particles were redispersed in THF and precipitated in diethyl ether twice. The particles were then repeatedly dispersed in THF and separated by centrifugation, and finally stored in a THF dispersion. The concentration of polymer brush-grafted particles in THF dispersion was

determined by gravimetric analysis. 0.362 g of hairy particles was obtained. SEC analysis of the free polymer (polystyrene standards): $M_{n,SEC}$ = 10,000 g/mol and $M_{w,SEC}$ = 12,400 g/mol.

1.2.8 Acylation Reaction of Sterically Hindered Alcohols with Hairy Particles as Catalyst. A typical procedure of acylation of (±)-1-(1-naphthyl)ethanol with acetic anhydride is described below. Hairy particles (35.4 mg, 0.025 mmol of VEMAP, 5 mol % with respect to the sterically hindered alcohol) were dispersed in THF (2.0 mL), followed by addition of (±)-1-(1-naphthyl)ethanol (86.1 mg, 0.5 mmol), triethylamine (75.9 mg, 0.75 mmol), and acetic anhydride (102.1 mg, 1.0 mmol). The reaction mixture was stirred at room temperature for 3 h. A portion of the reaction mixture (~ 0.4 mL) was taken and the solvent was removed in vacuum. ^{1}H NMR spectroscopy was used to determine the reaction yield. The hairy particles were isolated by centrifugation (11000 rpm, 25 min) and redispersed in THF. This washing process was repeated for additional three times. The hairy particles were reused for acylation reactions of sterically hindered alcohols.

1.2.9 Baylis-Hillman Reaction of 4-Nitrobenzaldehyde and Methyl Vinyl Ketone with Hairy Particles as Catalyst. A typical procedure for the Baylis-Hillman reaction of 4-nitrobenzaldehyde and methyl vinyl ketone with hairy particles as catalyst is described below. A dispersion of hairy particles (73.5 mg, 14.0 mg VEMAP, 0.0522 mmol) in THF (2.0 mL) was added into a 20 mL scintillation vial, followed by addition of 4-nitrobenzaldehyde (45.4 mg, 0.300 mmol), methyl vinyl ketone (105.1 mg, 1.50 mmol), and distilled water (54.0 mg, 3.00 mmol). The vial was sealed tightly with Teflon tape and placed in a 60 ^{o}C oil bath. After 24 h, the reaction yield was determined by ^{1}H NMR

spectroscopy analysis. The hairy particles were isolated by centrifugation (11000 rpm, 25 min) and redispersed in THF. This washing process was repeated for additional three times. The hairy particles were reused for the same Baylis-Hillman reaction.

1.3 Results and Discussion

Surface-initiated nitroxide-mediated radical polymerization (NMRP)[10] was employed to synthesize hairy particles. We prepared 1-(4-(2-(2-(4-vinylbenzyloxy)ethoxy)ethoxy) methyl)phenyl-1-(2′,2′,6′,6′-tetramethyl-1′-piperidinyloxy)ethane, which is an inimer (initiator/monomer)[11] containing an NMRP initiator (Scheme 1.2). The inimer was then incorporated into the shell layer of core-shell crosslinked PS particles by a seeded emulsion polymerization (Scheme 1.1). The average size of initiator particles, determined from the transmission electron microscopy (TEM) micrograph (Figure 1.1b), was 212 nm, 15 nm larger than that of PS seed particles (Figure 1.1a). The hairy particles were prepared by surface-initiated NMRP of a mixture of St and VEMAP with a molar ratio of 87 : 13 from the initiator particles in DMF at 120 ^{o}C with addition of a free initiator, 1-phenyl-1-(2′,2′,6′,6′-tetramethyl-1′-piperidinyloxy)-2-benzoyloxyethane. After the polymerization, the reaction mixture was cooled to room temperature and diluted with THF. The particles were separated by centrifugation and purified by repetitive dispersion in THF and isolation by centrifugation and/or precipitation in diethyl ether. The free random copolymer of St and VEMAP, poly(St-*co*-VEMAP), formed from the free initiator was purified by precipitation in hexanes and diethyl ether. From ^{1}H NMR spectrum (Figure 1.2a), the molar content of VEMAP in the free random copolymer was 16.6 mol %, close to the molar fraction in the feed (13.0 mol %). The average size of hairy particles measured

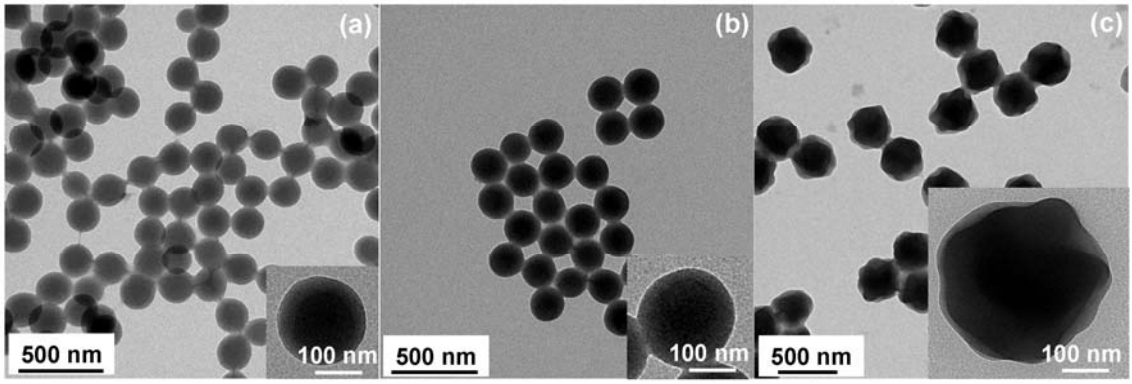

Figure 1.1. TEM micrographs of (a) polystyrene seed particles, (b) initiator-functionalized core-shell polystyrene particles, and (c) poly(St-*r*-VEMAP) brush-grafted particles.

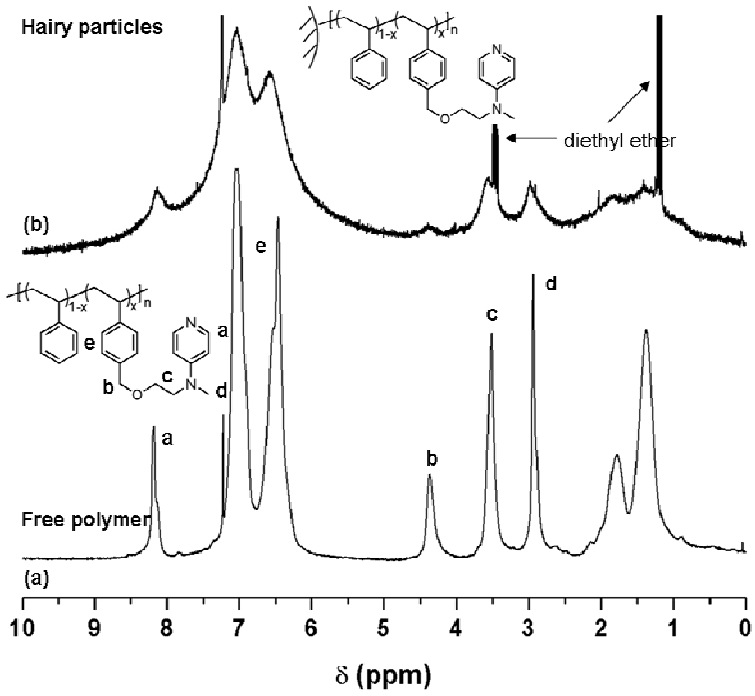

Figure 1.2. ^{1}H NMR spectra of (a) the free polymer poly(St-*r*-VBEGMAP) formed in the solution from the free initiator and (b) poly(St-*r*-VEMAP) brushes on the particles. $CDCl_3$ was used as solvent.

from the TEM micrograph (Figure 1.1c) was 375 nm, which was 163 nm larger than that of the initiator particles in the dry state. The observed relatively large particle size increase might be due to the porous nature of hairy particles causing collapse/deformation along the vertical direction during the solvent evaporation. The poly(St-*co*-VEMAP) brush layer can be clearly "seen" from ^{1}H NMR spectrum (Figure 1.2b). Although the peaks are broader than those of the free polymer, all characteristic peaks of VEMAP are present in the spectrum, indicating that the grafted polymer chains are mobile in the solvent. The N content of hairy particles from elemental analysis was 1.99 wt %, corresponding to 19.1 wt % of VEMAP or 0.71 mmol catalyst/g particles. If we assume that all particles are isolated during the centrifugation process and the grafted random copolymer has identical composition, molecular weight, and molecular weight distribution to those of the free polymer, the calculated weight percentage of VEMAP in the hairy particles is 21.0 wt %, which is close to the result from elemental analysis.

The hairy particles were first tested as catalyst for acylation of a secondary alcohol, (±)-1-(1-naphthyl)ethanol (Scheme 1.3a). The reaction was carried out at room temperature in THF at 5 mol % catalyst loading with 2 equiv. of acetic anhydride and1.5 equiv. of triethylamine. Note that the hairy particles were well dispersed in the reaction medium after sonication in an ultrasonic bath (Figure 1.3a). The reaction proceeded to completion in 3 h, which was evidenced by the complete shift of the peak of CH_3CH- from 5.68 to 6.65 ppm (Figure 1.4iii), demonstrating that the hairy particles exhibited a high catalytic activity for acylation of sterically hindered alcohols. In control experiments, the acylation of (±)-1-(1-naphthyl)ethanol with DMAP as catalyst was also complete after 3 h under the

Scheme 1.3. (a) Acylation Reaction of a Secondary Alcohol with Hairy Particles as Catalyst; (b) Baylis-Hillman Reaction with Hairy Particles as Catalyst

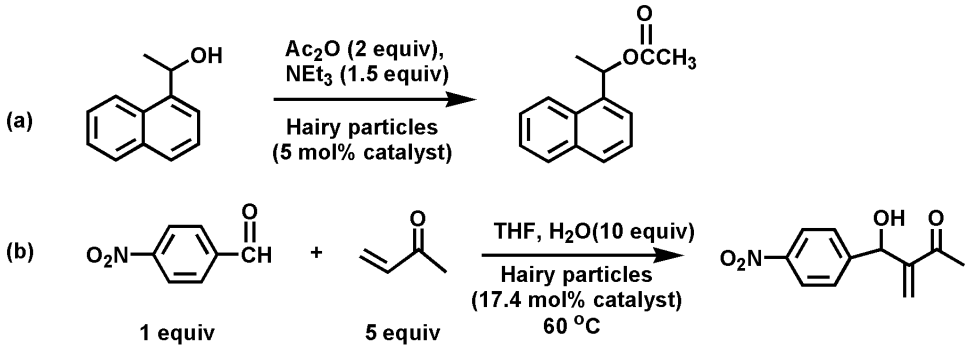

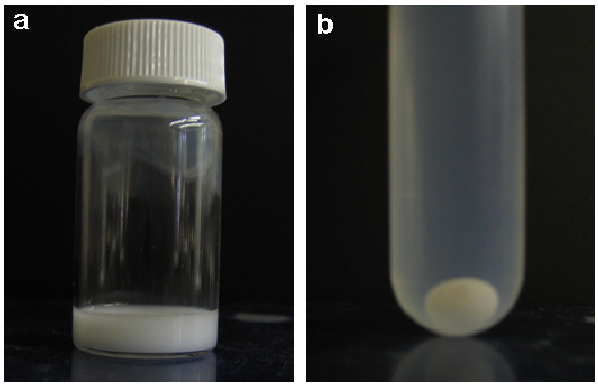

Figure 1.3. Optical pictures of (a) a dispersion of hairy particles in the reaction mixture and (b) the hairy particles isolated by centrifugation.

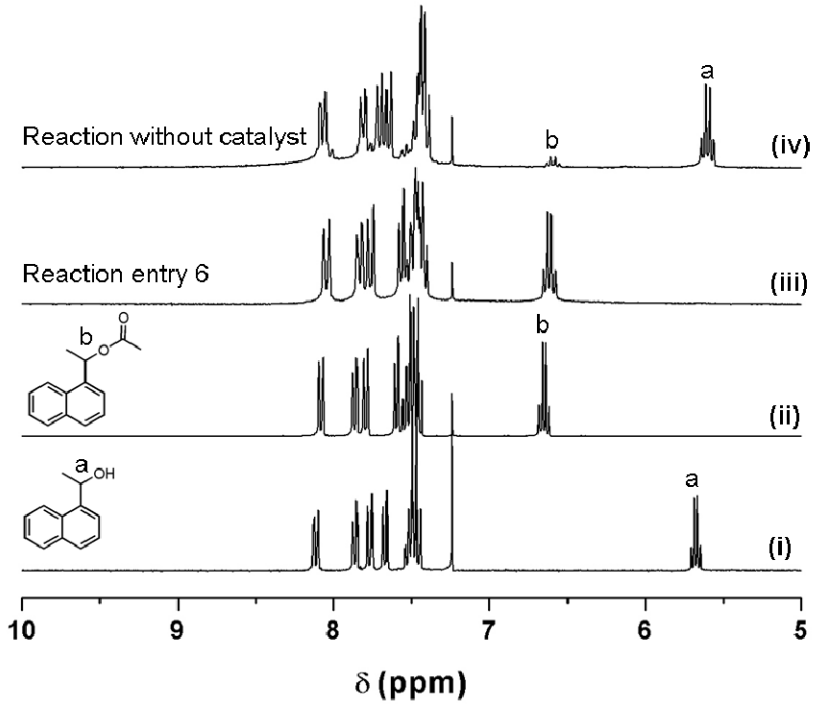

Figure 1.4. ^{1}H NMR spectra of (i) (±)-1-(1-naphthyl)ethanol, (ii) isolated, pure acylation product (±)-1-(1-naphthyl)ethyl acetate, (iii) acylation reaction mixture at 3 h from entry 6 in Table 1.1, and (iv) acylation reaction mixture in the absence of catalyst at 48 h. $CDCl_3$ was used as solvent for ^{1}H NMR spectroscopy analysis.

same reaction conditions. However, in the absence of DAAP catalyst, the reaction was very slow with a yield of only 4.9 mol % after 24 h and 10 mol % at 48 h (Figure 1.4iv). The hairy particles were separated by centrifugation. Figure 1.3b shows an optical picture of the isolated particles in the bottom of a centrifuge tube. The catalyst was washed with THF three times to remove the remaining starting materials and the residual product. The hairy particles were subsequently reused as catalyst in 7 iterative cycles for acylation of sterically hindered alcohols. In the third to sixth cycle, the reaction of (±)-1-(1-naphthyl)ethanol with acetic anhydride was essentially complete in 3 h (Table 1.1). In the seventh and eighth runs, a different alcohol, (±)-1-phenylethanol, was used and the yield decreased slightly (98 % in the 7^{th} cycle and 97 % in the 8^{th} cycle). These experiments demonstrated that the hairy particles were an efficient and reusable catalyst for acylation of secondary alcohols. The hairy particles were further evaluated as catalyst for a more challenging reaction – Baylis-Hillman reaction (Scheme 1.3b). Baylis-Hillman reaction is an important organic reaction for forming carbon-carbon bonds between aldehydes and α,β-unsaturated ketones or esters. Corma et al. recently reported a recyclable, Merrifield-type PS resin-supported DAAP catalyst.[3s] A stoichiometric amount of the catalyst was used to obtain fair yields within reasonable reaction times, and in some cases, the undesired diadduct and Michael adduct were observed. In contrast, the hairy particles efficiently catalyzed the Baylis-Hillman reaction of 4-nitrobenzaldehyde and methyl vinyl ketone in THF at a catalyst loading of 17.4 mol %. In the first cycle, the yield reached 95 % within 24 h. The reaction was clean; only the starting materials and the desired product were found in the ^{1}H NMR spectrum (Figure 1.5iv). No any undesired diadduct and Michael addition side

Table 1.1. Acylation Reaction of Sterically Hindered Alcohols

Entry [a]	Catalyst	Cycle	Alcohol	Yield (%) [b]
1	Hairy particles	1	NEA [c]	> 99
2	Hairy particles	2	NEA [c]	98
3	Hairy particles	3	NEA [c]	> 99
4	Hairy particles	4	NEA [c]	> 99
5	Hairy particles	5	NEA [c]	> 99
6	Hairy particles	6	NEA [c]	> 99
7	Hairy particles	7	PEA [d]	98
8	Hairy particles	8	PEA [d]	97
9	No catalyst	NA	NEA [c]	10 [e]
10	DMAP [f]	NA	NEA [c]	> 99 [g]

[a] Reaction conditions: sterically hindered alcohol (0.5 mmol), hairy particles (5 mol % of catalyst VEMAP with respect to the alcohol), acetic anhydride (2.0 equiv.), triethylamine (NEt_3, 1.5 equiv.), THF (2.0 mL), room temperature, 3 h. [b] The yields were determined by ^1H NMR spectroscopy analysis. [c] NEA: (±)-1-(1-naphthyl)ethanol. [d] PEA: (±)-1-phenylethanol. [e] The reaction yield at 48 h determined by ^1H NMR spectroscopy analysis. [f] DMAP: 4-*N,N*-dimethylaminopyridine. [g] The reaction yield at 3 h determined by ^1H NMR spectroscopy analysis.

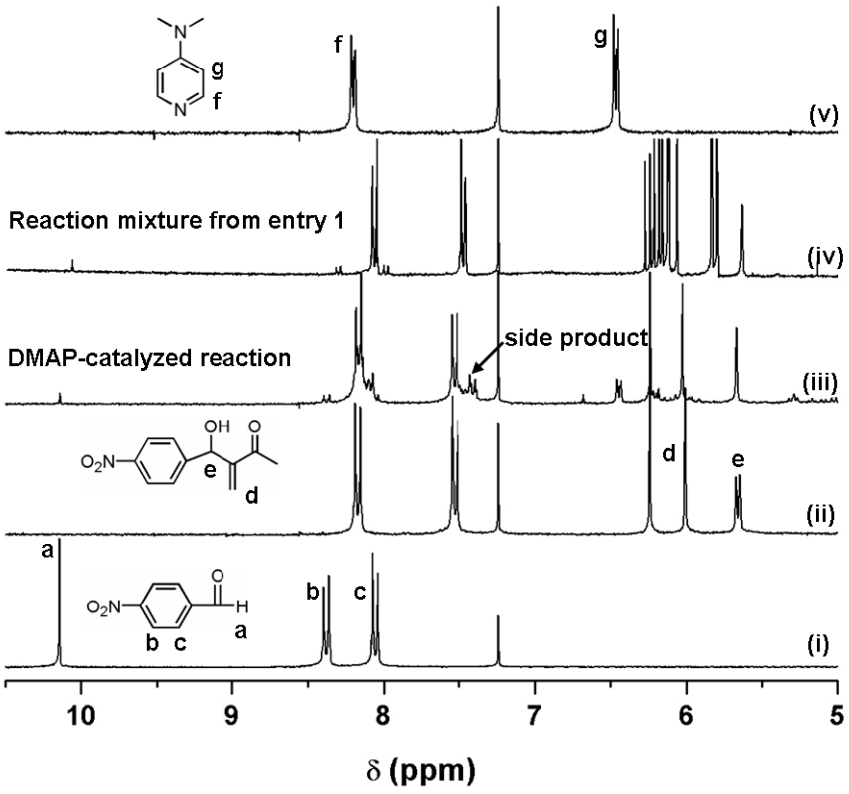

Figure 1.5. ^{1}H NMR spectra of (i) 4-nitrobenzaldehyde, (ii) isolated pure product of Baylis-Hillman reaction, (iii) reaction mixture with 4-*N,N*-dimethylaminopyridine (DMAP) as catalyst after 24 h (catalyst loading 17.4 mol %), (iv) reaction mixture with hairy particles as catalyst after 24 h (catalyst loading: 17.4 mol %), and (v) DMAP. $CDCl_3$ was used as solvent for ^{1}H NMR spectroscopy analysis.

products were observed even at relatively high reaction temperature (60 ^{o}C). Conversely, when DMAP was used as catalyst, the same reaction was reported to give rise to a mixture of the desired product and side products.[3a] Our control experiment using DMAP as catalyst also gave a undesired side product (Figure 1.5iii).

The hairy particles were isolated by centrifugation and reused as catalyst for the same reaction. In the subsequent 2nd to 6th cycles, the reaction yields were ≥ 90 % (Table 1.2),[13] demonstrating a good recyclability of hairy particle-supported catalyst. It should be noted here that the sixth Baylis-Hillman reaction was carried out after the hairy particles were stored in THF for three weeks, indicating that the catalytic activity of the hairy particles can be maintained over an extended period of time.

1.4 Conclusions

In summary, we successfully developed an efficient and recyclable hairy particle-supported DAAP catalyst by surface-initiated NMRP from initiator-functionalized PS particles. The presence of polymer brushes on the particles was confirmed by ^{1}H NMR spectroscopy study. The hairy particles efficiently catalyzed the acylation of secondary alcohols at a loading of 5 mol %, and were recycled 8 times with no or negligible decrease in the yield (yields ≥ 97 %). This supported catalyst was also efficient in catalyzing Baylis-Hillman reaction of 4-nitrobenzaldehyde and methyl vinyl ketone at a catalyst loading of 17.4 mol %. The reaction was clean and no undesired side products were observed from ^{1}H NMR spectrum, which is in contrast to the same reaction catalyzed by small molecule DMAP. The hairy particles were recycled six times with yields ≥ 90 %.

Table 1.2. Baylis-Hillman Reaction of 4-Nitrobenzaldehyde and Methyl Vinyl Ketone

Entry [a]	Catalyst	Cycle	Yield (%) [b]
1	Hairy particles	1	95
2	Hairy particles	2	91
3	Hairy particles	3	91
4	Hairy particles	4	91
5	Hairy particles	5	90
6	Hairy particles	6	90
7	DMAP [c]	NA	96 [d]

[a] Reaction conditions: 4-nitrobenzaldehyde (0.3 mmol), methyl vinyl ketone (5 equiv), H_2O (10 equiv), hairy particles (catalyst VEMAP loading: 17.4 mol % with respect to 4-nitrobenzaldehyde), THF (2.0 mL), 60 ^oC, 24 h. [b] The yields were determined by ^1H NMR spectroscopy analysis. [c] DMAP: 4-*N,N*-dimethylaminopyridine. [d] Side product was observed from ^1H NMR spectroscopy analysis (Figure 1.5iii).

References

1. (a) Scriven, E. F. V. *Chem. Soc. Rev.* **1983**, *12*, 129-161. (b) Heinrich, M. R.; Klisa, H. S.; Mayr, H.; Steglich, W.; Zipse, H. *Angew. Chem. Int. Ed.* **2003**, *42*, 4826-4828. (c) Spivey, A. C.; Arseniyadis, S. *Angew. Chem. Int. Ed.* **2004**, *43*, 5436-5441.

2. (a) Cozzi, F. *Adv. Synth. Catal.* **2006**, *348*, 1367-1390. (b) Benaglia, M.; Puglisi, A.; Cozzi, F. *Chem. Rev.* **2003**, *103*, 3401-3429. (c) Bergbreiter, D. E. *Chem. Rev.* **2002,** *102*, 3345-3383. (d) Piotti, M. E.; Rivera, F.; Bond, R.; Hawker, C. J.; Fréchet, J. M. J. *J. Am. Chem. Soc.* **1999,** *121*, 9471-9472. (e) Ochiai, B.; Endo, T. *J. Polym. Sci.,Part A: Polym. Chem.* **2007**, *45*, 5673-5678. (f) Faucher, S.; Zhu, S. P. *J. Polym. Sci., Part A: Polym. Chem.* **2007**, *45*, 553-565. (g) Hizal, G.; Tunca, U.; Aras, S.; Mert, H. *J. Polym. Sci.,Part A: Polym. Chem.* **2006**, *44*, 77-87.

3. (a) Chen, H. -T.; Huh, S.; Wiench, J. W.; Pruski, M.; Lin, V. S. -Y. *J. Am. Chem. Soc.* **2005**, *127*, 13305-13311. (b) Ó Dálaigh, C.; Corr, S. A.; Gun'ko, Y.; Connon, S. J. *Angew. Chem. Int. Ed.* **2007**, *46*, 4329-4332. (c) Hierl, M. A.; Gamson, E. P.; Klotz, I. M. *J. Am. Chem. Soc.* **1979**, *101*, 6020-6021. (d) Delaney, E. J.; Wood, L. E.; Klotz, I. M. *J. Am. Chem. Soc.* **1982**, *104*, 799-807. (e) Rubinsztajn, S.; Zeldin, M.; Fife, W. K. *Macromolecules* **1991**, *24*, 2682-2688. (f) Bergbreiter, D. E.; Osburn, P. L.; Li, C. M. *Org. Lett.* **2002**, *4*, 737-740. (g) Bergbreiter, D. E.; Li, C. M. *Org. Lett.* **2003**, *5*, 2445-2447. (h) Price, K. E.; Mason, B. P.; Bogdan, A. R.; Broadwater, S. J.; Steinbacher, J. L.; McQuade, D. T. *J. Am. Chem. Soc.* **2006**, *128*, 10376-10377. (i) Mason, B. P.; Bogdan, A. R.; Goswami, A.; McQuade, D. T. *Org. Lett.* **2007**, *9*, 3449-3451. (j) Liang, C. O.; Helms, B.; Hawker, C. J.; Fréchet, J. M. J. *Chem.*

Commum. **2003**, *20*, 2524-2525. (k) Helms, B.; Liang, C. O.; Hawker, C. J.; Fréchet, J. M. J. *Macromolecules* **2005**, *38*, 5411-5415. (l) Helms, B.; Guillaudeu, S. J.; Xie, Y.; McMurdo, M.; Hawker, C. J.; Fréchet, J. M. J. *Angew. Chem. Int. Ed.* **2005**, *44*, 6384-6387. (m) Tomoi, M.; Akada, Y.; Kakiuchi, H. *Makromol. Chem. Rapid Commum.* **1982,** *3*, 537-542. (n) Menger, F. M.; McCann, D. J. *J. Org. Chem.* **1985**, *50*, 3928-3930. (o) Deratani, A.; Darling, G. D.; Fréchet, J. M. J. *Polymer* **1987**, *28*, 825-830. (p) Deratani, A.; Darling, G. D.; Horak, D.; Fréchet, J. M. J. *Macromolecules* **1987**, *20*, 767-772. (q) Storck, W.; Manecke, G. *J. Mol. Catal.* **1985**, *30*, 145-169. (r) Guendouz, F.; Jacquier, R.; Verducci, J. *Tetrahedron* **1988**, *44*, 7095-7108. (s) Corma, A.; García, H.; Leyva, A. *Chem. Commum.* **2003**, *22,* 2806-2807. (t) Huang, J. -W.; Shi, M. *Adv. Synth. Catal.* **2003**, *345*, 953-958.

4. (a) Tsujii, Y.; Ohno, K.; Yamamoto, S.; Goto, A.; Fukuda, T. *Adv. Polym. Sci.* **2006**, *197*, 1-45. (b) Zhao, B.; Brittain, W. J. *Prog Polym. Sci.* **2000**, *25*, 677-710. (c) Advincula, R. C. *J. Dispersion Sci. and Technol.* **2003**, *24*, 343-361.

5. (a) Li, D. J.; Sheng, X.; Zhao, B. *J. Am. Chem. Soc.* **2005**, *127*, 6248-6256. (b) Li, D. J.; Jones, G. L.; Dunlap, J. R.; Hua, F. J.; Zhao, B. *Langmuir* **2006**, *22*, 3344-3351.

6. (a) Prucker, O.; Rühe, J. *Macromolecules* **1998**, *31*, 592-601. (b) Ejaz, M.; Yamamoto, S.; Ohno, K.; Tsujii, Y.; Fukuda, T. *Macromolecules* **1998**, *31*, 5934-5936. (c) Husseman, M.; Malmström, E. E.; McNamara, M.; Mate, M.; Mecerreyes, D.; Benoit, D. G.; Hedrick, J. L.; Mansky, P.; Huang, E.; Russell, T. P.; Hawker, C. J. *Macromolecules* **1999**, *32*, 1424-1431. (d) von Werne, T.; Patten, T. E. *J. Am. Chem. Soc.* **1999**, *121*, 7409-7410. (e) Bartholome, C.; Beyou, E.;

Bourgeat-Lami, E.; Chaumont, P.; Zydowicz, N. *Macromolecules* **2003**, *36*, 7946-7952. (f) Ohno, K.; Koh, K.; Tsujii, Y.; Fukuda, T. *Angew. Chem. Int. Ed.* **2003**, *42*, 2751-2754. (g) Skaff, H.; Emrick, T. *Angew. Chem. Int. Ed.* **2004**, *43*, 5383-5386. (h) Li, C. Z.; Benicewicz, B. C. *Macromolecules* **2005**, *38*, 5929-5936. (i) Andruzzi, L.; Senaratne, W.; Hexemer, A.; Sheets, E. D.; Ilic, B.; Kramer, E. J.; Baird, B.; Ober, C. K. *Langmuir* **2005**, *21*, 2495-2504. (j) Xu, C.; Wu, T.; Drain, C. M.; Batteas, J. D.; Fasolka, M. J.; Beers, K. L. *Macromolecules* **2006**, *39*, 3359-3364. (k) Sankhe, A. Y.; Husson, S. M.; Kilbey, S. M. *Macromolecules* **2006**, *39*, 1376-1383. (l) Bao, Z. Y.; Bruening, M. L.; Baker, G. L. *J. Am. Chem. Soc.* **2006**, *128*, 9056-9060. (m) Li, D. J.; Zhao, B. *Langmuir* **2007**, *23*, 2208-2217. (n) Matyjaszewski, K.; Dong, H. C.; Jakubowski, W.; Pietrasik, J.; Kusumo A. *Langmuir* **2007**, *23*, 4528-4531. (o) Guerrini, M. M.; Charleux, B.; Vairon, J. -P. *Macromol. Rapid Commun.* **2000**, *21*, 669-674. (p) Jayachandran, K. N.; Takacs-Cox, A.; Brooks, D. E. *Macromolecules* **2002**, *35*, 4247-4257. (q) Zheng, G. D.; Stöver, H. D. H. *Macromolecules* **2002**, *35*, 6828-6834. (r) Schmidt, R.; Zhao, T. F.; Green, J. B.; Dyer, D. J. *Langmuir* **2002**, *18*, 1281-1287. (s) Tomlinson, M. R.; Efimenko, K.; Genzer, J. *Macromolecules* **2006**, *39*, 9049-9056. (t) Zhao, B.; Zhu, L. *J. Am. Chem. Soc.* **2006**, *128*, 4574-4575. (u) Hotchkiss, J. W.; Lowe, A. B.; Boyes, S. G. *Chem. Mater.* **2007**, *19*, 6-13. (v) Jhaveri, S. B.; Koylu, D.; Maschke, D.; Carter, K. R. *J. Polym. Sci., Part A: Polym. Chem.* **2007**, *45*, 1575-1584. (w) Ishizu, K.; Kobayakawa, N.; Takano, S.; Tokuno, Y.; Ozawa, M. *J. Polym. Sci., Part A: Polym. Chem.* **2007**, *45*, 1771-1777. (x) Wang, F.; Hu, J. H.; Yang, W.; Wang, C. C. *J. Polym. Sci., Part A: Polym. Chem.* **2007**, *45*,

4552-4563.

7. (a) Koning, C. E.; Brinkhuis, R.; Wevers, R.; Challa, G. *Polymer* **1987**, *28*, 2310-2316. (b) Koning, C. E.; Viersen, F. J.; Challa, G.; Reedijk, J. *J. Mol. Catal.* **1988**, *44*, 245-257. (c) Mei, Y.; Lu, Y.; Polzer, F.; Ballauff, M.; Drechsler, M. *Chem. Mater.* **2007**, *19*, 1062-1069.

8. (a) Hawker, C. J. *J. Am. Chem. Soc.* **1994**, *116*, 11185-11186. (b) Zhao, B.; He, T. *Macromolecules* **2003**, *36*, 8599-8602.

9. Dao, J.; Benoit, D.; Hawker, C. J. *J. Polym. Sci., Part A: Polym. Chem.* **1998**, *36*, 2161-2167.

10. (a) Hawker, C. J.; Bosman, A. W.; Harth, E. *Chem. Rev.* **2001**, *101*, 3661-3688. (b) Hua, F. J.; Jiang, X. G.; Li, D. J.; Zhao, B. *J. Polym. Sci., Part A: Polym. Chem.* **2006**, *44*, 2454-2467. (c) Jiang, X. G.; Zhao, B. *J. Polym. Sci., Part A: Polym. Chem.* **2007**, *45*, 3707-3721.

11. Foreman, E. A.; Puskas, J. E.; Kaszas, G. *J. Polym. Sci., Part A: Polym. Chem.* **2007**, *45*, 5847-5856.

12. The ^{1}H NMR spectrum of reaction mixture from entry 1 in Table 1.2 (Figure 1.5iv) was recorded on a Varian Mercury 300 NMR spectrometer without removing the solvent and methyl vinyl ketone. The ^{1}H NMR spectrum of the DMAP-catalyzed reaction mixture was recorded on a Bruker AC 250 spectrometer after removing most of the solvent and methyl vinyl ketone. The slight differences in the chemical shifts of peaks f and g might be due to the different chemical environments.

13. Corma et al. reported in reference 3s that the decrease in the yield might be due to the

covalent attachment of methyl vinyl ketone to the pyridine nitrogen of the polymer. They observed from IR spectra the presence of carbonyl group in the deactivated supported catalyst.

Chapter 2. Thermosensitive Polymer Brush-Supported 4-*N*,*N*-Dialkylaminopyridine on Silica Particles as Catalyst for Hydrolysis of an Activated Ester in Aqueous Buffers: Comparison of Activity with Linear Polymer-Supported Version and Effect of LCST Transition

Abstract

This chapter presents the synthesis of a thermosensitive polymer brush-supported 4-*N*,*N*-dialkylaminopyridine catalyst and the comparison of its catalytic activity with the corresponding linear polymer-supported version in the hydrolysis of *p*-nitrophenyl acetate (NPA) as well as the effect of LCST transition on catalytic activity. The polymer brushes were synthesized from initiator-functionalized silica particles by surface-initiated ATRP of methoxytri(ethylene glycol) methacrylate and 2-(*N*-methyl-*N*-(4-pyridyl)amino)ethyl methacrylate in the presence of a free initiator. Dynamic light scattering studies showed that the onset temperatures of the LCST transition of polymer brushes in pH 7.52 and 7.82 buffers were 42 and 38 ^{o}C, respectively. Under the same reaction conditions, the net initial rate of the hydrolysis of NPA catalyzed by hairy particles was 70 - 80 % of that catalyzed by the free copolymer at the temperature below the LCST of polymer brushes. With further increasing the temperature above the LCST, the plot of logarithm of net initial rate versus inverse temperature exhibited a shift for the reactions catalyzed by hairy particles and leveled off or decreased slightly in the case of using the free copolymer as catalyst, presumably because the structures of the aggregates of hairy particles and free copolymer chains were different.

2.1 Introduction

4-*N*,*N*-Dialkylaminopyridines (DAAPs) are widely recognized and used as highly efficient nucleophilic catalysts for many important organic reactions, including acylation of sterically hindered alcohols, hydrolysis of activated esters, and Baylis-Hillman reaction.[1] DAAP-containing polymers have been a subject of intensive research in the past decades. The covalent attachment of a DAAP to a polymer support, e.g., crosslinked polymer resin, allows facile recovery and reuse of the catalyst.[2] Moreover, polymers create for the supported DAAP a distinct microenviroment, which can be tailored by varying polymer structures and can be designed to respond to external stimuli, allowing the tuning of their catalytic activity and the control of their compatibility with other types of catalytic groups.[3] Various polymers, including linear soluble polymers,[3a-3f] dendrimers and dendritic polymers,[3g,3h] multiarm star copolymers,[3i] and crosslinked insoluble polymers,[3j-3p] have been employed for developing polymer-supported DAAP catalysts. The first macromolecular DAAP catalysts, reported by Klotz et al.,[3a,3b] were prepared by covalently attaching DAAPs onto laurylated polyethylenimines. Compared with small molecule DAAPs, these polymer catalysts exhibited a marked increase in the catalytic effectiveness for the hydrolysis of *p*-nitrophenyl caproate in aqueous buffer solutions, which was attributed to the decreased pK_a of macromolecular DAAPs. Vaidya and Mathias synthesized a linear water-soluble homopolymer consisting of 4-(pyrrolidino)pyridine by cyclopolymerization of 4-diallylaminopyridine.[3c] For the same reason, the homopolymer was more effective than small molecule 4-(pyrrolidino)pyridine for the hydrolysis of *p*-nitrophenyl esters under the homogeneous aqueous conditions. Liang et al. incorporated

DAAPs into dendrimers and dendritic polymers and studied the effects of polymer architecture and nanoenvironment on the catalytic activities of supported DAAPs in acylation reactions.[3g] They found that the nanoenvironment played a crucial role in determining the activities of polymer catalysts.[3g,3h] Very recently, Helms et al. synthesized two multi-arm star copolymers, each containing a different catalyst (DAAP or *p*-toluenesulfonic acid) confined in its core, and used them as catalysts in a one-pot reaction cascade.[3i] The hairy structure of multi-arm star copolymers allowed the use of otherwise incompatible acid and base catalysts in one-pot reactions, an excellent example demonstrating the power of tailoring polymer structures for the creation of novel polymer catalysts.

We have been interested in developing supported organocatalysts by the use of polymer brushes,[4] a strategy that has not been much explored but potentially could combine the advantages of both linear soluble polymer- (high activity) and crosslinked polymer-supported organocatalysts (excellent recyclability). Polymer brushes are an assembly of macromolecular chains that are densely grafted by one end via a covalent bond on a solid surface.[5] Unlike covalently immobilized small molecules that are completely fixed on the solid substrate, polymer brushes are a dynamic system possessing a certain degree of mobility, which can be "seen" from ^{1}H NMR spectra of polymer brush-grafted particles.[6] Therefore, if an organic catalyst is incorporated into the grafted polymer chains, this supported catalyst would resemble linear soluble polymer-supported catalysts, exhibiting a high catalytic activity. On the other hand, the substrate for polymer brushes can be silica particles, magnetic nanoparticles, porous materials, etc., allowing facile recovery

and reuse of the catalyst.

Chapter 1 presents the synthesis of a polymer brush-supported DAAP catalyst by surface-initiated nitroxide mediate radical polymerization of styrene and 4-*N*-(4-vinylbenzyl)oxyethyl-*N*-methylaminopyridine from initiator-functionalized core-shell polymeric particles. The polymer brush-grafted particles (hairy particles) efficiently catalyzed the acylation of secondary alcohols and Baylis-Hillman reaction of 4-nitrobenzaldehyde and methyl vinyl ketone, and were recycled ≥ six times with no or negligible decrease in the reaction yields after the same period of time. In this chapter, we synthesized thermosensitive poly(methoxytri(ethylene glycol)methacrylate-*co*-2-(*N*-methyl -*N*-(4-pyridyl)amino)ethyl methacrylate) (P(TEGMMA-*co*-MAPMA)) brushes from initiator-functionalized silica particles by surface-initiated atom transfer radical polymerization (ATRP) in the presence of a free initiator (Scheme 2.1). Note that PTEGMMA is a thermosensitive water-soluble polymer with a lower critical solution temperature (LCST) at 48 ^{o}C in water.[6b,7] The hairy particles and the free copolymer formed from the free initiator were used as catalysts for the hydrolysis of *p*-nitrophenyl acetate (NPA) in aqueous buffer solutions (Scheme 2.2).[3a-c,8] The goal of this work was two-fold: (i) examining and comparing the catalytic activities of the polymer brush-supported and the corresponding linear soluble polymer-supported DAAPs in the hydrolysis of NPA; (ii) studying the effect of thermo-induced LCST transition on catalytic activity.

Scheme 2.1. Synthesis of Thermosensitive Polymer Brush-Supported DAAP on Silica Particles

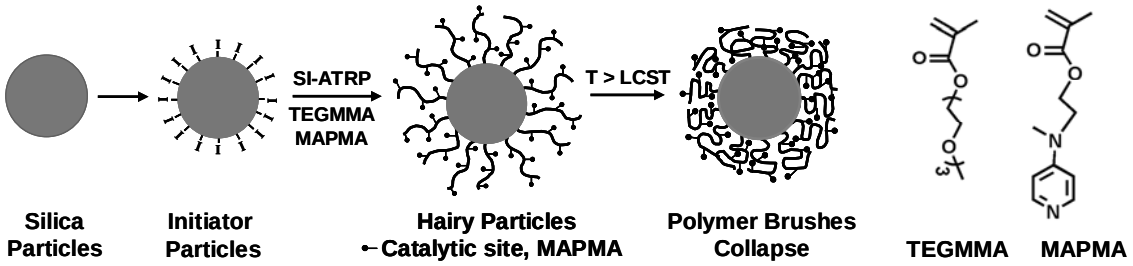

Scheme 2.2. Hydrolysis of *p*-Nitrophenyl Acetate with DAAP as Catalyst

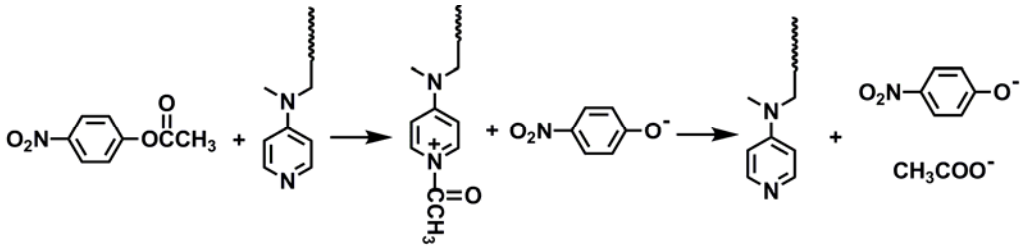

2.2 Experimental

2.2.1 Materials

Methacryloyl chloride (97%), tri(ethylene glycol) monomethyl ether (95%), potassium dihydrogen phosphate (≥ 99%), and 1,1,4,7,10,10-hexamethyltriethylenetetramine (97%) were obtained from Aldrich-Sigma. Hydrogen hexachloroplatinate (IV) hydrate, $CuCl_2$ (anhydrous, 99%), *p*-nitrophenyl acetate (97%), acetonitrile (99.5%), *N*,*N*-dimethylformamide (extra dry, with molecular sieves), and sodium tetraborate decahydrate were purchased from Acros and used as received. Chlorodimethylsilane (98%) was obtained from Alfa Aesar and stored in a refrigerator. Tetrahydrofuran (THF) was distilled from sodium and benzophenone and stored in a solvent storage bottle prior to use. CuCl (99.995%, Aldrich) was purified according to a procedure described in the literature.[9] Ethyl 2-bromoisobutyrate (98%, Aldrich) was dried over calcium hydride, distilled under a reduced pressure, and stored in a dessicator prior to use.

2.2.2 Characterization

Size exclusion chromatography (SEC) was carried out at ambient temperature using PL-GPC 50 Plus (an integrated GPC/SEC system from Polymer Laboratories, Inc) with a differential refractive index detector, one PSS GRAL guard column (50 × 8 mm, 10 micron particles, Polymer Standards Service-USA, Inc.), and two PSS GRAL linear columns (each 300 × 8 mm, 10 micron, molecular weight range from 500 to 1,000,000 according to Polymer Standards Service-USA, Inc.). The data were processed using Cirrus™ GPC/SEC software (Polymer Laboratories, Inc.). *N,N*-Dimethylformamide was used as the carrier solvent at a flow rate of 1.0 mL/min. Standard polystyrenes with narrow PDIs (Polymer

Laboratories, Inc.) were used for calibration. ^{1}H (300 MHz) and ^{13}C NMR (75 MHz) spectra were recorded on a Varian Mercury 300 NMR spectrometer and the residual solvent proton signal was used as the internal standard. Mass spectroscopy analysis was performed at the Mass Spectrometry Center of the Department of Chemistry at the University of Tennessee at Knoxville using a JEOL (Peabody, MA) AccuTOF-D time-of-flight mass spectrometer with a DART (direct analysis in real time) ionization source. Thermogravimetric analysis was performed in air at a heating rate of 20 ºC/min from room temperature to 800 ºC using TA Q-series Q50. Scanning electron microscopy (SEM) was carried out by an environmental SEM (FEI XL30) at an acceleration voltage of 10 kV. The SEM samples were prepared by dispersing particles in THF with the concentration of 0.1 wt %. 10 μL solutions were drop cast on the glass slides and spin coated at 1000-3000 rpm for 60 seconds. The glass slides were then dried under vacuum overnight to completely remove the solvent. Before SEM testing, platinum coating (30 s, 40 mA) was performed by using a Gressington Sputter Coater 208HR in order to increase the conductivity of the particles.

The cloud points of P(TEGMMA-*co*-MAPMA), formed from the free initiator in the synthesis of hairy particles, in 10 mM KH_2PO_4/$KNaHPO_4$ buffer solutions with pH of 7.52 at concentrations of 0.5, 0.2, and 0.1 wt % were determined by the use of UV-vis spectrometry. The optical transmittances of polymer solutions at wavelength of 500 nm at various temperatures during a heating process were recorded using a UV-vis spectrometer (Biomate 5 from Thermospectronic, Inc.). The sample cell was thermostated with an external water bath of a Fisher Scientific Isotemp refrigerated circulator and the

temperature was increased at a step of 1 or 2 ^{o}C. At each temperature, the solutions were equilibrated for 20 min. The onset temperatures of the LCST transition of P(TEGMMA-*co*-MAPMA) in two phosphate buffer solutions with pH of 7.52 and 7.82 at a polymer concentration of 0.01 wt % were determined by dynamic light scattering (DLS). DLS measurements were conducted with a Brookhaven Instruments BI-200SM goniometer equipped with a PCI BI-9000AT digital correlator, a temperature controller, and a solid-state laser (model 25-LHP-928-249, λ = 633 nm) at a scattering angle of 90^{o}. The polymer solutions were filtered into borosilicate glass tubes with an inner diameter of 7.5 mm by the use of Millipore Teflon filters (0.2 μm pore size). The glass tubes were then sealed with PE stoppers. The solutions were gradually heated from 35 ^{o}C. At each temperature, the solutions were equilibrated for 15 min prior to data recording.

The apparent hydrodynamic sizes of P(TEGMMA-*co*-MAPMA) brush-grafted silica particles or aggregates of hairy particles in 10 mM KH_2PO_4/$KNaHPO_4$ buffers with pH of 7.52 and 7.82 at various temperatures during heating were measured by DLS. The time correlation functions were analyzed with a Laplace inversion program (CONTIN). At each temperature, the particle dispersion was equilibrated for 30 min and multiple measurements (at least 8) were made to give an average apparent hydrodynamic diameter.

2.2.3 Synthesis of 2-(*N*-Methyl-*N*-(4-pyridyl)amino)ethyl Methacrylate (MAPMA)

4-(*N*-Methyl-*N*-(2-hydroxyethyl)amino)pyridine (EGMAP) was synthesized by following a procedure described in the literature.[31] ^{1}H NMR ($CDCl_3$): δ (ppm) 8.12 (d, 2H, N(C*H*)$_2$, aromatic), 6.50 (d, 2H, N(CHC*H*)$_2$, 3.82 (t, 2H, NCH_2), 3.52 (t, 2H, OCH_2), 3.02 (s, 3H, NCH_3), 2.34 (br s, 1H, OH). ^{13}C NMR: δ (ppm) 149.25 (N(*C*H)$_2$ and N*C*(CH)$_2$),

106.68 (N(CH*C*H)$_2$), 59.71 (N*C*H$_2$), 53.57 (NCH$_2$*C*H$_2$), 38.24 (N*C*H$_3$).

A solution of methacryloyl chloride (3.75 g, 35.9 mmol) in dry methylene chloride (9 mL) was added dropwise from an additional funnel under N_2 atmosphere into a 100 mL three-necked flask that contained a solution of 4-(*N*-methyl-*N*-(2-hydroxyethyl)-amino)pyridine (3.26 g, 21.5 mmol) and triethylamine (3.45 g, 34.1 mmol) in dry CH_2Cl_2 (15 mL) in an ice/water bath. After being stirred at room temperature for 12 h, the mixture was poured into an aqueous NaOH solution (2.5 M, 100 mL). The organic layer was then separated and the aqueous layer was extracted with $CHCl_3$ (50 mL × 3). The organics were combined and dried over anhydrous Na_2SO_4. The solvents were removed by using a rotary evaporator and the crude product was purified by silica gel column chromatography with methanol as eluent. After being dried in high vacuum to completely remove methanol, the desired product, 2-(*N*-methyl-*N*-(4-pyridyl) amino)ethyl methacrylate, was obtained as a light yellow liquid (1.53 g, 32.3 %). The product was subsequently dissolved in dry *N*,*N*-dimethylformamide and the solution was stored in a refrigerator. ^{1}H NMR δ (ppm) 8.21 (d, 2H, aromatic), 6.52 (d, 2H, aromatic), 6.02 (s, 1H, C*H*H=C), 5.54 (s, 1H, CH*H*=C), 4.30 (t, 2H, COOC*H*$_2$), 3.66 (t, 2H, COOCH$_2$C*H*$_2$N), 3.01 (s, 1H, NC*H*3), 1.87 (s, 3H, CC*H*$_3$); ^{13}C NMR δ (ppm) 167.08 (*C*=O), 153.20 (-N-*C*(CH)$_2$), 149.88 (-N-*C*H-CH), 135.66 (CH$_2$=*C*(CH$_3$)), 126.07 (*C*H$_2$=C), 106.50 (-C-*C*HCH), 61.29 (-O*C*H$_2$CH$_2$), 49.55 (OCH$_2$*C*H$_2$N), 37.67 (-N-*C*H$_3$), 18.14 (-C-*C*H$_3$); MS (ESI+): 221.12930 ([M + H]$^+$); calculated: 221.12900.

2.2.4 Synthesis of (3-(2-Bromo-2-methylpropionyloxy)propyl)dimethylchlorosilane and the Immobilization on Silica Particles

Allyl 2-bromo-2-methylpropionate was synthesized according to the procedure reported in the literature.[10,11] ^{1}H NMR ($CDCl_3$): δ (ppm) 5.94-5.83 (m, 1H, CH_2=C*H*), 5.37-5.21 (m, 2H, C*H*$_2$=CH), 4.63 (d, 2H, OCH_2), 1.90 (s, 6H, C(C*H*$_3$)$_2$Br. ^{13}C NMR: δ (ppm) 171.22 (*C*=O), 131.34 (CH_2=*C*H), 118.45 (*C*H_2=CH), 66.28 (O*C*H_2), 55.58 (*C*(CH_3)$_2$Br), 30.70 (C(*C*H_3)$_2$).

Chlorodimethylsilane (4.0 mL) was injected via a disposable syringe into a 25 mL two-necked flask that contained allyl 2-bromo-2-methylpropionate (0.522 g, 2.52 mmol) under nitrogen atmosphere, followed by addition of a solution of hydrogen hexachloroplatinate (IV) hydrate (7.0 mg) in a mixture of diethyl ether (0.2 mL) and absolute ethanol (0.2 mL). The flask was placed in an oil bath with a preset temperature of 35 ºC. The reaction was monitored by ^{1}H NMR spectroscopy. After the reaction was complete, excess chlorodimethylsilane was removed in high vacuum, and the product was used directly for functionalization of silica particles. The product was dissolved in dry THF (5 mL) and the solution was transferred via a syringe to a flask that contained a dispersion of bare silica particles (0.682 g) in dry THF (13 mL). The bare silica particles were dried in vacuum at 90 ºC overnight before being dispersed in dry THF. The reaction mixture was stirred at 70 ºC under N_2 atmosphere for 60 h. The particles were then isolated by centrifugation, re-dispersed in THF, and centrifugated again. This washing process was repeated for additional four times, followed by drying with a stream of air flow to yield the initiator-functionalized silica particles (0.607 g).

2.2.5 Synthesis of Poly(methoxytri(ethylene glycol) methacrylate-*co*-2-(*N*-methyl-*N*-(4-pyridyl)amino)ethyl methacrylate) Brushes from Initiator-Functionalized Silica Particles by Surface-Initiated ATRP

A typical procedure for the synthesis of P(TEGMMA-*co*-MAPMA) brush-grafted silica particles is described below. The initiator-functionalized silica particles (0.215 g) were added into a 25 mL two-necked flask and dried in vacuum at 45 ºC for 12 h. The particles were dispersed in *N*,*N*-dimethylformamide (8.2 mL) by sonication in a ultrasonic bath and transferred via a syringe into another 25 mL two-necked flask that contained CuCl (12.2 mg, 0.123 mmol), $CuCl_2$ (6.0 mg, 0.045 mmol), ethyl 2-bromoisobutyrate (10.9 mg, 0.0559 mmol), 1,1,4,7,10,10-hexamethyltriethylenetetramine (27.9 mg, 0.121 mmol), 2-(*N*-methyl-*N*-(4-pyridyl)amino)ethyl methacrylate (0.224 g, 1.02 mmol), methoxytri(ethylene glycol) methacrylate (7.827 g, 33.7 mmol), and DMF (0.255 g). After the reaction mixture was degassed by three freeze-pump-thaw cycles, an aliquot was taken immediately for ^{1}H NMR spectroscopy analysis and the flask was placed in an oil bath with a preset temperature of 90 ºC. The polymerization was monitored by ^{1}H NMR spectroscopy analysis using the peaks located at 4.23 ppm (the methylene groups of -$COOCH_2$- of monomers TEGMMA and MAPMA) and 4.00 ppm (the methylene groups of -$COOCH_2$- in P(TEGMMA-*co*-MAPMA)); the conversion at a particular polymerization time was calculated from the integral values of these two peaks (the sum of the integral values of two peaks was a constant throughout the polymerization). After the polymerization proceeded for 660 min, the flask was removed from the oil bath and opened to air, and the mixture was diluted with THF. The particles were isolated by centrifugation (Eppendorf 5840,

11000 rpm, 15 min), and the supernatant was passed through a short column of basic aluminum oxide (top)/silica gel (bottom) (1/2, v/v) with THF as eluent. The free copolymer solution was concentrated and purified by precipitation first in hexane and then in diethyl ether. The particles from centrifugation were dispersed in THF and separated by centrifugation. Methanol was then used to disperse particles, and three drops of an ammonia aqueous solution (25%) were added to the dispersion to facilitate the removal of copper catalyst. The particles were separated by centrifugation, re-dispersed in methanol, and isolated again. This process was repeated for addition two times. The hairy particles were dried with a stream of air flow. A portion of particles was further dried in high vacuum and used in thermogravimetric analysis. The rest of polymer brush-grafted particles were washed by two cycles of dispersing in water and separation via centrifugation, and finally dispersed in water. The concentration of hairy particles in the aqueous dispersion was 5.94 mg/g, determined by gravimetric analysis. The hairy particles were then used as catalyst for hydrolysis of *p*-nitrophenyl acetate in aqueous buffer solutions. The free copolymer, P(TEGMMA-*co*-MAPMA), was analyzed by SEC using polystyrene calibration. The SEC results were: $M_{n,SEC}$= 40100 Da, polydispersity index (PDI) = 1.23.

2.2.6 Determination of pK_a Values of the MAPMA Units in the Free Copolymer P(TEGMMA-*co*-MAPMA) and Small Molecule 4-(*N*-Methyl-*N*-(2-hydroxyethyl)-amino)pyridine (EGMAP)

A series of 10 mM aqueous buffer solutions were made by dissolving sodium tetraborate decahydrate (borax) or potassium dihydrogen phosphate in deionized water. The pH values of buffer solutions were adjusted by adding a NaOH solution or a HCl solution.

To determine the pK_a value of the MAPMA units in P(TEGMMA-*co*-MAPMA), an aqueous polymer solution (0.227 wt %, 40 μL) was injected into a quartz cuvette via a microsyringe, followed by addition of either a borax (for pH > 8) or a phosphate buffer solution (for pH < 8) with a known pH value via a syringe (1.0 mL). The UV-vis spectrum of the solution was recorded with a UV-vis spectrometer (Biomate 5 from Thermospectronic, Inc.). The absorbances of protonated and nonprotonated DAAPs were known to be at 280 nm and 260 nm, respectively. Similarly, the UV-vis spectra of EGMAP in aqueous buffers with various pH values were recorded. The absorbances of EGMAP and the MAPMA units of P(TEGMMA-*co*-MAPMA) at pH = 1 and 13 were recorded from 0.1 N aqueous HCl and 0.1 N NaOH solutions, respectively.

2.2.7 Kinetics Studies of the Hydrolysis of NPA in Aqueous Buffers Using P(TEGMMA-*co*-MAPMA) Brush-Grafted Particles, Free Copolymer P(TEGMMA-*co*-MAPMA), and EGMAP as Catalysts

The hydrolysis reactions of NPA were performed in 10 mM aqueous KH_2PO_4/$KNaHPO_4$ buffer solutions with pH of 7.52 and 7.82. The buffers were made by dissolving KH_2PO_4 in deionized water; the pH values were adjusted by addition of an aqueous NaOH solution and were measured with a pH meter (Accumet AB 15 pH meter from Fisher Scientific, calibrated with pH = 4.01, 7.00, and 10.01 standard buffer solutions).

The kinetics studies of the hydrolysis of NPA were conducted in a quartz cuvette using a Hewlett Packard 8542A Diode Array UV-vis spectrophotometer equipped with a Hewlett Packard 89090A Peltier temperature controller. The total weight of the reaction mixture in

the cuvette was 1.0 g. The absorbance of the ionized form of the hydrolysis product *p*-nitrophenol at 400 nm was recorded as a function of time by a computer program. The concentrations of NPA and MAPMA units in the buffer were 1.5×10^{-4} M and 1.5×10^{-5} M, respectively. A typical procedure using hairy particles as catalyst is described below. Similar procedures were employed for studying the kinetics of the hydrolysis of NPA with P(TEGMMA-*co*-MAPMA) or EGMAP as catalyst or without any DAAP catalyst.

The dispersion of hairy particles in water (82.1 mg, 0.488 mg hairy particles, 1.5×10^{-5} mmol MAPMA units) was added into a quartz cuvette equipped with a small magnetic stirrer, followed by addition of a 10 mM phosphate buffer with pH of 7.52 to bring the total weight to 1.0 g. The concentration of polymer brush-supported catalyst [MAPMA] was 1.5×10^{-5} M. The cuvette was then placed into the cell holder of the UV-vis spectrometer with a preset temperature. After the dispersion was equilibrated at the preset temperature for 30 min under the stirring condition, a solution of NPA in acetonitrile (7.51 mM, 20 μL) was injected into the cuvette via a microsyringe and the reaction mixture was immediately agitated with a glass pipette for 3 sec. The molar concentration of NPA was 1.5×10^{-4} M. The UV-vis spectra of the reaction mixture were recorded every 10 or 20 sec depending on the reaction temperature. The time at which the NPA solution was injected was taken as t = 0 sec.

The initial rates of the hydrolysis of NPA were calculated by using the following equation:[12]

$$V = \frac{\mathrm{d}(A_{400}-A_{550})}{\mathrm{d}t}\,\frac{1}{\varepsilon b}\,\frac{1}{f} \qquad (1)$$

where $d(A_{400}-A_{550})/dt$ is the initial slope of the variation of the difference between the absorbances at 400 (A_{400}) and 550 nm (A_{550}) with time, ε is the extinction coefficient of ionized *p*-nitrophenol, b is the optical path length (1 cm), and f is the fraction of ionized *p*-nitrophenol. We found from DLS studies that the P(TEGMMA-*co*-MAPMA) brush-grafted silica particles in aqueous phosphate buffers underwent aggregation when the temperature was above the LCST transition of P(TEGMMA-*co*-MAPMA) brushes. For the hydrolysis of NPA, we agitated the reaction mixture immediately with a glass pipette for 3 sec to make it uniform after the injection of 20 μL NPA solution. This disturbed the aggregates of hairy particles in the buffer solutions at temperatures above the LCST of polymer brushes and caused a slight fluctuation in the absorbances at 400 nm. Since this effect was essentially the same on the absorbances at wavelengths of 400 and 550 nm, we used the initial slope of $d(A_{400}-A_{550})/dt$ instead of dA_{400}/dt [12] to calculate the initial reaction rate in order to eliminate/minimize the agitation effect on the absorbance. Details were presented in the section of Results and Discussion. For every data point presented in this article, two identical experiments were performed and the average value was used. The product of extinction coefficient ε and fraction of ionized *p*-nitrophenol f was equal to the apparent coefficient ε' of *p*-nitrophenol in a buffer with a specific pH, which was determined by using the concentration of *p*-nitrophenol instead of the concentration of ionized *p*-nitrophenol. The values of apparent extinction coefficient ε' of *p*-nitrophenol in pH 7.52 and 7.82 buffers were 11337 and 14690 L/(mol•cm), respectively.

2.3 Results and Discussion

This work was intended to compare the catalytic activities of a polymer

brush-supported DAAP catalyst and the corresponding linear soluble polymer-supported version. We chose the hydrolysis of NPA in aqueous buffer solutions for studying and comparing the catalytic activities of polymer brush- and linear polymer-supported DAAPs because this reaction proceeds cleanly to yield *p*-nitrophenol via a known pathway (Scheme 2.2) and the reaction can be conveniently followed by UV-vis spectrometry due to the absorbance of ionized *p*-nitrophenol at 400 nm. A new methacrylate monomer that contains a DAAP group, MAPMA (Scheme 2.1), was prepared and used along with TEGMMA for the synthesis of random copolymer brushes from initiator-functionalized silica particles by surface-initiated polymerization[4-6,9,13] in the presence of a free initiator.[6a,13c,13f] It has been confirmed by a number of research groups that the molecular weight and molecular weight distribution of the grafted polymer on silica particles synthesized by surface-initiated "living"/controlled radical polymerization are essentially identical to those of the free copolymer formed from the free initiator.[6a,13c,13f] The composition of the free random copolymer is believed to be the same as that of the polymer brushes on silica particles. Thus, to compare the catalytic activities of polymer brush- and linear soluble polymer-supported DAAPs, we simply used the hairy particles and the corresponding free copolymer as catalysts for the hydrolysis of NPA under the same conditions at various temperatures and measured the reaction rates. We also investigated the hydrolysis of NPA using 4-(*N*-methyl-*N*-(2-hydroxyethyl)amino)pyridine (EGMAP) as catalyst in order to compare polymer catalysts with a small molecule DAAP.

The homopolymer of TEGMMA (PTEGMMA) is a thermosensitive water-soluble polymer with a cloud point at 48 ^{o}C in water.[6b,7] It belongs to a new family of

thermosensitive water-soluble polymers that contain short oligo(ethylene glycol) pendants.[7,14] The collapse of polymer brushes on silica particles and the coil-to-globule transition of the free copolymer in water likely present a higher steric hindrance for the diffusion of NPA molecules to the catalytic sites. The second goal of this work was to study the effects of thermo-induced LCST transitions of polymer brushes and the free copolymer on the catalytic activities of supported DAAPs.

2.3.1 Synthesis of Catalyst Monomer MAPMA and Initiator-Functionalized Silica Particles

MAPMA was prepared by reaction of methacryloyl chloride with 4-*N*-methyl-*N*-(2-hydroxyethyl)aminopyridine in the presence of triethylamine. The product was thoroughly purified by silica gel column chromatography and its molecular structure was confirmed by ^{1}H and ^{13}C NMR spectroscopy as well as mass spectroscopy analysis. The synthesis of TEGMMA and the precursor of the immobilizable ATRP initiator, allyl 2-bromo-2-methylpropionate, followed the procedures described in the literature.[6b,10,11] Silica particles with an average diameter of 202 nm, measured from a scanning electron microscopy (SEM) micrograph (Figure 2.1a), were prepared by the Stöber process, which involves the hydrolysis and condensation of tetraethoxysilane in an ammonia/ethanol solution.[6a] This process is well known to produce spherical silica particles with a relatively uniform size distribution. The particles were functionalized with an ATRP initiator by immobilizing a monochlorosilane, (3-(2-bromo-2-methyl-propionyloxy)propyl)dimethylchlorosilane, on the surface of silica particles. Figure 2.2 shows the thermogravimetric analysis (TGA) results; the weight retention of silica particles

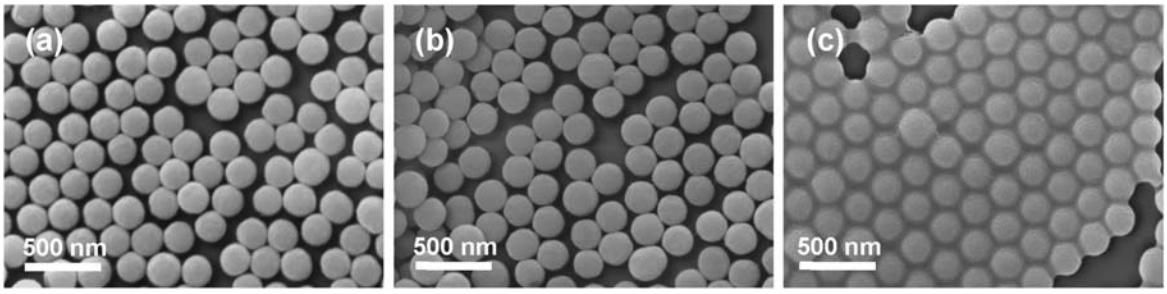

Figure 2.1. Scanning electron microscopy micrographs of (a) bare silica particles, (b) initiator-functionalized silica particles, and (c) P(TEGMMA-*co*-MAPMA) brush-grafted silica particles. The particles were drop cast from THF dispersions.

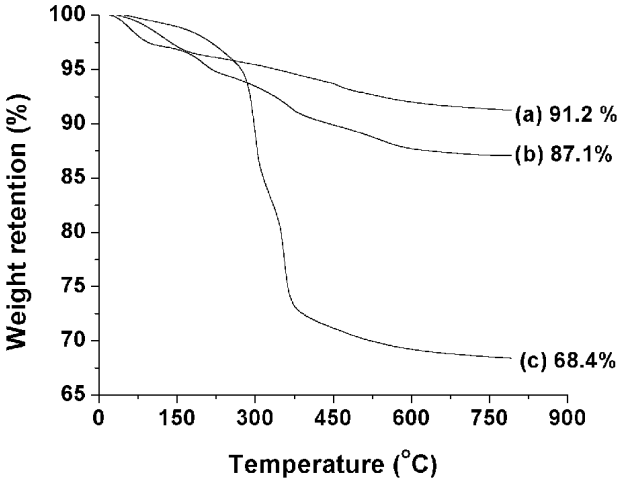

Figure 2.2. Thermogravimetric analysis (TGA) of bare silica particles (a), initiator-functionalized silica particles (b), and P(TEGMMA-*co*-MAPMA) brush-grafted silica particles (c). TGA was performed in air at a heating rate of 20 ºC/min from room temperature to 800 ºC.

at 800 ^{o}C decreased from 91.2 % (bare silica particles) to 87.1 % (after surface functionalization). This difference was similar to the results reported in previous publications from our group.[6]

2.3.2 Synthesis of Thermosensitive P(TEGMMA-*co*-MAPMA) Brush-Grafted Silica Particles by Surface-Initiated Atom Transfer Radical Polymerization

P(TEGMMA-*co*-MAPMA) brushes were grown from initiator-functionalized silica particles by surface-initiated ATRP, which was carried out in *N*,*N*-dimethylformamide (DMF) at 90 ^{o}C using CuCl/$CuCl_2$/1,1,4,7,10,10-hexamethyltriethylenetetramine (HMTETA) as catalytic system in the presence of a free initiator, ethyl 2-bromoisobutyrate (EBiB). The molar ratios of [EBiB] : [CuCl] : [$CuCl_2$] : [HMTETA] : [TEGMMA] : [MAPMA] = 1 : 2.2 : 0.8 : 2.2 : 603 : 18. We chose to use a small amount of MAPMA in the copolymerization for two reasons: (i) it has been reported that DAAPs are superior nucleophilic catalysts for the hydrolysis of *p*-nitrophenyl esters;[3a,b] (ii) the incorporation of a small amount of MAPMA into the polymer chain will not change the thermosensitive property too much. The polymerization was monitored by ^{1}H NMR spectroscopy and the monomer conversion was calculated by using the peak at 4.23 ppm, which was from the methylene groups of –$COOCH_2$– of both TEGMMA and MAPMA monomers, and the peak at 4.00 ppm, which was from the methylene groups of –$COOCH_2$– in the copolymer. Note that the sum of the integral values of the two peaks was a constant throughout the polymerization. The polymerization was stopped after 660 min and the particles were isolated by centrifugation and repeatedly washed with THF and methanol. The free copolymer was purified and analyzed by size exclusion chromatography (SEC) against

polystyrene calibration.

Figure 2.3a shows the kinetics plot of the polymerization. A linear relationship between $\ln([M]_o/[M])$ and reaction time was observed (the point at 660 min was slightly low than expected), indicating that the number of growing polymer chains was a constant during the polymerization. SEC analysis showed that the polymer peak continuously shifted to the high molecular weight side with the increase of polymerization time. The number average molecular weight $M_{n,SEC}$ increased linearly with the monomer conversion and the polydispersity index remained narrow (≤ 1.25) throughout the polymerization (Figure 2.3b). Both kinetics and SEC analysis confirmed that the ATRP of TEGMMA and MAPMA was a controlled process under the chosen polymerization conditions. The $M_{n,SEC}$ of the final copolymer after precipitation was 40100 Da and the polydispersity index was 1.23. The degree of polymerization (DP) of the final copolymer was 258, calculated from the monomer conversion and monomer-to-initiator ratio assuming every free initiator molecule initiated a polymer chain.

The molar ratio of TEGMMA and MAPMA units in the free copolymer P(TEGMMA-*co*-MAPMA) was determined from the ^{1}H NMR spectrum shown in Figure 2.4. From the integral values of the peaks located at 8.21 and 6.60 ppm (2H each from the pyridyl ring of MAPMA) and 4.07 ppm (2H from –$COOCH_2$– of both TEGMMA and MAPMA units in the copolymer P(TEGMMA-*co*-MAPMA)), the molar content of MAPMA units in the free copolymer was 3.13 %, virtually identical to that of MAPMA monomer in the polymerization feed (2.94 mol %).

The (PTEGMMA-*co*-MAPMA) brush-grafted silica particles were characterized by

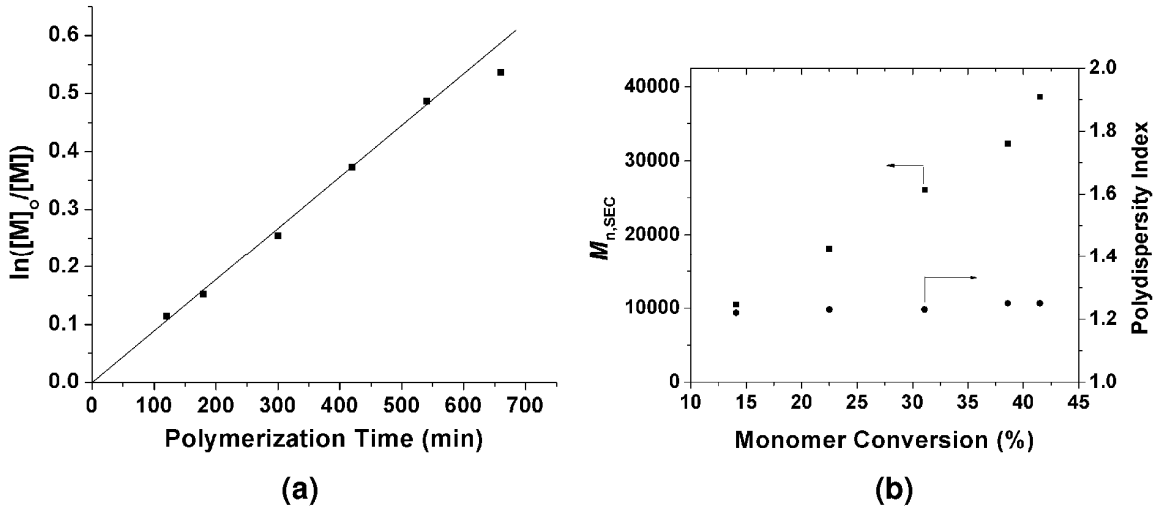

Figure 2.3. Plot of $\ln([M]_o/[M])$ versus reaction time (a) and plot of $M_{n,SEC}$ (▪) and polydispersity index (●) versus monomer conversion (b) for the ATRP of TEGMMA and MAPMA at 90 ^oC in DMF in the synthesis of P(TEGMMA-*co*-MAPMA) brush-grafted silica particles. The molar ratios of $[TEGMMA]_o$: $[MAPMA]_o$: [ethyl 2-bromoisobutyrate]$_o$: $[CuCl]_o$: $[CuCl_2]_o$: [1,1,4,7,10,10-hexamethyltriethylenetetramine]$_o$ were 603 : 18 : 1 : 2.2 : 0.8 : 2.2. $M_{n,SEC}$ and polydispersity index were determined by size exclusion chromatography analysis of the samples taken from the polymerization mixture against polystyrene calibration.

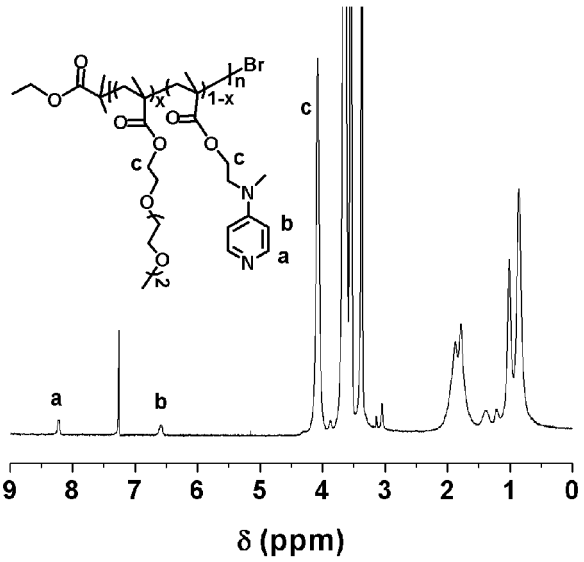

Figure 2.4. ^{1}H NMR spectrum of free copolymer P(TEGMMA-*co*-MAPMA) formed from the free initiator in the synthesis of hairy particles. $CDCl_3$ was used as the solvent.

TGA and SEM. TGA showed that the weight retention of the hairy particles at 800 ^{o}C was 68.4 % (Figure 2.2c), in contrast to 87.1 % for the initiator-functionalized silica particles. If we use the mass of the residual silica at 800 ^{o}C as reference and take into consideration the weight retention difference at 100 ^{o}C between initiator-functionalized particles (97.4 wt %) and hairy particles (99.5 wt %), the polymer content in the hairy particles is 23.3 wt %. Figure 2.1c shows a typical SEM micrograph of P(TEGMMA-*co*-MAPMA) brush-grafted silica particles, in which the grafted polymer can be clearly seen. The average size of hairy particles (the average distance between the centers of two neighboring particles) was 234 nm, 32 nm larger than those of bare particles and initiator particles. By the use of the average size of bare silica particles (202 nm), DP of the free copolymer (DP = 258), and TGA data, the grafting density of polymer brushes on silica particles was calculated to be 4.2 nm^2/chain, assuming that the silica particles were spherical and the density of the silica particles was identical to that of bulk silica (2.07 g/cm^3).[6a] The average distance between the grafting sites was 2.0 nm, which was much smaller than the thickness of polymer brushes in the dry state (16 nm from SEM micrograph Figure 2.1c), indicating that the grafted polymer chains were in the brush regime. It has been confirmed by a number of research groups that the molecular weight and polydispersity index of the grafted polymer on silica particles are essentially identical to those of the free polymer formed from the free initiator in the solution.[6a,13c,13f] The chemical composition of the free copolymer is believed to be identical to that of polymer brushes in the hairy particles.

2.3.3 pK_a of MAPMA Units in the Free Copolymer P(TEGMMA-*co*-MAPMA) and Small Molecule EGMAP

Since the hydrolysis rate of NPA in the presence of a DAAP catalyst is heavily dependent on the concentration of the nonprotonated DAAP,[3a-c] it is necessary to study its pK_a. The pK_a values of the MAPMA units in free copolymer P(TEGMMA-*co*-MAPMA) and small molecule EGMAP were determined spectrophotometrically following a method described in the literature.[8a] DAAPs are known to exhibit a 20-nm shift in λ_{max} when the basic (B, nonporotonated) and conjugated acid forms (BH^+, protonated) are compared, peaks appearing typically at 260 and 280 nm, respectively.[3a-c,8a] The following equation was used to calculate the molar fraction of nonprotonated DAAP species/units, x(B), at pH = *p*:[8a]

$$x(B) = \frac{[A_{280}/A_{260}]_{pH\ 1} - [A_{280}/A_{260}]_{pH\ p}}{[A_{280}/A_{260}]_{pH\ 1} - [A_{280}/A_{260}]_{pH\ 13}} \qquad (2)$$

where A_{280} and A_{260} are the absorbances at 280 and 260 nm, respectively. The absorbances at pH = 1 and 13 were obtained from the UV-vis spectra of EGMAP or the free copolymer in a 0.1 N aqueous HCl solution and a 0.1 N NaOH solution, respectively. A series of aqueous buffers with salt concentrations of 10 mM and various pH values were prepared and used to make solutions of EGMAP and P(TEGMMA-*co*-MAPMA) for UV-vis measurements. The ratio of $[B]/[BH^+]$ at each pH was calculated, and the pK_a value was then determined by the use of Henderson-Hasselbalck equation:

$$pH = pK_a + n \log([B]/[BH^+]) \qquad (3)$$

where *n* is a measure of deviation from ideal titration behavior.[8a]

Figure 2.5 shows the plots of log([B]/[BH^+]) versus pH for EGMAP and P(TEGMMA-*co*-MAPMA). The pK_a of EGMAP was 9.31, obtained by linear regression (R = 0.999, n = 1.02, Figure 2.5a), which is very close to that of 4-*N*,*N*-dimethylaminopyridine (pK_a = 9.7)[3a] and is within the range of the pK_a values of a series of DAAPs reported by Klotz et al. (pK_a = 8.60 – 9.96).[3b] The apparent pK_a of the MAPMA units in P(TEGMMA-*co*-MAPMA) was 7.95 (obtained by linear regression, R = 0.995, n = 1.40, Figure 2.5b), which is 1.36 pH units lower than that of EGMAP, indicating that the incorporation of a DAAP into a polymer has a significant effect on its pK_a value. This observation is consistent with those reported in the literature for the polymer-supported DAAPs.[3a-c,8a] Since the molar content of MAPMA units in the copolymer was only 3.13 % (approximately one MAPMA unit every 32 monomer units), the electrostatic repulsive interaction among protonated DAAP units, which has been used to explain the lower pK_a values of polymer-supported DAAPs,[3c] is unlikely the predominant cause of the decrease of pK_a of P(TEGMMA-*co*-MAPMA). We speculate that the main reason, as discussed by Urry,[15] is that the introduction of charges (protonation of DAAP) onto a thermosensitive water-soluble polymer chain disrupts the "ordered" water structures around the hydrophobic moieties and the charges compete with the hydrophobic groups for water molecules for hydration. Thus, achieving the same degree of protonation of MAPMA units on a thermosensitive polymer chain requires a lower solution pH compared with small molecule EGMAP. Considering the low segment density in the brush layer of hairy particles in aqueous solutions and the low content of MAPMA in the copolymer, we assume that the pK_a of MAPMA in the brush is the same as that of MAPMA in the free

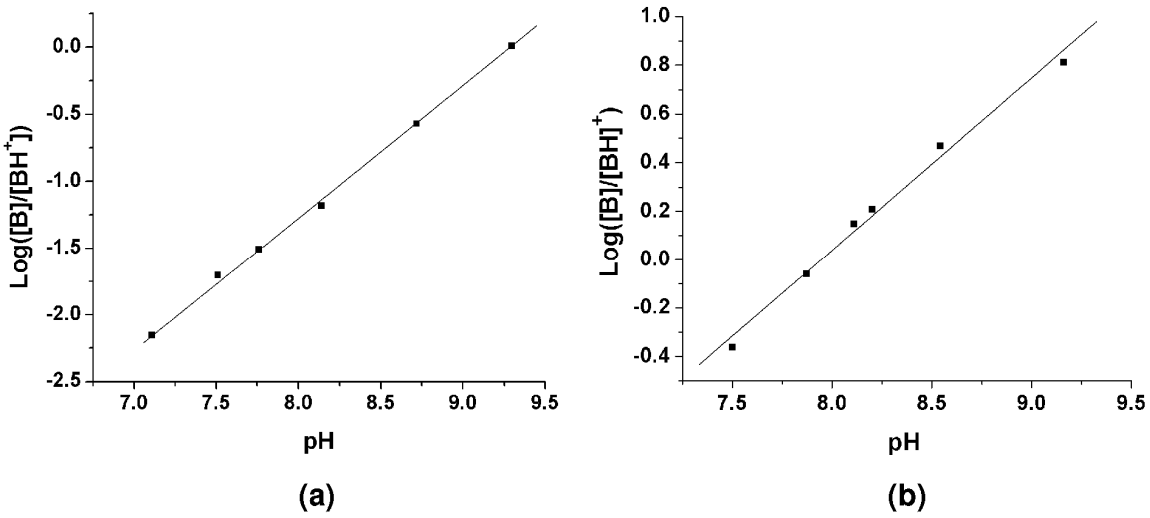

Figure 2.5. Plot of log([B]/[BH^+]) versus pH for 4-(*N*-methyl-*N*-(2-hydroxyethyl)-amino)pyridine (EGMAP) (a) and the MAPMA units in free copolymer P(TEGMMA-*co*-MAPMA) (b) in aqueous buffers with various pH values, where [B] and [BH^+] are the concentrations of nonprotonated and protonated DAAP species/units, respectively.

copolymer. Since the nonprotonated DAAP is the actual nucleophilic catalyst, a lower pK_a makes the polymer catalyst more attractive than small molecules because the reaction can be carried out at a milder pH at a reaction rate that can only be obtained at a higher pH with a small molecule DAAP as catalyst. For the same reason, we chose phosphate buffers with pH of 7.52 and 7.82, which were close to the pK_a of P(TEGMMA-*co*-MAPMA) (pK_a = 7.95), as reaction media for the hydrolysis of NPA with hairy particles and free copolymer P(TEGMMA-*co*-MAPMA) as catalysts.

2.3.4 Thermosensitive Properties of Free Copolymer P(TEGMMA-*co*-MAPMA) and P(TEGMMA-*co*-MAPMA) Brush-Grafted Silica Particles

Since one goal of this work was to investigate the effects of thermo-induced LCST transitions on the catalytic activities of the supported DAAPs in the hydrolysis of NPA, we studied the thermoresponsive properties of free copolymer P(TEGMMA-*co*-MAPMA) and the polymer brush-grafted silica particles in aqueous phosphate buffers with pH of 7.52 and 7.82, the solutions used as media for the hydrolysis of NPA. The cloud points of P(TEGMMA-*co*-MAPMA) in the pH 7.52 buffer at concentrations of 0.5, 0.2, and 0.1 wt % were 47.5, 48, and 50 ^{o}C, respectively, which were obtained from the plots of optical transmittance at wavelength of 500 nm versus temperature. The cloud point of P(TEGMMA-*co*-MAPMA) at a concentration of 0.5 wt % (47.5 ^{o}C) was almost identical to that of PTEGMMA at the same concentration (48 ^{o}C),[6b] indicating that the incorporation of 3.13 mol % MAPMA units into the polymer chain has little effect on the thermosensitive property. Note that the cloud point increased with the decrease of polymer concentration, consistent with our previous observations.[14c,d]

Measurement of cloud points of the copolymer at further lower concentrations (e.g., 0.01 wt % – the concentration used in the hydrolysis of NPA) by UV-vis spectrometry was not practical because of the small optical transmittance changes involved in the transition. Therefore, we used dynamic light scattering (DLS) to determine the onset temperatures of the LCST transition of P(TEGMMA-*co*-MAPMA) in the two buffers. Figure 2.6a shows the plot of scattering intensity at 90 ^{o} versus temperature for two polymer solutions with pH of 7.52 and 7.82. The concentrations of P(TEGMMA-*co*-MAPMA) in the two aqueous phosphate buffers were 0.01 wt %. For each polymer solution, the scattering intensity was very low when the temperature was below a certain point, above which the scattering intensity increased dramatically, signaling the LCST transition of P(TEGMMA-*co*-MAPMA). The onset temperature of the LCST transition of the copolymer was 51 ^{o}C in the pH 7.82 buffer and 53 ^{o}C in the pH 7.52 buffer. The higher transition temperature at pH 7.52 is due to the larger number of protonated MAPMA (BH^{+}) units in the copolymer chain. As shown in the previous section, the apparent pK_a of P(TEGMMA-*co*-MAPMA) was 7.95. Calculations using equation (3) showed that the ratio of nonprotonated MAPMA (B) units to protonated (BH^{+}) units was 0.49 at pH = 7.52 and 0.81 at pH = 7.82. Thus, more MAPMA units were charged at pH = 7.52, making the polymer chains more hydrophilic than in the pH 7.82 buffer, and hence the LCST transition occurred at a higher temperature.

The thermoresponsive properties of P(TEGMMA-*co*-MAPMA) brush-grafted silica particles in the two buffers were also studied by DLS. Figure 2.6b shows the average apparent hydrodynamic size of hairy particles/aggregates as a function of temperature

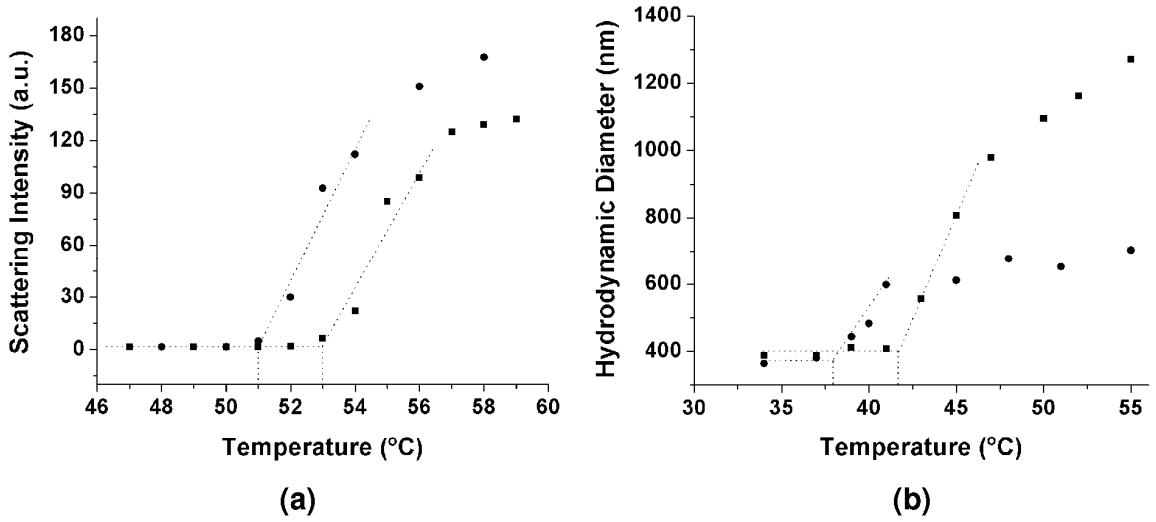

Figure 2.6. (a) The intensity of scattered light at 90^{o} obtained from DLS studies of solutions of free copolymer P(TEGMMA-*co*-MAPMA) in 10 mM phosphate buffers with pH of 7.52 (▪) and 7.82 (●) as a function of temperature during heating processes. The polymer concentrations in both buffers were 0.01 wt %. (b) The plot of average apparent hydrodynamic size of P(TEGMMA-*co*-MAPMA) brush-grafted silica particles/aggregates in 10 mM phosphate buffers with pH of 7.52 (▪) and 7.82 (●) versus temperature upon heating. The concentrations of hairy particles in the two buffers were ~0.06 mg/g. At temperatures ≥ 39 ^{o}C in the pH 7.82 buffer and ≥ 43 ^{o}C in the pH 7.52 buffer, two size distributions were often observed.

during the course of heating. For hairy particles in the pH 7.82 buffer, a single size distribution was observed when the temperature was ≤ 37 ^{o}C. With increasing the temperature ≥ 39 ^{o}C, two size distributions were often observed from DLS measurements; the reported hydrodynamic sizes in Figure 2.6b were the averages over all size distributions. This indicated that the polymer brushes underwent a LCST transition and the hairy particles began to form aggregates.[16] The onset temperature of the LCST transition from Figure 2.6b was ~ 38 ^{o}C. Similarly, the hairy particles underwent aggregation in the pH 7.52 buffer upon heating, but the onset temperature was slightly higher (42 ^{o}C), consistent with the observation of the LCST transitions of free copolymer P(TEGMMA-*co*-MAPMA) in the two buffers. Note that the LCST transition temperatures of polymer brushes on silica particles were significantly lower than those of free copolymer P(TEGMMA-*co*-MAPMA) in the two buffers, which is presumably due to the interactions among neighboring polymer chains in the polymer brush layer where the density of segments is much higher than that in the random coil of a free copolymer chain in the solution.[6b,13j]

2.3.5 P(TEGMMA-*co*-MAPMA) Brush-Grafted Silica Particles and Free Copolymer P(TEGMMA-*co*-MAPMA) as Catalysts for Hydrolysis of *p*-Nitrophenyl Acetate

The hydrolysis reactions of NPA were carried out in a 10 mM aqueous phosphate buffer with pH of either 7.52 or 7.82 under the stirring condition. In all hydrolysis experiments with hairy particles and the free copolymer as catalysts, the concentrations of NPA and the MAPMA units in the hairy particles or in the free copolymer were 1.5×10^{-4} and 1.5×10^{-5} M, respectively. Figure 2.7a shows the UV-vis spectra of a reaction mixture with hairy particles as catalyst in the pH 7.52 buffer at 37 ^{o}C at various times. Note that the

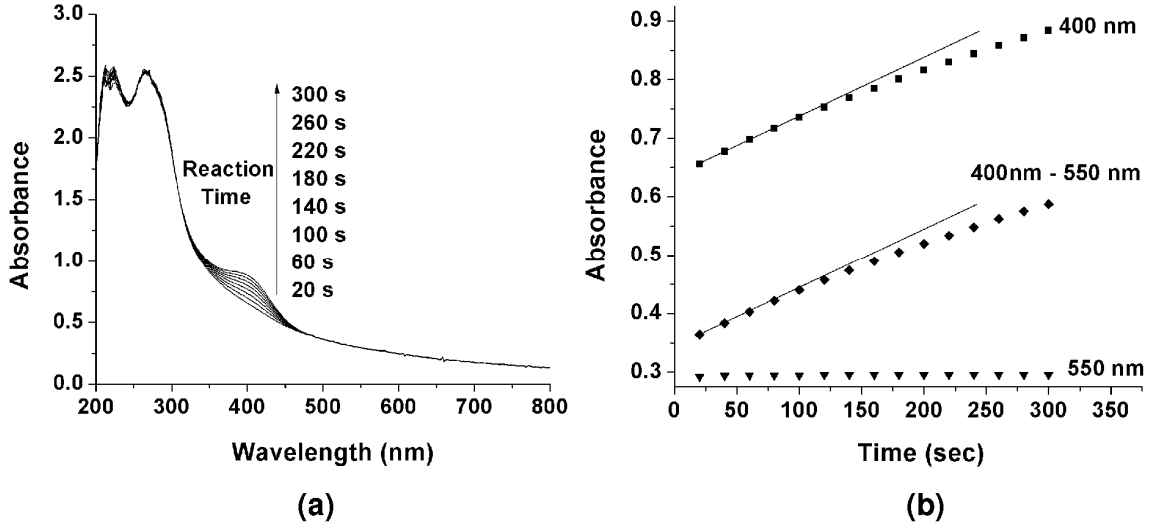

Figure 2.7. (a) UV-vis spectra of a reaction mixture with hairy particles as catalyst for the hydrolysis of *p*-nitrophenyl acetate in the pH 7.52 phosphate buffer at 37 ^{o}C at various reaction times. [NPA] = 1.5×10^{-4} M and [MAPMA unit] = 1.5×10^{-5} M. (b) Absorbances at 400 ($A_{400\ nm}$) and 550 nm ($A_{550\ nm}$) and the difference between the absorbances at 400 and 550 nm ($A_{400\ nm} - A_{550\ nm}$) as a function of reaction time.

temperature was below the LCST of polymer brushes. Because of the absorbance of hairy particles, the baselines of the UV-vis spectra were not flat. From Figure 2.7b, one can see that the absorbance at 400 nm (A_{400}), from the ionized product *p*-nitrophenol, increased smoothly with the increase of reaction time, while the absorbance at 550 nm (A_{550}) remained constant throughout the reaction because *p*-nitrophenol and its ion do not exhibit an absorbance at this wavelength. Figure 2.8a shows the UV-vis spectra of another reaction mixture under the same conditions as in Figure 2.7 except the temperature at 52 ^{o}C, which was above the LCST of polymer brushes. Different from Figure 2.7b, the absorbance at wavelength of 400 nm did not increase smoothly with the time but fluctuated to some degree even after the dispersion of hairy particles was equilibrated for 30 min under the stirring condition (Figure 2.8b). As shown in Figure 2.6b, the hairy particles underwent aggregation when the temperature was above the LCST of polymer brushes. In the hydrolysis experiments, immediately after the injection of a NPA solution into the quartz cuvette, we agitated the reaction mixture with a glass pipette for 3 sec to make the NPA concentration uniform. The fluctuation in the absorbance was likely due to the agitation with the glass pipette, which might disturb some loose aggregates of hairy particles. This effect can also be seen from the continuous decrease of the absorbances at 550 and 270 nm and the fluctuations of the absorbances at two wavelengths follow the same trend (Figure 2.8b). To eliminate/minimize the agitation effect on the absorbance, we subtracted the absorbance at 550 nm (A_{550}) from that at 400 nm (A_{400}) and made a plot of ($A_{400} - A_{550}$) versus time, assuming that the agitation effect on the absorbance at 400 nm was the same as that at 550 nm. As shown in Figure 2.8b, a smooth curve was obtained for the hydrolysis at

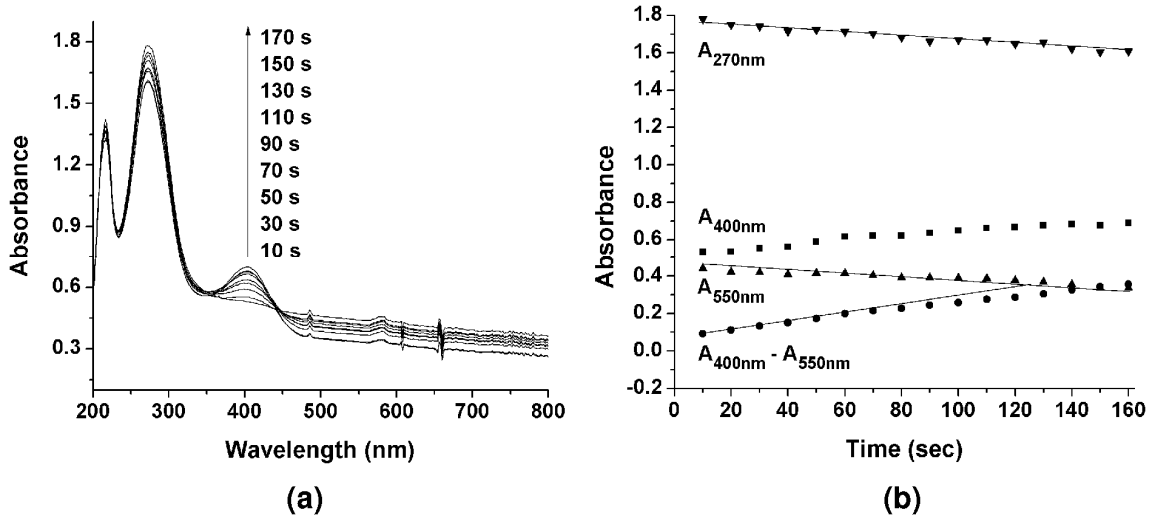

Figure 2.8. (a) UV-vis spectra of a reaction mixture with hairy particles as catalyst for the hydrolysis of *p*-nitrophenyl acetate in the pH 7.52 phosphate buffer at 52 ^{o}C at various reaction times. [NPA] = 1.5×10^{-4} M and [MAPMA unit] = 1.5×10^{-5} M. (b) Absorbances at 400 ($A_{400\ nm}$) and 550 nm ($A_{550\ nm}$) and the difference between the absorbances at 400 and 550 nm ($A_{400\ nm} - A_{550\ nm}$) as a function of reaction time.

52 ^{o}C, from which the initial reaction rate was derived by linear regression of the first five points and the use of equation (1). To be consistent, we also used this method to calculate the initial reaction rates at temperatures below the LCST, where the absorbances at 550 nm were a constant (Figure 2.7b).

2.3.6 Comparison of Net Initial Rates of Hydrolysis of *p*-Nitrophenyl Acetate Catalyzed by Hairy Particles and Free Copolymer at Temperatures below the LCST of Polymer Brushes

A series of hydrolysis reactions of NPA with hairy particles as catalyst in the pH 7.52 and 7.82 buffers were carried out under the same conditions except temperature and the initial rates were obtained from the UV-vis data using the aforementioned method. For comparison, we determined the initial rates of hydrolysis with free copolymer P(TEGMMA-*co*-MAPMA) and small molecule EGMAP as catalysts under the same conditions (EGMAP was used as catalyst only for the reactions in the pH 7.52 phosphate buffer). Since the buffer was slightly basic and might also contribute to the initial rate of the hydrolysis of NPA, we measured the background rates by performing the reactions under the same conditions except without addition of any DAAP catalyst. We found that the background rate accounted for a small fraction of the total rate, e.g., 6.3 % of the total rate catalyzed by hairy particles in the pH 7.52 buffer at 34 ^{o}C and 15.3 % at 55 ^{o}C. For better comparison, we derived the net initial rates of hydrolysis of NPA catalyzed by hairy particles, free copolymer, and EGMAP by subtracting the corresponding background rates from the overall rates for all temperatures.

The effect of temperature on reaction rate constant is usually expressed by Arrhenius

equation, that is, ln*k* changes linearly with inverse temperature. Figure 2.9 shows the plot of logarithm of net initial rate (logV) versus inverse temperature for the reactions with hairy particles, free copolymer P(TEGMMA-*co*-MAPMA), and EGMAP as catalysts as well as the background rate. As expected, for hydrolysis of NPA in the absence of any DAAP catalyst and in the presence of small molecule EGMAP catalyst, logV changed with 1/T in a linear fashion throughout the studied temperature range (from 34 to 58 ^{o}C in the pH 7.52 buffer and from 31 to 55 ^{o}C in the pH 7.82 buffer). For the reactions with hairy particles as catalyst at temperatures below the LCST, a linear relationship between logV and 1/T was observed in the range of 34 to 43 ^{o}C in the pH 7.52 buffer and 31 to 39 ^{o}C in the pH 7.82 buffer. Note that the onset temperature of LCST transition of polymer brushes was 42 ^{o}C in the pH 7.52 buffer and 38 ^{o}C in the pH 7.82 buffer. The two curves for the reactions with hairy particles and the free copolymer as catalysts in these temperature ranges were in parallel (Figure 2.9a and b). On average, the net initial rate using hairy particles was 70% of that using free copolymer P(TEGMMA-*co*-MAPMA) as catalyst in the pH 7.52 buffer and 80% in the pH 7.82 buffer. These results suggested that the catalytic activity of polymer brush-supported DAAP at the grafting density of 4.2 nm^2/chain was on the same level as that of the linear polymer-supported DAAP catalyst under the same reaction conditions. It has been observed that the catalytic performance difference between hairy particles and the free polymer was slightly greater at pH 7.52 than that at pH 7.82. This might be because more MAPMA units were charged at pH 7.52, making the free copolymer coil slightly more expanded and thus the catalytic sites more accessible. Note that the reaction catalyzed by either hairy particles or free copolymer at pH = 7.82 was consistently

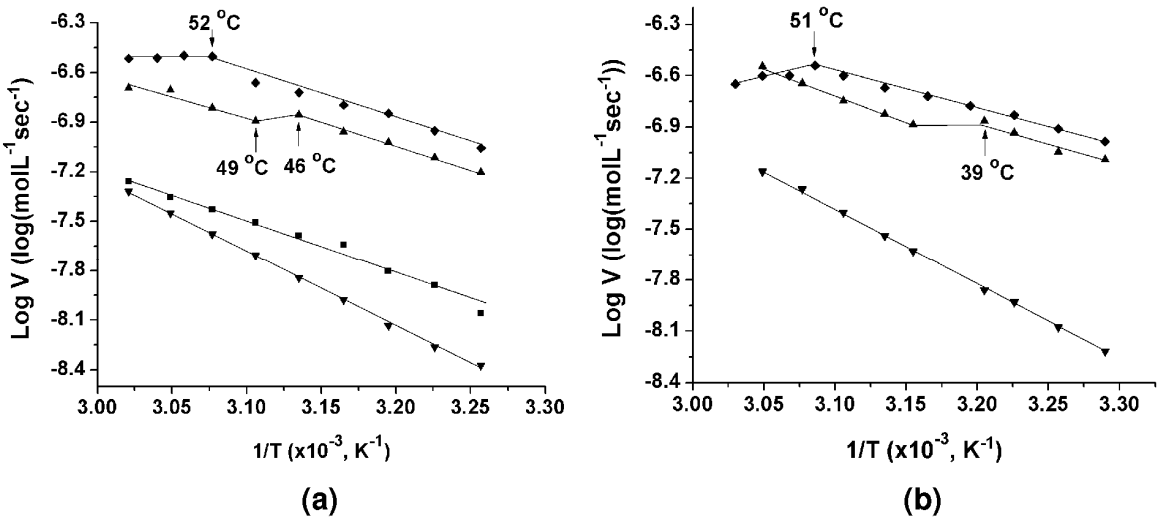

Figure 2.9. Plot of logarithm of net initial reaction rate versus inverse temperature for the hydrolysis of *p*-nitrophenyl acetate in the pH 7.52 (a) and pH 7.82 (b) phosphate buffers with P(TEGMMA-*co*-MAPMA) brush-grafted silica particles (▲), free copolymer P(TEGMMA-*co*-MAPMA) (♦), and EGMAP (■) as catalyst, and without any catalyst (▼). For all reactions, [NPA] = 1.5×10^{-4} M and [catalyst] = 1.5×10^{-5} M.[a]

[a.] Reaction rates, not rate constants, were used in these two plots. We did not derive the activation parameters.

faster than that at pH = 7.52 at the same temperature. For example, the net initial rates of reactions with hairy particles and free copolymer as catalysts at 34 ^{o}C were 6.3×10^{-8} and 8.8×10^{-8} $molL^{-1}sec^{-1}$ in the pH 7.52 buffer, respectively, and 9.0×10^{-8} and 1.2×10^{-7} $molL^{-1}sec^{-1}$ in the pH 7.82 buffer. This is because the concentration of nonprotonated MAPMA units in the pH 7.82 buffer was higher than that in the pH 7.52 buffer.

In contrast, the net initial rate for the reaction catalyzed by small molecule EGMAP at any temperature was much lower than that using either hairy particles or the free copolymer as catalyst (Figure 2.9a). For example, at 37 ^{o}C in the 7.52 buffer, the net initial rates of the reactions with hairy particles, free copolymer, and EGMAP as catalysts were 7.7×10^{-8}, 1.1×10^{-7}, 1.3×10^{-8} $molL^{-1}sec^{-1}$. The net hydrolysis rates using hairy particles and the free copolymer were 5.9 and 8.5 times faster than that using EGMAP as catalyst. This is understandable because the pK_a of EGMAP (pK_a = 9.31) is much higher than that of polymer catalysts (pK_a = 7.95). Calculations show that at pH = 7.52, only 2 % of EGMAP molecules were not protonated while 32 % MAPMA units in the copolymer were nonprotonated. Thus, the normalized catalytic activity (expressed as the net initial rate) of small molecule EGMAP was 2.7 and 1.9 times higher than that of free copolymer and polymer brush-supported DAAP catalysts, respectively. This comparison is based on the use of EGMAP as small molecule and the polymer brush- and linear polymer-supported MAPMA. The catalytic activity of EGMAP might be slightly different from that of small molecule MAPMA. In summary, the catalytic activities of polymer brush-supported and linear soluble polymer-supported DAAPs were very close to each other and these polymer catalysts were 6-8 times more effective than EGMAP in the pH 7.52 buffer under the same

reaction conditions.

2.3.7 Effects of Thermo-Induced LCST Transitions on the Catalytic Activities of P(TEGMMA-*co*-MAPMA) Brushes on Silica Particles and Free Copolymer P(TEGMMA-*co*-MAPMA)

As shown in Figure 2.6, when the temperature was high enough, the free copolymer P(TEGMMA-*co*-MAPMA) and polymer brushes on silica particles underwent LCST transitions, resulting in the formation of polymer aggregates and particle aggregates in the buffers. The onset temperatures of the LCST transition of free copolymer P(TEGMMA-*co*-MAPMA) in the pH 7.52 and 7.82 buffers were 53 and 51 ^{o}C, respectively, while the onset temperatures for the hairy particles in the two buffers were 42 and 38 ^{o}C, respectively. From Figure 2.9, one can see that all plots of logV versus 1/T for the reactions with hairy particles and the free copolymer as catalysts in both buffers did not follow the Arrhenius equation in the entire temperature range as for the reactions with small molecule EGMAP as catalyst or without any DAAP catalyst; the curve shifted noticeably to the left side in the case of hairy particles or leveled off/decreased slightly in the case of free copolymer as catalyst when the temperature was higher than a certain point. For example, for the reactions with hairy particles as catalyst in the pH 7.52 buffer, the initial rate of hydrolysis at 49 ^{o}C was slightly lower than that at 46 ^{o}C; the transition occurred around 46 ^{o}C, just above the onset temperature of the LCST transition of polymer brushes (42 ^{o}C), indicating that the collapse of polymer brushes did exert an effect on the reaction rate. At temperatures above 49 ^{o}C, the increase of initial rate with increasing temperature was resumed with the slope almost identical to that before the LCST transition. A similar

phenomenon was observed for the reactions with hairy particles as catalyst in the pH 7.82 buffer (Figure 2.9b). The shift occurred in the temperature range of 39 to 44 ^{o}C, slightly lower than that in the pH 7.52 buffer but again just above the onset temperature of the LCST transition of polymer brushes in this buffer (38 ^{o}C). In contrast, for the reactions using the free copolymer P(TEGMMA-*co*-MAPMA) as catalyst, the initial rate leveled off or decreased slightly when the temperature was above a critical point (Figure 2.9a and b). The transition occurred at 52 ^{o}C in the pH 7.52 buffer and 51 ^{o}C in the pH 7.82 buffer, which matched the LCSTs of the free copolymer in the two buffers (53 and 51 ^{o}C, respectively).

Above the LCSTs, both the free copolymer and the polymer brush-grafted silica particles formed aggregates (Figure 2.6), presenting a higher steric barrier to the diffusion of NPA molecules to the catalytic sites and thus exerting effects on the reaction rates. In the case of using the free copolymer as catalyst, with increasing temperature, the polymer chains became more dehydrated and the aggregates became tighter and larger. The surface-to-volume ratio decreased dramatically compared with the coiled, highly swelled polymer chains below the LCST, resulting in a mass transfer limitation of substrate molecules to the catalytic sites buried inside the aggregates. Consequently, the reaction rate leveled off or decreased slightly with the increase of temperature. The situation for hairy particles was slightly different; the NPA molecules could still diffuse quickly through the interstitial space among the particles in the aggregates to the catalytic sites in the collapsed polymer brushes. Unlike the dehydrated free copolymer chains forming large aggregates, the collapsed polymer brushes remained a single brush layer on the surface of silica

particles even after the hairy particles aggregated. Thus, the surface-to-volume ratio decreased, but not as drastically as in the case of free copolymer. Therefore, the steric barrier for the diffusion of NPA molecules to the DAAP sites inside polymer brushes was not increased as much as in the large aggregates of collapsed copolymer chains above the LCST transition. With further increasing temperature, the diffusion was accelerated and the increase of reaction rate with temperature was resumed. Note that the modulation of catalytic activities of supported metal catalysts by thermo-induced LCST transitions has been reported in the literature.[17] For example, Ballauff et al. reported the use of crosslinked thermosensitive core-shell particles as carrier for Ag nanoparticles for catalysis of reduction of 4-nitrophenol.[17a] They observed that the dependence of apparent rate constant on temperature did not follow Arrhenius equation, which was attributed to the temperature-induced volume phase transition of crosslinked poly(*N*-isopropylacrylamide) shell layer of the carrier particles. In summary, the thermo-induced LCST transitions were observed to have noticeable effects on the catalytic activities of thermosensitive polymer brush-supported and linear soluble polymer-supported DAAP catalysts in the hydrolysis of NPA. The effects were different, likely because of the different structures of aggregates of collapsed polymer chains and thermosensitive hairy particles.

2.4 Conclusions

We synthesized P(TEGMMA-*co*-MAPMA) brushes on silica particles by surface-initiated ATRP of a mixture of TEGMMA and MAPMA with a molar ratio of 100 : 3 in DMF at 90 ^{o}C in the presence of a free initiator using CuCl/$CuCl_2$/HMTETA as catalytic system. ^{1}H NMR spectroscopy analysis of the free copolymer formed from the

free initiator showed that the molar content of MAPMA units was 3.13 %, virtually identical to that in the feed (2.94 %). DLS studies showed that the onset temperatures of LCST transition of the free copolymer in 10 mM phosphate buffers with pH of 7.52 and 7.82 were 53 and 51 ^{o}C, respectively, while the onset temperatures of the LCST transition of polymer brushes were 42 and 38 ^{o}C, respectively. Both hairy particles and the free copolymer P(TEGMMA-*co*-MAPMA) were used as catalysts for the hydrolysis of NPA in the two buffers at various temperatures and the reactions were monitored by UV-vis spectrometry at wavelength of 400 nm. We found that the catalytic activity of polymer brush-supported DAAP was very close to that of the free copolymer under the same reaction conditions. The plot of logarithm of net initial rate versus inverse temperature exhibited a shift for the reactions with hairy particles as catalyst and leveled off/decreased slightly in the case of using the free copolymer as catalyst. The difference is likely because the collapsed free copolymer chains formed large aggregates in the buffers at temperatures above the LCST while the collapsed polymer brushes remained a single brush layer even in the aggregates of hairy particles and thus the steric barrier was not increased as much as in the aggregates of collapsed polymer chains.

References

1. (a) Scriven, E. F. V. *Chem. Soc. Rev.* **1983**, *12*, 129-161. (b) Chen, H. -T.; Huh, S.; Wiench, J. W.; Pruski, M.; Lin, V. S. -Y. *J. Am. Chem. Soc.* **2005**, *127*, 13305-13311. (c) Ó Dálaigh, C.; Corr, S. A.; Gun'ko, Y.; Connon, S. J. *Angew. Chem. Int. Ed.* **2007**, *46*, 4329-4332.

2. (a) Cozzi, F. *Adv. Synth. Catal.* **2006**, *348*, 1367-1390. (b) Benaglia, M.; Puglisi, A.; Cozzi, F. *Chem. Rev.* **2003**, *103*, 3401-3429. (c) Bergbreiter, D. E. *Chem. Rev.* **2002**, *102*, 3345-3383.

3. (a) Hierl, M. A.; Gamson, E. P.; Klotz, I. M. *J. Am. Chem. Soc.* **1979**, *101*, 6020-6021. (b) Delaney, E. J.; Wood, L. E.; Klotz, I. M. *J. Am. Chem. Soc.* **1982**, *104*, 799-807. (c) Vaidya, R. A.; Mathias, L. J. *J. Am. Chem. Soc.* **1986**, *108*, 5514-5520. (d) Rubinsztajn, S.; Zeldin, M.; Fife, W. K. *Macromolecules* **1991**, *24*, 2682-2688. (e) Bergbreiter, D. E.; Osburn, P. L.; Li, C. M. *Org. Lett.* **2002**, *4*, 737-740. (f) Price, K. E.; Mason, B. P.; Bogdan, A. R.; Broadwater, S. J.; Steinbacher, J. L.; McQuade, D. T. *J. Am. Chem. Soc.* **2006**, *128*, 10376-10377. (g) Liang, C. O.; Helms, B.; Hawker, C. J.; Fréchet, J. M. J. *Chem. Commun.* **2003**, *20*, 2524-2525. (h) Helms, B.; Liang, C. O.; Hawker, C. J.; Fréchet, J. M. J. *Macromolecules* **2005**, *38*, 5411-5415. (i) Helms, B.; Guillaudeu, S. J.; Xie, Y.; McMurdo, M.; Hawker, C. J.; Fréchet, J. M. J. *Angew. Chem. Int. Ed.* **2005**, *44*, 6384-6387. (j) Tomoi, M.; Akada, Y.; Kakiuchi, H. *Makromol. Chem. Rapid Commun.* **1982**, *3*, 537-542. (k) Menger, F. M.; McCann, D. J. *J. Org. Chem.* **1985**, *50*, 3928-3930. (l) Deratani, A.; Darling, G. D.; Fréchet, J. M. J. *Polymer* **1987**, *28*, 825-830. (m) Deratani, A.; Darling, G. D.; Horak, D.; Fréchet, J.

M. J. *Macromolecules* **1987**, *20*, 767-772. (n) Storck, W.; Manecke, G. J Mol Catal 1985, 30, 145-169. (o) Guendouz, F.; Jacquier, R.; Verducci, J. *Tetrahedron* **1988**, *44*, 7095-7108. (p) Corma, A.; García, H.; Leyva, A. *Chem. Commun.* **2003**, *22*, 2806-2807.

4. Zhao, B.; Jiang, X. M.; Li, D. J.; Jiang, X. G.; O'Lenick, T. G.; Li, B.; Li, C. Y. *J. Polym. Sci., Part A: Polym. Chem.* **2008**, *46*, 3438-3446.

5. (a) Tsujii, Y.; Ohno, K.; Yamamoto, S.; Goto, A.; Fukuda, T. *Adv. Polym. Sci.* **2006**, *197*, 1-45. (b) Zhao, B.; Brittain, W. J. *Prog. Polym. Sci.* **2000**, *25*, 677-710.

6. (a) Li, D. J.; Sheng, X.; Zhao, B. *J. Am. Chem. Soc.* **2005**, *127*, 6248-6256. (b) Li, D. J.; Jones, G. L.; Dunlap, J. R.; Hua, F. J.; Zhao, B. *Langmuir* **2006**, *22*, 3344-3351. (c) Li, D. J.; Dunlap, J. R.; Zhao, B. *Langmuir* **2008**, *24*, 5911-5918.

7. Han, S.; Hagiwara, M.; Ishizone, T. *Macromolecules* **2003**, *36*, 8312-8319.

8. (a) Mathias, L. J.; Cei, G. *Macromolecules* **1987**, *20*, 2645-2650. (b) Fife, W. K.; Rubinsztajn, S.; Zeldin, M. *J. Am. Chem. Soc.* **1991**, *113*, 8535-8537. (c) Wang, G.-J.; Ye, D.; Fife, W. K. *J. Am. Chem. Soc.* **1996**, *118*, 12536-12540. (d)Wang, G.-J.; Fife, W. K. *J. Am. Chem. Soc.* **1998**, *120*, 883-887.

9. Matyjaszewski, K.; Miller, P. J.; Shukla, N.; Immaraporn, B.; Gelman, A.; Luokala, B. B.; Siclovan, T. M.; Kickelbick, G.; Vallant, T.; Hoffmann, H.; Pakula, T. *Macromolecules* **1999**, *32*, 8716-8724.

10. Miller, P. J.; Matyjaszewski, K. *Macromolecules* **1999**, *32*, 8760-8767.

11. Ramakrishnan, A.; Dhamodharan, R.; Rühe, J. *Macromol. Rapid Commun.* **2002**, *23*, 612-616.

12. Okhapkin, I. M.; Bronstein, L. M.; Makhaeva, E. E.; Matveeva, V. G.; Sulman, E. M.; Sulman, M. G.; Khokhlov, A. R. *Macromolecules* **2004**, *37*, 7879-7883.

13. (a) Prucker, O.; Rühe, J. *Macromolecules* **1998**, *31*, 592-601. (b) Ejaz, M.; Yamamoto, S.; Ohno, K.; Tsujii, Y.; Fukuda, T. *Macromolecules* **1998**, *31*, 5934-5936. (c) Husseman, M.; Malmström, E. E.; McNamara, M.; Mate, M.; Mecerreyes, D.; Benoit, D. G.; Hedrick, J. L.; Mansky, P.; Huang, E.; Russell, T. P.; Hawker, C. J. *Macromolecules* **1999**, *32*, 1424-1431. (d) von Werne, T.; Patten, T. E. *J. Am. Chem. Soc.* **1999***, 121*, 7409-7410. (e) Kim, J. B.; Bruening, M. L.; Baker, G. L. *J. Am. Chem. Soc.* **2000**, *122*, 7616-7617. (f) Bartholome, C.; Beyou, E.; Bourgeat-Lami, E.; Chaumont, P.; Zydowicz, N. *Macromolecules* **2003**, *36*, 7946-7952. (g) Skaff, H.; Emrick, T. *Angew. Chem. Int. Ed.* **2004**, *43*, 5383-5386. (h) Ohno, K.; Morinaga, T.; Koh, K.; Tsujii, Y.; Fukuda, T. *Macromolecules* **2005**, *38*, 2137-2142. (i) Li, D. J.; Zhao, B. *Langmuir* **2007**, *23*, 2208-2217. (j) Jayachandran, K. N.; Takacs-Cox, A.; Brooks, D. E. *Macromolecules* **2002**, *35*, 4247-4257. (k) Tomlinson, M. R.; Efimenko, K.; Genzer, J. *Macromolecules* **2006**, *39*, 9049-9056. (l) Zhao, B.; Zhu, L. *J. Am. Chem. Soc.* **2006**, *128*, 4574-4575. (m) Wang, B. B.; Li, B.; Zhao, B.; Li, C. Y. *J. Am. Chem. Soc.* **2008**, *130*, 11594-11595. (n) Blomberg, S.; Ostberg, S.; Harth, E.; Bosman, A. W.; Van Horn, B.; Hawker, C. J. *J. Polym. Sci., Part A: Polym .Chem.* **2002**, *40*, 1309-1320. (o) Jhaveri, S. B.; Koylu, D.; Maschke, D.; Carter, K. R. *J. Polym. Sci. , Part A: Polym. Chem.* **2007**, *45*, 1575-1584. (p) Czaun, M.; Rahman, M. M.; Takafuji, M.; Ihara, H. *J. Polym. Sci., Part A: Polym. Chem.* **2008**, *46*, 6664-6671. (q) Cheng, Z. P.; Zheng, L. F.; Zhu, X. L.; Kang, E. T.; Neoh, K. G. *J. Polym. Sci.,*

Part A: Polym. Chem. **2008**, *46*, 2119-2131. (r) Yoshikawa, C.; Goto, A.; Tsujii, Y.; Ishizuka, N.; Nakanishi, K.; Fukuda, T. *J. Polym. Sci., Part A: Polym. Chem.* **2008**, *45*, 4795-4803.

14. (a) Aoshima, S.; Sugihara, S. *J. Polym. Sci., Part A: Polym. Chem.* **2000**, *38*, 3962-3965. (b) Zhao, B.; Li, D. J.; Hua, F. J.; Green, D. R. *Macromolecules* **2005**, *38*, 9509-9517. (c) Hua, F. J.; Jiang, X.G.; Li, D. J.; Zhao, B. *J. Polym. Sci., Part A: Polym. Chem.* **2006**, *44*, 2454-2467. (d) Hua, F. J.; Jiang, X. G.; Zhao, B. *Macromolecules* **2006,** *39*, 3476-3479. (e) Jiang, X. G.; Zhao, B. *J. Polym. Sci., Part A: Polym. Chem.* **2007**, *45*, 3707-3721. (f) Lutz, J. F.; Weichenhan, K.; Akdemir, O.; Hoth, A. *Macromolecules* **2007**, *40*, 2503-2508. (g) Wang, N.; Dong, A.; Radosz, M.; Shen, Y. Q. *J. Biomed. Mater. Res. Part A.* **2008**, *84A*, 148-157. (h) Anthimanikandan, S. V.; Thayumanavan, S. *J. Am. Chem. Soc.* **2005**, *127*, 14922-14929. (i) Jiang, X. G.; Lavender, C. A.; Woodcock, J. W.; Zhao, B. *Macromolecules* **2008**, *41*, 2632-2643. (j) Jiang, X. G.; Zhao, B. *Macromolecules* **2008**, *41*, 9366-9375.

15. Urry, D. W. *J. Phys. Chem. B* **1997,** *101*, 11007-11028.

16. This is different from the behavior of PTEGMMA brush-grafted particles in deionized water at a similar concentration where the hairy particles did not aggregate but shrank during the LCST transition. In a control experiment with PTEGMMA brush-grafted particles in the pH 7.52 and 7.82 buffers, we also observed the aggregation of hairy particles when the temperature was above the LCST, which is likely due to the salt effect in the aqueous buffer solutions.

17. (a) Lu, Y.; Mei, Y.; Drechsler, M.; Ballauff, M. *Angew. Chem. Int. Ed.* **2006**, *45*,

813-816; (b) Ballauff, M.; Lu, Y. *Polymer* **2007**, *48*, 1815-1823; (c) Lu, Y.; Mei, Y.; Ballauff, M.; Drechsler, M. *J. Phys. Chem. B* **2006**, *110*, 3930-3937.

Chapter 3. Evolution of Phase Morphology of Mixed Poly(*t*-butyl acrylate)/Polystyrene Brushes Grafted on Silica Particles with the Change of Chain Length Disparity

Abstract

This chapter presents the synthesis of a series of mixed poly(*t*-butyl acrylate) (P*t*BA)/polystyrene (PS) brushes with P*t*BA number average molecular weight (M_n) fixed at 24.5 kDa and PS M_n ranging from 14.8 to 30.4 kDa on 160 nm silica particles and the study of their microphase separation behavior using differential scanning calorimetry (DSC) and transmission electron microscopy (TEM). The samples were synthesized by a two-step "grafting from" process from asymmetric difunctional initiator- (Y-initiator-) functionalized silica particles using two different "living"/controlled radical polymerization techniques. P*t*BA brushes were grown first from Y-initiator-functionalized particles by surface-initiated atom transfer radical polymerization of *t*-butyl acrylate at 75 °C in the presence of a free initiator, followed by nitroxide-mediated radical polymerization (NMRP) of styrene at 120 °C. The "living" nature of NMRP allowed the synthesis of mixed P*t*BA/PS brushes with different PS molecular weights (14.8, 18.7, 24.9, and 30.4 kDa, respectively) in a one-pot polymerization. DSC studies showed that all thermally annealed mixed brush samples exhibited two glass transitions with the middle points located at ~ 47 and ~ 90 °C, respectively, suggesting that the two tethered polymers microphase separated in the brush layer. For TEM studies, the samples were dispersed in $CHCl_3$, a good solvent for both P*t*BA and PS, drop cast onto carbon films, thermally annealed in vacuum at 120 °C for 3 h, and then stained with RuO_4 vapor. All samples showed clear microphase separation, consistent with the DSC results. With increasing PS M_n from 14.8, to 18.7, and 24.9 kDa, the morphology of mixed brushes evolved from isolated, nearly spherical PS microdomains buried inside the P*t*BA matrix, to short PS cylindrical microdomains in the P*t*BA matrix,

and to nearly bicontinuous nanostructures. Further increasing the molecular weight of PS to 30.4 kDa resulted in the formation of isolated P*t*BA microdomains which were covered by PS chains.

3.1 Introduction

Binary mixed homopolymer brushes are composed of two chemically distinct homopolymers randomly or alternately immobilized by one end via a covalent bond on the surface of a solid substrate.[1-3] These brushes represent a new, intriguing class of environmentally responsive materials. The two grafted polymers, which are not necessarily stimuli-sensitive, can undergo spontaneous chain reorganization in response to environmental variations and exhibit different nanostructures and surface properties.[1-3] This response mechanism is different from those of traditional stimuli-sensitive, e.g., thermosensitive, polymer brushes where individual polymer chains exhibit different chain structures and properties upon application of an external stimulus.[4] Certainly, the use of stimuli-responsive polymers would further enrich the self-assembly behaviors and responsive properties of mixed brushes.[5]

The phase morphologies and responsive properties of mixed homopolymer brushes have been intensively investigated in the past two decades.[1-3,5-14] Theoretically, Marko and Witten studied whether symmetric mixed brushes on a flat substrate microphase separated laterally or vertically under equilibrium melt conditions and predicted that the lateral phase separation preempted the vertical phase separation, yielding a "rippled" nanostructure instead of a "layered" structure.[1a] The periodicity of the ripple pattern was predicted to be 1.97 times the chain root-mean-square end-to-end distance ($<R_{rms}>$). They also pointed out that by altering the compositions and molecular weights of mixed brushes, first order transitions between different ordered states could be achieved. The lateral phase separation of symmetric mixed brushes under melt or near-melt conditions and in nonselective

solvents was also revealed by other researchers in theoretical or simulation studies.[1c,d,2,6,7] In selective solvents, surface-tethered micellar structures with the solvophobic polymer packing into a core and the solvophilic chains forming the corona were predicted.[2d] By tuning parameters, including chain lengths, grafting densities, chemical compositions, solvent quality, and temperature, a variety of surface nanostructures could be formed by mixed brushes.[1-3,6-8] Moreover, different structures formed from the same brushes are fully reversible because of the covalent grafting of polymer chains to the substrate.

Experimentally, many methods have been developed to prepare mixed brushes.[5,9-14] Sidorenko et al. reported the synthesis of first mixed brushes by a two-step surface-initiated conventional free radical polymerization process and demonstrated the switching properties of mixed brushes by treating them with selective solvents.[9] Besides the two-step conventional free radical polymerization,[10] "grafting to" and other "grafting from" methods were also developed.[11-14] For example, Minko et al. reported a "grafting to" method, in which carboxyl-terminated polystyrene (PS) and poly(2-vinylpyridine) were grafted sequentially onto silicon wafers that were functionalized with 3-glycidoxypropyl-trimethoxysilane.[11a] Wang et al. prepared mixed PS/poly(methyl methacrylate) brushes on silicon wafers by grafting ABC triblock copolymers with a short central B block that can form covalent bonds with silicon wafers in a one-step reaction.[11f] Our group reported a "grafting from" method for the synthesis of mixed brushes with controlled molecular weights, narrow polydispersities, and high grafting densities by using two different "living"/controlled radical polymerization techniques,[12a,b] atom transfer radical polymerization (ATRP) and nitroxide-mediated radical polymerization (NMRP), from

asymmetric difunctional initiator- (Y-initiator-) functionalized silica surfaces.[12c-f] The responsive properties of mixed brushes upon environmental variations, including solvent changes and heating, have been intensively investigated and well documented in the literature.[9-14]

Of particular interest to the present work are asymmetric mixed homopolymer brushes in which the chain lengths or grafting densities of two polymers or both are different.[2a,6,7] Here we focus on asymmetric mixed brushes that are composed of two distinct homopolymers with different molecular weights but similar grafting densities. The effect of chain length disparity on phase morphology of mixed brushes in solvents has been theoretically studied.[6,7] Using computer simulations, Roan investigated the microphase separation of immiscible mixed brushes grafted on spherical nanoparticles with a radius comparable to the polymer size $<R_{rms}>$.[6] By varying chain lengths, grafting densities, and grafting patterns, a variety of well-ordered nanostructures can form. For example, the equilibrium nanostructure changes from rippled, to 12-islanded, and then layered with the increase of chain length disparity when the grafting densities of two polymers are identical. Wang and Müller recently used single-chain-in-mean-field simulations to study the phase behavior of asymmetric mixed brushes on flat substrates.[7] At a large chain length asymmetry, two layers can be distinguished in a solvent that is marginally good for both polymers with a slight preference for one polymer: a laterally structured bottom layer and a top layer that contains only the longer polymer species.

Asymmetric mixed brushes on planar substrates have been experimentally studied.[12d,14] Minko et al. prepared a series of asymmetric mixed brushes by a "grafting to" method and

investigated them by AFM and contact angle measurements.[14] They found that for small chain length asymmetry, the brushes exhibited lateral and perpendicular segregation, depending on the solvent quality. Upon increasing the molecular weight asymmetry, a transition from a "rippled" to a layered (sandwich-like) structure occurred. Using Y-initiator-functionalized silicon wafers, Our group previously synthesized mixed brushes with various chain length asymmetries and studied their responsive properties upon exposure to different solvents by AFM, XPS, and contact angle measurements.[12d] Although interesting results have been obtained from these studies, the phase morphologies of asymmetric mixed brushes have not been directly visualized.

Transmission electron microscopy (TEM) has been proven to be a powerful means for the study of phase morphologies of block copolymers in bulk and in solutions.[15] However, the use of silicon wafers as substrates for mixed brushes makes TEM studies difficult because microtoming of silicon wafers for the preparation of TEM samples is very challenging. Quite differently, silica particles can be directly used or microtomed into thin sections for visualization by TEM. Our group synthesized Y-initiator-functionalized silica particles and grew mixed poly(*t*-butyl acrylate) (P*t*BA)/PS brushes by sequential ATRP of *t*BA and NMRP of styrene.[12f] TEM studies showed that symmetric P*t*BA/PS brushes with P*t*BA M_n of 24.2 kDa and PS M_n of 23.0 kDa underwent lateral microphase separation in the melt and in nonselective solvents.[16,17] The feature sizes were on the order of $<R_{rms}>$ values of polymers in an unperturbed state (~10 nm). In this work, we synthesized a series of asymmetric mixed P*t*BA/PS brushes from 160 nm Y-initiator-functionalized silica particles by sequential ATRP and NMRP, and studied their microphase separation

behaviors in the melt after thermal annealing using differential scanning calorimetry (DSC) and TEM. P*t*BA brushes were grown first from Y-initiator particles by surface-initiated ATRP, followed by NMRP of styrene. By taking advantage of the "living" nature of NMRP,[18] mixed brushes with PS M_n smaller than, comparable to, and higher than that of P*t*BA were prepared in a one-pot reaction (Scheme 3.1). We note here that Motornov et al. reported the preparation of amphiphilic mixed brush-grafted particles by using a quaternization reaction between 11-bromoundodecyltrimethoxysilane-functionalized silica particles and the pyridine groups in a triblock copolymer PS-*b*-poly(2-vinyl pyridine)-*b*-poly(ethylene oxide) and the responsive properties of their particles.[19]

3.2 Experimental Section

3.2.1 Materials

Styrene (99%, Aldrich) and *tert*-butyl acrylate (*t*-BA, 99%, Aldrich) were dried with CaH_2, distilled under a reduced pressure, and stored in a refrigerator prior to use. CuBr (98%, Aldrich) was purified according to the procedure described in the literature[20] and stored in a desiccator. *N*, *N*, *N′*, *N′*, *N″*-pentamethyldiethylenetriamine (PMDETA, 99 %, Aldrich) was dried with calcium hydride, distilled under a reduced pressure, and stored in a desiccator. Tetrahydrofuran (THF) was distilled from sodium and benzophenone and used immediately. Tetraethoxysilane (98%) and ammonium hydroxide (25% in water) were purchased from Arcos and used as received. Chlorodimethylsilane (98%) was purchased from Aldrich and used as received. Platinum-divinyltetramethyldisiloxane complex in xylene (2.1~2.4% Pt concentration in xylene) was obtained from Gelest, Inc. and used as received. 2-[4-(But-3-enyl)phenyl]-2-(2',2',6',6'-tetramethyl-1'-piperidinyloxy)ethyl

Scheme 3.1. Schematic Illustration for the Synthesis of Mixed P*t*BA/PS Brushes with a Fixed P*t*BA M_n and Various PS Molecular Weights by Sequential Atom Transfer Radical Polymerization (ATRP) and Nitroxide-Mediated Radical Polymerization (NMRP) from Y-Initiator-Functionalized Silica Particles.

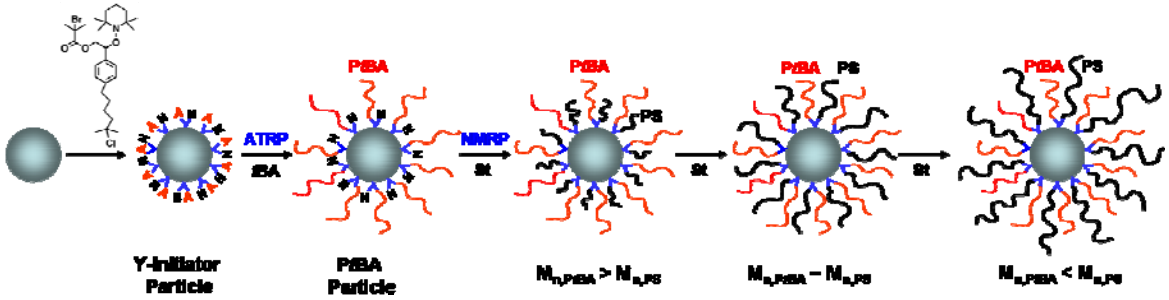

2-bromo-2-methylpropanoate (Y-initiator) was synthesized according to the procedure described in a previous publication from our group.[12f] All other chemical reagents were purchased from either Aldrich or Fisher and used without further purification.

3.2.2 Characterization. Size exclusion chromatography (SEC) was carried out at ambient temperature using PL-GPC 20 (an integrated GPC system from Polymer Laboratories, Inc.) with a refractive index detector, one PLgel 5 μm guard column (50 × 7.5 mm), and two PLgel 5 μm mixed-C columns (each 300 × 7.5 mm, linear range of molecular weight from 200 to 2,000,000 according to Polymer Laboratories, Inc.). The data were processed using Cirrus^{TM} GPC/SEC software (Polymer Laboratories). THF was used as the carrier solvent at a flow rate of 1.0 mL/min. Polystyrene standards (Polymer Laboratories) were used for calibration. The ^{1}H and ^{13}C NMR spectra were recorded on a Varian Mercury 300 MHz NMR spectrometer and the residual solvent proton peak was used as the internal standard. Thermogravimetric analysis (TGA) was performed in air at a heating rate of 20 °C/min from room temperature to 800 °C using TA Q-series Q50. The hairy particle samples for TGA were dried at 50 °C in vacuum for at least 5 h.

3.2.3 Synthesis of 1-Phenyl-1-(2',2',6',6'-tetramethyl-1'-piperidinyloxy)ethane (STEMPO). STEMPO, an initiator for nitroxide-mediated radical polymerization, was synthesized according to the procedure described in the literature.[21] ^{1}H NMR (300 MHz, $CDCl_3$) δ(ppm): 0.63 (s, C*H*$_3$, 3H), 1.00 (s, C*H*$_3$, 3H), 1.14 (s, CH_3, 3H), 1.27 (s, CH_3, 3H), 1.30–1.56 (m, 9H, C*H*$_2$ and CHC*H*$_3$), 4.75 (q, 1H, C*H*CH_3), and 7.20–7.30 (m, 5H, Ar*H*); ^{13}C NMR ($CDCl_3$) δ(ppm): 17.20, 20.32, 23.63, 34.10, 40.30, 83.11, 126.58, 126.75, 127.99, and 145.84.

3.2.4 Synthesis of Bare Silica Particles. Ammonium hydroxide (25% in water, 13.860 g) and tetraethoxysilane (TEOS, 6.964 g) were dissolved separately in ethanol (each 5 mL). The solutions were added into a 500 mL flask that contained 190 mL of ethanol under stirring. The concentrations of NH_3, TEOS, and water in the solution were 0.44 M, 0.15 M, 3.03 M, respectively. The mixture was stirred vigorously at room temperature for 6 h. The particles were isolated by centrifugation (Eppendorf 5804 Centrifuge, 6000 rpm), redispersed in ethanol, and centrifugated again. This washing process was repeated with ethanol one more time, water four times, and ethanol again. Particles were then dried with a stream of air flow (2.261 g). The average size of particles was 160 nm, determined by TEM image analysis.

3.2.5 Synthesis of Y-Initiator-Functionalized Silica Particles. 2-[4-(But-3-enyl)phenyl]-2-(2',2',6',6'-tetramethyl-1'-piperidinyloxy)ethyl 2-bromo-2-methylpropanoate (Y-initiator, 0.261 g, 0.545 mmol) was added into a 25 mL two-necked flask and dried at room temperature in vacuum for 30 min. Chlorodimethylsilane (2.0 mL, 18.4 mmol) was injected via a disposable syringe into the flask under N_2 atmosphere, followed by addition of Pt complex in xylene (15 μL). The mixture was stirred under nitrogen atmosphere at room temperature and the hydrosilylation reaction was monitored by ^{1}H NMR spectroscopy analysis. Once the reaction was complete, excess chlorodimethylsilane was removed by vacuum and the product (Y-silane) was used directly in the next step for the preparation of Y-initiator-functionalized silica particles.

Silica particles (1.081 g) were dried at 110 °C in vacuum (~ 30 millitorr) for 6-7 h, and were dispersed in dry THF (10 mL). A solution of Y-silane freshly synthesized from 0.261

g of Y initiator in dry THF (2 mL) was injected into the dispersion via a syringe. The mixture was stirred at 70 °C under N_2 atmosphere for 49 h. The particles were then isolated by centrifugation, re-dispersed in THF, and centrifugated again. This washing process was repeated four times, followed by drying with a stream of air flow to yield dry particles (0.853 g).

3.2.6 Synthesis of Poly(*t*-butyl acrylate) (P*t*BA) Brush-Grafted Silica Particles. Y-initiator-functionalized silica particles (Y-initiator particles, 0.406 g) and anisole (9.888 g) were added into a 50 mL two-necked flask. The mixture was ultrasonicated in an ultrasonic water bath to form a stable dispersion. CuBr (53.9 mg, 0.374 mmol), *tert*-butyl acrylate (*t*BA, 19.37 g, 151.3 mmol), *N*, *N*, *N*′, *N*′, *N*″-pentamethyldiethylenetriamine (PMDETA, 65.9 mg, 0.380 mmol), and ethyl 2-bromoisobutyrate (EBiB, 48.6 mg, 0.249 mmol) were added into a separate 100 mL three-necked flask and stirred under N_2 atmosphere. The particle dispersion was then transferred into the three-necked flask via a syringe and the reaction mixture was degassed by three freeze-pump-thaw cycles. The flask was placed in an oil bath with a preset temperature of 75 °C and the polymerization was monitored by SEC and ^{1}H NMR spectroscopy analysis. After the reaction proceeded for 38 h, the flask was removed from the oil bath and opened to air. THF (20 mL) was added into the flask to dilute the mixture. The particles were separated by centrifugation and the supernatant was passed through a column of neutral, activated aluminum oxide to remove the copper catalyst. The particles were re-dispersed in THF, allowed to stand at ambient conditions for 2 h (the green precipitate was removed), and centrifugated again. This washing process was repeated with THF one more time and chloroform three times,

followed by drying the particles with a stream of air flow, yielding P*t*BA brush-grafted silica particles (0.405 g). The $M_{n,SEC}$ and polydispersity index (PDI) of the free P*t*BA formed from the free initiator in the polymerization were 24.5 kDa and 1.11, respectively, determined from SEC analysis using polystyrene calibration.

3.2.7 Synthesis of Mixed P*t*BA/PS Brush-Grafted Silica Particles. The P*t*BA brush-grafted silica particles (0.342 g) were dispersed in anisole (18.218 g) in a 50 mL two-necked flask using an ultrasonic water bath. The particle dispersion was then transferred into a 100 mL three-necked flask that contained free NMRP initiator STEMPO (65.4 mg, 0.251 mmol), followed by the addition of styrene (26.016 g, 250.2 mmol). The mixture was degassed by three freeze-pump-thaw cycles. The flask was then placed in a 120 °C oil bath and the polymerization was monitored by ^{1}H NMR spectroscopy and SEC analysis. Samples were taken from the reaction mixture using a degassed syringe when the molecular weight of the free polystyrene formed from the free initiator reached desired values. The samples were diluted with THF. The particles were separated from the free polymer by centrifugation, re-dispersed in THF, and centrifugated again. For each sample, this washing process was repeated four times to remove the physically adsorbed polymer. The particles were then dried with a stream of air flow.

3.2.8 Differential Scanning Calorimetry (DSC) Study of P*t*BA Brush- and Mixed P*t*BA/PS Brush-Grafted Silica Particles. DSC analysis of polymer brush-grafted particles was conducted on a TA Q-1000 DSC instrument that was calibrated with the sapphire standard. The hairy particles were thermally annealed at 120 °C in vacuum for 3 h and then cooled to room temperature. For each sample, approximately 10 ~ 15 mg of particles was

used in the analysis. The heating and cooling rates were 10 °C/min; the second heating thermogram was used to determine the glass transitions.

3.2.9 Transmission Electron Microscopy (TEM) Study. Chloroform, a good solvent for both P*t*BA and PS, was used to prepare the particle dispersions. For each sample, about 1 mg of particles was dispersed in 2 mL of chloroform in a vial by ultrasonication for 5 min. A drop of the particle dispersion was cast onto a carbon-coated mica and allowed to dry at ambient temperature. The sample-loaded carbon films on mica were floated onto the surface of double-distilled water in a crystallization dish, and picked up with 400-mesh copper grids. The samples were thermally annealed in vacuum at 120 °C for 3 h and then stained with RuO_4 vapor at room temperature for 30 min. TEM experiments were performed on a JEOL 1200EX at an accelerating voltage of 80 kV. The images were analyzed using the Image Processing Tool Kit 2.5 software (Reindeer, Inc.).

3.3 Results and Discussion

3.3.1 Synthesis of Mixed P*t*BA/PS Brushes on Silica Particles with a Fixed P*t*BA M_n and Various PS Molecular Weights. The Y-initiator-functionalized silica particles were prepared via a procedure that was reported before from our laboratory using the Y-initiator-terminated monochlorosilane (Y-silane) and 160 nm bare silica particles.[12f] The bare silica particles were synthesized by the Stöber process, which involves the hydrolysis and condensation of tetraethoxysilane in an ammonia/ethanol solution and is known to produce silica particles with a relatively uniform size distribution.[22] Thermogravimetric analysis (TGA) showed that the weight loss of Y-initiator particles relative to bare silica particles was comparable to our previous result if the difference at 100 °C between the two

curves was taken into consideration (Figure 3.1).[12f]

The Y-initiator particles were then used for preparing mixed P*t*BA/PS brush samples. The surface-initiated ATRP of *t*-butyl acrylate from Y-initiator particles was carried out in anisole at 75 °C using CuBr/PMDETA as catalyst in the presence of a free initiator, ethyl 2-bromoisobutyrate (EBiB). Our group confirmed before that the TEMPO group in the Y-initiator was stable under this ATRP condition.[12] The addition of a free initiator to the polymerization mixture not only made it possible to control the surface-initiated polymerization by the solution polymerization, but also allowed us to conveniently monitor the polymerization by ^{1}H NMR spectroscopy and SEC analysis.

We found that the $M_{n,SEC}$ of free P*t*BA were 14.1 kDa and 1.13, respectively, at polymerization time of 16 h, 19.6 kDa and 1.10, respectively, at 24 h, and 24.5 kDa and 1.11, respectively, at 38 h, indicating that the reaction was a controlled process. The polymerization was stopped at the monomer conversion of 31.4 %, which corresponded to a degree of polymerization (DP) of P*t*BA of 191. The P*t*BA brush-grafted particles were isolated by centrifugation and repeatedly washed with THF and $CHCl_3$ to remove the physically adsorbed free polymer. The $M_{n,SEC}$ and PDI of the free P*t*BA formed from the free initiator EBiB were 24.5 kDa and 1.11, respectively, determined by SEC using polystyrene standards. TGA showed that the weight retention of P*t*BA brush-grafted silica particles at 800 °C was 69.5 %. It has been confirmed that the molecular weight and molecular weight distribution of polymer brushes synthesized by "living"/controlled radical polymerization were essentially identical to those of the free polymer formed from the free initiator.[12f,23] By using the average size of bare silica particles, TGA data, and the DP of

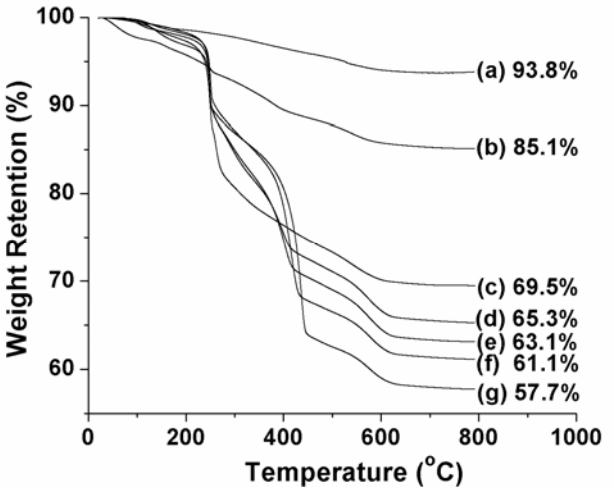

Figure 3.1. Thermogravimetric analysis (TGA) of (a) bare particles, (b) Y-initiator particles, (c) P*t*BA brush-grafted particles, (d) mixed brush-grafted particles with P*t*BA $M_{n,SEC}$ of 24.5 kDa and PS M_n of 14.8 kDa (particle-**1**), (e) mixed brush-grafted particles with P*t*BA $M_{n,SEC}$ of 24.5 kDa and PS M_n of 18.7 kDa (particle-**2**), (f) mixed brush-grafted particles with P*t*BA $M_{n,SEC}$ of 24.5 kDa and PS M_n of 24.9 kDa (particle-**3**), and (g) mixed brush-grafted particles with P*t*BA $M_{n,SEC}$ of 24.5 kDa and PS M_n of 30.4 kDa (particle-**4**). TGA was performed in air at a heating rate of 20 ºC/min from room temperature to 800 ºC.

free P*t*BA, and assuming that the density of silica particles was identical to bulk SiO_2 (2.07 g/cm^3), the grafting density of P*t*BA brushes on silica particles was calculated to be 2.8 nm^2/chain or 0.36 chains/nm^2. This value was very close to that of P*t*BA brushes on 180 nm silica particles reported in reference 12f.

Mixed P*t*BA/PS brush-grafted particles were obtained after the surface-initiated NMRP of styrene from the P*t*BA brush-grafted particles. Again, a free initiator, 1-phenyl-1-(2',2',6',6'-tetramethyl-1'-piperidinyloxy)ethane (STEMPO), was added into the reaction mixture. The polymerization was carried out at 120 °C and monitored by SEC. Four samples with different PS molecular weights were taken from the reaction mixture at different polymerization times. The hairy particles were isolated by centrifugation and repeatedly washed with THF. The free polymers were precipitated in methanol and analyzed by SEC. Note that the C-Br bond at the grafted P*t*BA chain end is relatively weak and might participate in the chain transfer process in the NMRP of styrene. Our group previously used tri(*n*-butyl)tin hydride to remove the bromine atom from the P*t*BA chain end,[12f] however it was difficult to completely remove the tin compound and any tin residue could interfere with the NMRP of styrene. In the synthesis of block copolymers from asymmetric difunctional initiators by combining ATRP and NMRP, Tunca et al. did not remove the bromine atom from the polymer chain end but used the polymer directly for the preparation of block copolymers by NMRP,[24] suggesting that the possible chain transfer to the P*t*BA chain end in the NMRP of styrene was negligible. In this work, we synthesized mixed P*t*BA/PS brushes by surface-initiated NMRP of styrene from P*t*BA brush-grafted particles without dehalogenation.

Figure 3.2 shows the SEC traces of four polymers taken at different polymerization times. The M_n of PS increased from 14.8 kDa (PS-**1**; the corresponding mixed P*t*BA/PS brush-grafted particle sample designated as particle-**1**), to 18.7 kDa (PS-**2**; the corresponding mixed P*t*BA/PS brush-grafted particle sample designated as particle-**2**), to 24.9 kDa (PS-**3**; the corresponding mixed P*t*BA/PS brush-grafted particle sample designated as particle-**3**), and 30.4 kDa (PS-**4**; the corresponding mixed P*t*BA/PS brush-grafted particle sample designated as particle-**4**), while the PDI remained narrow (< 1.25). From Figure 3.1, the weight retention of mixed brush-grafted particles at 800 °C decreased with the increase of PS M_n, from 65.3 % for particle-**1**, to 63.1 % for particle-**2**, to 61.1 % for particle-**3**, and 57.7 % for particle-**4**. If the residue (silica) at 800 °C is used as reference, the amount of the polymers grafted on silica particles can be calculated. Figure 3.3 shows the relative mass of the grafted polymers versus the molecular weight of PS; the amount of the grafted polymers increased with PS M_n in a nearly linear fashion, indicating that the polymerization was controlled.

Based on the size of bare silica particles, TGA data, and PS molecular weight, the grafting density of PS for each sample was calculated. The results are summarized in Table 3.1. The grafting densities of two polymers in these samples were reasonably close to each other. Calculations showed that the average distance between grafting sites in these mixed brushes was 1.2 – 1.3 nm, indicating that the polymers were densely grafted. To confirm that the tethered polymers were in the brush regime, we estimated the radii of gyration ($<R_g>$) of free polymers having the same molecular weights in their unperturbed states[25] and found that they were more than twice larger than the average distance between the

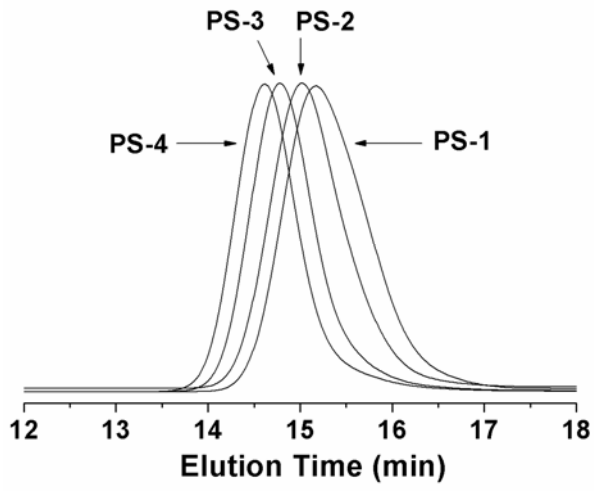

Figure 3.2. Size exclusion chromatography traces of four polymers formed from free initiator STEMPO at different polymerization times in the synthesis of mixed P*t*BA/PS brush-grafted silica particles by NMRP of styrene at 120 °C from P*t*BA brush-grafted particles.

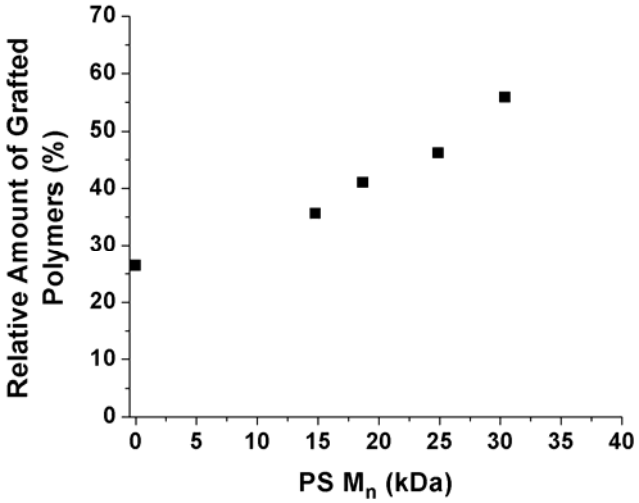

Figure 3.3. The amount of the grafted polymers relative to the silica residue calculated from TGA data versus polystyrene molecular weight.

Table 3.1. Molecular Characteristics of Mixed P*t*BA/PS Brushes with a fixed P*t*BA $M_{n,SEC}$ of 24.5 kDa and various PS molecular weights on 160 nm Silica Particles and the Corresponding Free Polymers [a]

Sample No.	PS M_n (Da), PDI, and DP [b]	σ_{PS} and σ_{total} (chains/nm^2) [c]	$\langle R_{rms} \rangle$ and $\langle R_g \rangle$ (nm) [d]
Particle-**1**	14800, 1.24, 142	0.21, 0.57	8.0, 3.3
Particle-**2**	18700, 1.20, 180	0.26, 0.62	9.0, 3.7
Particle-**3**	24900, 1.17, 239	0.27, 0.63	10.4, 4.2
Particle-**4**	30400, 1.14, 292	0.32, 0.68	11.5, 4.7

[a] The $M_{n,SEC}$ and PDI of P*t*BA were 24.5 kDa and 1.11, respectively, determined by SEC using PS calibration; the degree of polymerization (DP) of P*t*BA was 191, calculated by using the monomer conversion and the monomer-to-initiator ratio; the grafting density of P*t*BA (σ_{PtBA}) was 0.36 chains/nm^2, calculated by using the DP of P*t*BA, TGA data, and the average size of bare silica particles (160 nm).

[b] The M_ns and the values of polydispersity index (PDI) of polystyrenes were determined by SEC using PS standards; the DPs of polystyrenes were calculated from M_ns.

[c] The polystyrene grafting density (σ_{PS}) in each sample was calculated based on the size of bare particles (160 nm), DP of free polystyrene, and TGA data along with the assumptions that the particles were spherical and the silica particle density was 2.07 g/cm^3. The total grafting density $\sigma_{total} = \sigma_{PtBA} + \sigma_{PS}$.

[d] $\langle R_{rms} \rangle$ and $\langle R_g \rangle$ are root-mean-square end-to-end distance (nm) and radius of gyration (nm) of polymer chains in an unperturbed state, respectively. The values of $\langle R_{rms} \rangle$ were calculated by using $\langle R_{rms} \rangle = (C_\infty n l^2)^{1/2}$, where C_∞ is the Flory's characteristic ratio for an infinite chain, n the number of C-C bonds in the chain (n = 2DP), and l the bond length of C-C bond (1.54 Å).[25] The values of $\langle R_g \rangle$ were calculated by using $\langle R_g \rangle = (\langle R_{rms} \rangle^2/6)^{1/2}$. The value of C_∞ for P*t*BA was not available in the literature. We used the value of C_∞ of PS in the calculation of the $\langle R_{rms} \rangle$ value of P*t*BA. The calculated values of $\langle R_{rms} \rangle$ and $\langle R_g \rangle$ of P*t*BA with a DP of 191 in the unperturbed state were 9.3 and 3.8 nm, respectively.

(see Table 3.1). According to the results from Cheng et al.,[26] when the reduced tethering density, defined as $\sigma\pi R_g^2$ (where σ is the reciprocal of the cross-sectional area per chain and R_g is the radius of gyration of the free polymer), is greater than 14.3, the grafted polymer chains are in the highly stretched brush regime. If the reduced tethering density is between 3.7 and 14.3, the tethered chains are in the crossover zone between the polymer mushroom and highly stretched polymer brush regimes. Calculations show that the reduced total grafting densities of four mixed P*t*BA/PS brush samples were > 23 (the average of the $<R_g>$ values of the two polymers in each sample was used in the calculation), which further confirmed that the grafted polymers in these samples were in the highly stretched brush regime.

3.3.2 DSC Study of Mixed P*t*BA/PS Brush-Grafted Silica Particles with a Fixed P*t*BA M_n and Various PS Molecular Weights. It was previously observed that for microphase separated mixed P*t*BA/PS brushes on silica particles, two glass transitions appeared in the DSC thermogram, while miscible mixed brushes exhibited only one broad glass transition.[16] This observation evidences that DSC is a powerful means to determine whether the two grafted polymers in the brush layer microphase separate or not. Therefore, we performed DSC analysis of all four mixed brush-grafted particle samples. For comparison, P*t*BA brush-grafted particles were also studied. Prior to the analysis, the particles were thermally annealed at 120 °C in vacuum for 3 h and then cooled in vacuum to room temperature. The results from DSC studies are shown in Figure 3.4. The glass transition of P*t*BA homopolymer brushes on silica particles occurred at 45 °C (thermogram **1**), which was about 10 °C higher than the T_g of free P*t*BA with a similar molecular

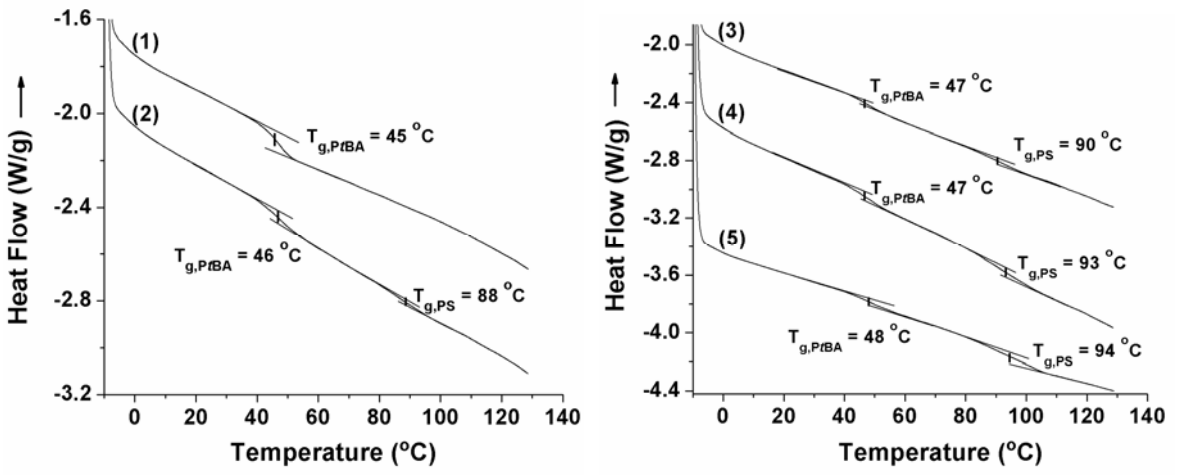

Figure 3.4. Differential scanning calorimetry (DSC) analysis of (1) P*t*BA brush-grafted silica particles (P*t*BA $M_{n,SEC}$ = 24.5 kDa), (2) particle-**1** (P*t*BA $M_{n,SEC}$ = 24.5 kDa and PS M_n = 14.8 kDa), (3) particle-**2** (P*t*BA $M_{n,SEC}$ = 24.5 kDa and PS M_n = 18.7 kDa), (4) particle-**3** (P*t*BA $M_{n,SEC}$ = 24.5 kDa and PS M_n = 24.9 kDa), and (5) particle-**4** (P*t*BA $M_{n,SEC}$ = 24.5 kDa and PS M_n = 30.4 kDa). The heating and cooling rates in the DSC analysis were 10 °C/min.

weight,[16] consistent with our previous observation. This is believed to be the result of surface tethering effect. Savin et al. also observed an increase in the T_g of homopolymer brushes grafted on silica nanoparticles compared with the corresponding free polymer.[27] All four mixed P*t*BA/PS brush-grafted particle samples exhibited two distinct glass transitions with the middle points being located at ~ 47 and ~ 90 °C (thermograms **2**, **3**, **4**, and **5**). These two transitions corresponded to the glass transitions of P*t*BA and PS, respectively, suggesting that the two grafted polymers phase separated into separate microdomains that consisted of nearly pure polymer species. Since one end of the polymer chains was fixed via a covalent bond on the surface of silica particles, the microphase separation was confined in the brush layer.

A closer examination of thermograms of mixed brush-grafted particles in Figure 3.4 revealed that with the increase of PS molecular weight, the magnitude and width of PS glass transition increased (using the P*t*BA glass transition as reference). In particular, the glass transition of PS in particle-**4** occurred over a temperature range of 20 °C (thermogram **5**), which could be due to the fact that the chain length of PS (DP = 292) was substantially longer than that of P*t*BA (DP = 191). As suggested by simulation studies,[7] it is very likely that the P*t*BA chains and the inner part of PS chains undergoes lateral microphase separation in the bottom layer, while the outer part of PS chains forms a thin layer that covers the microphase separated microdomains of PS and P*t*BA. The broad glass transition could be the result of different mobilities of PS segments in the two layers. Interestingly, with the increase of PS M_n from 14.8, to 18.7, to 24.9, and 30.4 kDa, the glass transition temperatures of both polymers shifted to slightly higher values. While the increase of P*t*BA

T_g was quite small (1 – 2 °C), the middle point of the PS T_g increased noticeably from 88, to 90, to 93, and 94 °C, which might be due to the molecular weight effect on T_g. It is known that the glass transition temperature is higher when the polymer molecular weight is higher before a plateau value is reached.[25] In summary, for all four mixed brush samples, two distinct glass transitions were observed from DSC analysis, implying that the two grafted polymers phase separated in the brush layer.

3.3.3 TEM Study of Mixed P*t*BA/PS Brushes on Silica Particles with P*t*BA $M_{n,SEC}$ of 24.5 kDa and PS M_n Varying from 14.8 to 30.4 kDa. To prepare samples for the TEM study, the mixed brush-grafted particles were dispersed in $CHCl_3$, a nonselective good solvent for both P*t*BA and PS, and drop cast onto carbon films. After the solvent was evaporated, the samples were thermally annealed at 120 °C in vacuum for 3 h and then stained with RuO_4 vapor at room temperature for 30 min. Figure 3.5 shows the typical top-view TEM micrographs of four mixed brush particle samples. Note that RuO_4 selectively stains PS chains, making PS and P*t*BA microdomains appear dark and bright, respectively. By quickly looking through the four TEM images, one can easily find out that the phase morphology of mixed P*t*BA/PS brushes grafted on silica particles changes with the molecular weight of PS. For particle-**1** in which the molecular weight of PS (14.8 kDa) was substantially smaller than that of P*t*BA (24.5 kDa), relatively short PS chains segregated into isolated, nearly spherical microdomains (Figure 3.5A). A distinctive feature of Figure 3.5A is that the silica particles were separated from each other by a bright gap that was filled with "invisible" (i.e., unstained) P*t*BA chains, though occasionally dark PS nanodomains were found to bridge neighboring particles. Thus, it was very likely that PS

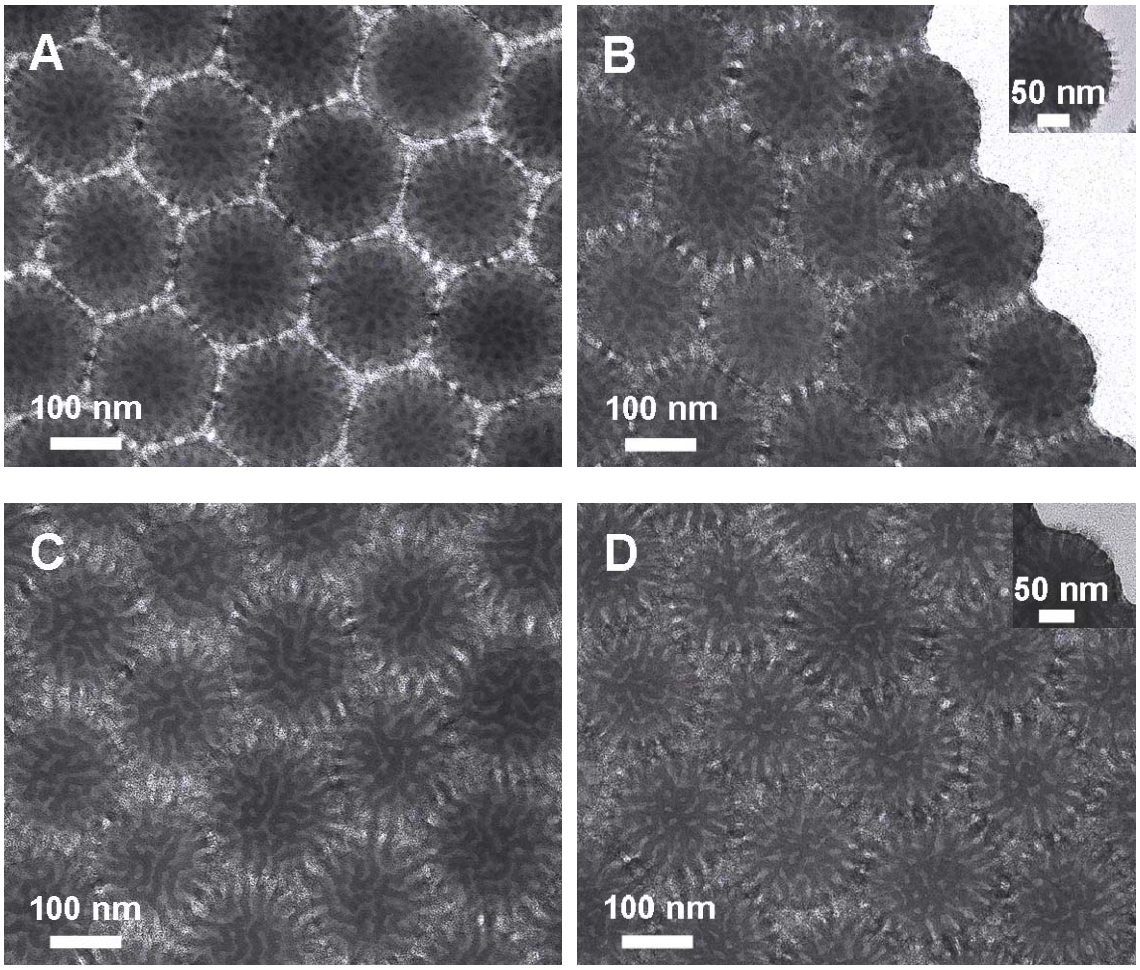

Figure 3.5. Top-view TEM micrographs of (A) particle-**1** (P*t*BA $M_{n,SEC}$ = 24.5 kDa, PS M_n = 14.8 kDa), (B) particle-**2** (P*t*BA $M_{n,SEC}$ = 24.5 kDa, PS M_n = 18.7 kDa), (C) particle-**3** (P*t*BA $M_{n,SEC}$ = 24.5 kDa, PS M_n = 24.9 kDa), and (D) particle-**4** (P*t*BA $M_{n,SEC}$ = 24.5 kDa, PS M_n = 30.4 kDa) after being cast from $CHCl_3$, a nonselective good solvent for both P*t*BA and PS, and thermally annealed at 120 °C in vacuum for 3 h. The samples were stained with RuO_4 vapor.

microdomains were buried inside the P*t*BA matrix (Scheme 3.2a).

The size of PS nanodomains was retrieved from TEM image analysis using Image Processing Tool Kit 2.5 software. We were aware that TEM only showed a two-dimensional projection image of mixed brush features on spherical SiO_2 particles. However, restoring the three-dimensional (3D) image from a 2D image was nontrivial, and we had to ignore the 3D effect on the actual feature sizes in our image analysis. To minimize errors, we purposely chose areas in the center of spherical particles for the analysis of feature size. The average equivalent diameter of PS microdomains in Figure 3.5A was 11.5 nm (Figure 3.6A). Note that the $<R_{rms}>$ of PS with a molecular weight of 14.8 kDa in the unperturbed state was 8.0 nm, reasonably comparable to the equivalent diameter. With the increase of PS molecular weight to 18.7 kDa, the isolated PS nanodomains began to merge into short cylinders but did not fully connect (Figure 3.5B), though the PS chain length (DP = 180) was quite close to that of P*t*BA (DP = 191).This is likely because the PS grafting density (0.26 chains/nm^2) is slightly lower than that of P*t*BA (0.36 chains/nm^2). A calculation shows that the volume ratio of P*t*BA to PS is 65 : 35;[28] an immiscible diblock copolymer with such a volume ratio for the two blocks is most likely to exhibit a cylindrical phase.[29] The grafted polymer chains spread out and covered the interstitials of particles. Moreover, some dark domains formed bridges among neighboring particles. From the edge of the hairy particle shown in the inset of Figure 3.5B, both dark and bright nanodomains appear to be present at the brush-vacuum interface. Note that the surface free energies of P*t*BA and PS are close to each other.[30,31] The average equivalent diameter and cylinder length of PS microdomains from the image analysis were 14.5 and

Scheme 3.2. Schematic Illustration of Phase Morphologies of Mixed P*t*BA/PS Brushes with a Fixed P*t*BA Molecular Weight and Varying PS Molecular Weight

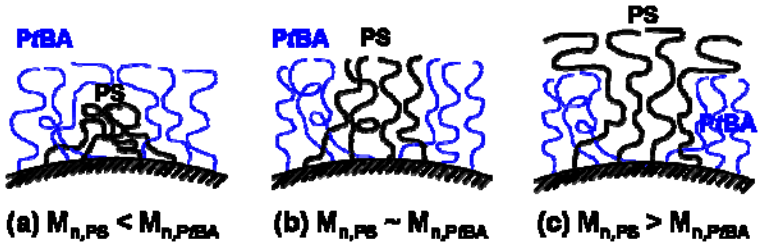

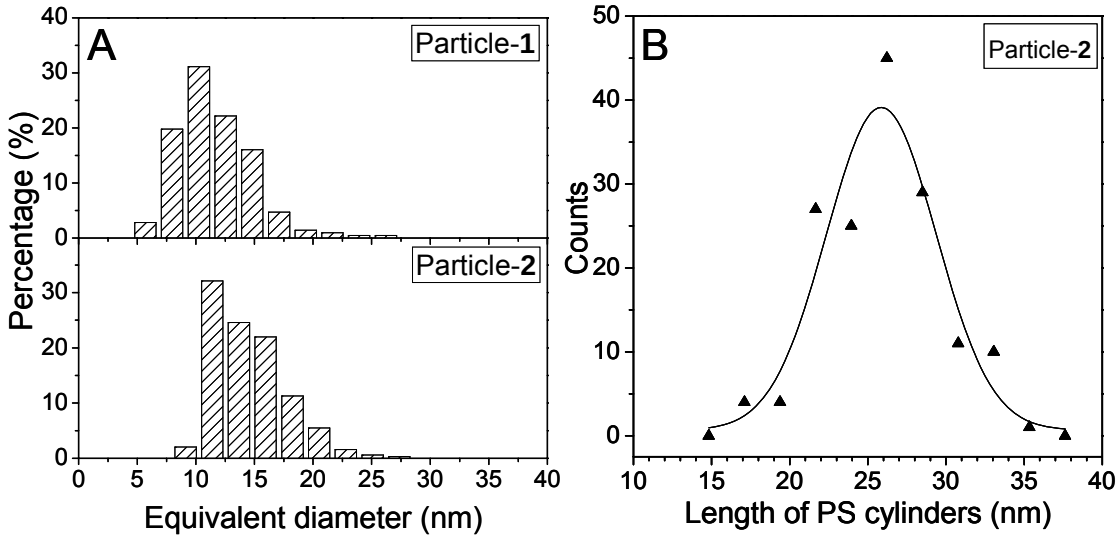

Figure 3.6. Equivalent diameter distributions (A) of polystyrene nanodomains in particle-**1** (P*t*BA $M_{n,SEC}$ = 24.5 kDa, PS M_n = 14.8 kDa) and -**2** (P*t*BA $M_{n,SEC}$ = 24.5 kDa, PS M_n = 18.7 kDa) and cylinder length distribution (B) of PS nanodomains from TEM image analysis. Gaussian function was used to fit the statistical data in order to guide eyes.

26.0 nm, respectively (Figure 3.6).

For particle-**3** in which the P*t*BA $M_{n,SEC}$ was 24.5 kDa and the PS M_n was 24.9 kDa (the grafting densities of P*t*BA and PS were 0.36 and 0.27 chains/nm^2, respectively), a nearly bicontinuous, random worm-like morphology was observed, which is the same as the phase separated nanostructure of mixed P*t*BA/PS brushes with P*t*BA $M_{n,SEC}$ of 24.2 kDa and PS M_n of 23.0 kDa on 180 nm silica particles that was reported before (Scheme 3.2b)[17] and is similar to the results obtained from computer simulations by Wang and Müller.[7] Again, the grafted polymer chains were highly stretched and spread out; the interstitials among silica particles were completely covered by the phase separated PS and P*t*BA chains. Some dark PS and bright P*t*BA stripes bridged among neighboring particles. From the image analysis, the widths of PS and P*t*BA stripes were 14.0 and 12.3 nm, respectively. The distributions of the widths of PS and P*t*BA microdomains are shown in Figure 3.7. Note that the values of $<R_{rms}>$ of the corresponding free PS and P*t*BA in the unperturbed states were 10.4 and 9.3 nm, respectively. Our results again corroborate the theoretical prediction that the ripple wavelength is about twice the $<R_{rms}>$ of polymers. It should be noted here that for this sample the DPs of P*t*BA and PS were not identical but 191 and 239, respectively. Computer simulation studies have shown that the bicontinuous "rippled" nanostructure can tolerate small chain length asymmetries.[6,7]

Figure 3.5D shows a typical micrograph of particle-**4** in which the P*t*BA $M_{n,SEC}$ (24.5 kDa) was lower than that of PS M_n (30.4 kDa) and the grafting densities of P*t*BA and PS were 0.36 and 0.32 chains/nm^2, respectively. Compared with the image in Figure 3.5C, a morphology transition can be seen; bridges that connected the dark PS stripes began to

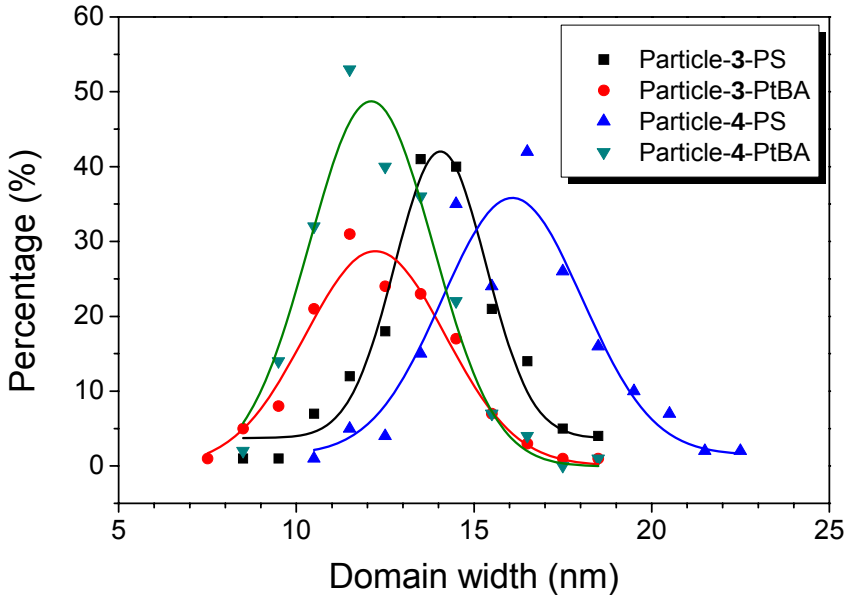

Figure 3.7. Width distributions of PS and P*t*BA microdomains in particle-**3** (P*t*BA $M_{n,SEC}$ = 24.5 kDa, PS M_n = 24.9 kDa) and particle-**4** (P*t*BA $M_{n,SEC}$ = 24.5 kDa, PS M_n = 30.4 kDa) from the TEM image analysis. Gaussian function was used to fit the statistical data in order to guide eyes.

form and more bright P*t*BA domains became isolated. Unlike the PS nanodomains in Figure 3.5A, the shape of the P*t*BA nanodomains here appeared to be more irregular. An examination of the interstitials among silica particles and the edge of the hairy particle (the inset in Figure 3.5D) suggested that the isolated P*t*BA nanodomains were buried in the continuous PS matrix (Scheme 3.2c), which can be explained by the fact that the grafting densities of P*t*BA and PS were very close to each other and the chain length of PS (DP = 292) was longer by 101 than that of P*t*BA (DP = 191). This observation is consistent with the prediction for asymmetric mixed brushes that at a large chain length asymmetry, a two-layered structure is formed in which the bottom layer is laterally microphase separated and covered by the longer polymer species that form the upper layer.[7] A quantitative analysis shows that the width of PS domains increased slightly from 14.0 nm in particle-**3** to 16.2 nm for particle-**4** (Figure 3.7), while the width of P*t*BA nanodomains remained the same, i.e., 12.3 nm. Thus, our TEM studies evidently showed that when the P*t*BA chain length was fixed, the phase morphology of mixed P*t*BA/PS brushes changed from the isolated PS nanodomains in the P*t*BA matrix at a relatively low DP of PS, to bicontinuous worm-like nanostructures at the PS chain length slightly higher but comparable to that of P*t*BA, and to a two-layer structure in which the bottom layer was laterally phase separated and covered by a thin PS layer at the PS M_n much higher than that of P*t*BA. Note that we cannot rule out the contribution of the slight difference in the grafting densities of two polymers in the first three samples, but the morphology evolution appears to be mainly governed by the chain length disparity.

3.4 Conclusions

We synthesized a series of mixed P*t*BA/PS brushes with a fixed P*t*BA $M_{n,SEC}$ of 24.5 kDa and the PS M_n varying from 14.8, to 18.7, to 24.9, and to 30.4 kDa on 160 nm Y-initiator-functionalized silica particles by combining ATRP and NMRP. Based on the TGA data, the size of silica particles, and the DPs of free polymers, the grafting densities of two polymers in these samples were calculated and found to be comparable to each other. Two distinct glass transitions, located at ~ 47 and ~ 90 °C, were observed from DSC analysis for all four mixed brush particle samples, suggesting that the two grafted polymers underwent microphase separation. TEM studies evidently showed that the phase morphology of mixed brushes on silica particles evolved from isolated PS nanodomains in the P*t*BA matrix, to bicontinuous, random worm-like nanostructures, and to a two-layer structure in which the bottom layer was laterally phase separated and covered by the longer polymer chains with the increase of PS molecular weight from below to above that of P*t*BA. This is the first time that the theoretically predicted morphology evolution of mixed brushes with the change of chain length disparity between two grafted polymers was directly observed from TEM. The results could open up new opportunities in the preparation of novel nanostructured hairy particles and the applications of mixed homopolymer brushes in technological uses.

References:

1. (a) Marko, J. F.; Witten, T. A. *Phys. Rev. Lett.* **1991,** *66*, 1541-1544. (b) Marko, J. F.; Witten, T. A. *Macromolecules* **1992,** *25*, 296-307. (c) Dong, H. *J. Phys. II Fr.* **1993,** *3*, 999-1020. (d) Brown, G.; Chakrabarti, A.; Marko, J. F. *Europhys. Lett.* **1994,** *25*, 239-244. (e) Luzinov, I.; Minko, S.; Tsukruk, V. V. *Prog. Polym. Sci.* **2004**, *29*, 635-698. (f) Luzinov, I.; Minko, S.; Tsukruk, V. V. *Soft Matter* **2008**, *4*, 714-725. (g) Zhao, B.; Brittain, W. J. *Prog. Polym. Sci.* **2000**, *25*, 677-710.
2. (a) Lai, P. Y. *J. Chem. Phys.* **1994,** *100*, 3351-3357. (b) Soga, K. G.; Zuckermann, M. J.; Guo, H. *Macromolecules* **1996,** *29*, 1998-2005. (c) Zhulina, E.; Balazs, A. C. *Macromolecules* **1996,** *29*, 2667-2673. (d) Singh, C.; Pickett, G. T.; Balazs, A. C. *Macromolecules* **1996,** *29*, 7559-7570. (e) Müller, M. *Phys. Rev. E* **2002,** *65*, 030802. (f) Minko, S.; Müller, M.; Usov, D.; Scholl, A.; Froeck, C.; Stamm, M. *Phys. Rev. Lett.* **2002,** *88*, 035502. (g) Wenning, L.; Müller, M.; Binder, K. *Europhys. Lett.* **2005**, *71*, 639-645.
3. Zhao, B.; Zhu, L. *Macromolecules* **2009**, *42*, 9369-9383.
4. (a) Zhu, M.-Q.; Wang, L.-Q.; Exarhos, G. J.; Li, A. D. Q. *J. Am. Chem. Soc.* **2004**, *126*, 2656-2657. (b) Li, D. J.; Jones, G. L.; Dunlap, J. R.; Hua, F. J.; Zhao, B. *Langmuir* **2006**, *22*, 3344-3351. (c) Li, D. J.; Zhao, B. *Langmuir* **2007**, *23*, 2208-2217. (d) Li, D. J.; Dunlap, J. R.; Zhao, B. *Langmuir* **2008**, *24*, 5911-5918. (e) Jiang, X. M.; Wang, B. B.; Li, C. Y.; Zhao, B. *J. Polym. Sci. Part A: Polym. Chem.*, **2009**, *47*, 2853-2870. (f) Wu, T.; Zou, G.; Hu, J.; Liu, S. *Chem. Mater.* **2009**, *21*, 3788-3798.
5. Boyer, C.; Whittaker, M. R.; Luzon, M.; Davis, T. P. *Macromolecules* **2009**, *42*,

6917-6926.

6. Roan, J.-R. *Phys. Rev. Lett.* **2006**, *96*, 248301.

7. Wang, J.; Müller, M. *J. Phys. Chem. B.* **2009**, *113*, 11384-11402.

8. Merlitz, H.; He, G. L.; Sommer, J. U.; Wu, C. X. *Macromolecules* **2009**, *42*, 445-451.

9. Sidorenko, A.; Minko, S.; Schenk-Meuser, K.; Duschner, H.; Stamm, M. *Langmuir* **1999,** *15*, 8349-8355.

10. (a) Minko, S.; Usov, D.; Goreshnik, E.; Stamm, M. *Macromol. Rapid Commun.* **2001,** *22*, 206-211. (b) Motornov, M.; Minko, S.; Eichhorn, K. J.; Nitschke, M.; Simon, F.; Stamm, M. *Langmuir* **2003,** *19*, 8077-8085. (c) Lemieux, M.; Usov, D.; Minko, S.; Stamm, M.; Shulha, H.; Tsukruk, V. V. *Macromolecules* **2003,** *36*, 7244-7255. (d) Usov, D.; Gruzdev, V.; Nitschke, M.; Stamm, M.; Hoy, O.; Luzinov, I.; Tokarev, I.; Minko, S. *Macromolecules* **2007**, *40*, 8774-8783. (e) Santer, S.; Kopyshev, A.; Yang, H. K.; Rühe, J. *Macromolecules* **2006,** *39*, 3056-3064.

11. (a) Minko, S.; Patil, S.; Datsyuk, V.; Simon, F.; Eichhorn, K. J.; Motornov, M.; Usov, D.; Tokarev, I.; Stamm, M. *Langmuir* **2002,** *18*, 289-296. (b) Minko, S.; Müller, M.; Motornov, M.; Nitschke, M.; Grundke, K.; Stamm, M. *J. Am. Chem. Soc.* **2003,** *125*, 3896-3900. (c) Ionov, L.; Minko, S.; Stamm, M.; Gohy, J. F.; Jerome, R.; Scholl, A. *J. Am. Chem. Soc.* **2003,** *125*, 8302-8306. (d) Ionov, L.; Sidorenko, A.; Stamm, M.; Minko, S.; Zdyrko, B.; Klep, V.; Luzinov, I. *Macromolecules* **2004**, *37*, 7421-7423. (e) LeMieux, M. C.; Julthongpiput, D.; Bergman, K. N.; Cuong, P. D.; Ahn, H. S.; Lin, Y. H.; Tsukruk, V. V. *Langmuir* **2004,** *20*, 10046-10054. (f) Wang, J.; Kara, S.; Long, T. E.; Ward, T. C. *J. Polym. Sci., Polym. Chem.* **2000**, *38*, 3742-3750. (g) Julthongpiput,

D.; Lin, Y. H.; Teng, J.; Zubarev, E. R.; Tsukruk, V. V. *Langmuir* **2003,** *19*, 7832-7836. (h) Tsujii, Y.; Ohno, K.; Yamamoto, S.; Goto, A.; Fukuda, T. *Adv. Polym. Sci.* **2006**, *197*, 1-45. (i) Ionov, L.; Houbenov, N.; Sidorenko, A.; Stamm, M.; Luzinov, I.; Minko, S. *Langmuir* **2004,** *20*, 9916-9919. (j) Ionov, L.; Sidorenko, A.; Stamm, M.; Minko, S.; Zdyrko, B.; Klep, V.; Luzinov, I. *Macromolecules* **2004**, *37*, 7421-7423. (k) Motornov, M.; Sheparovych, R.; Tokarev, I.; Roiter, Y.; Minko, S. *Langmuir* **2007**, *23*, 13-19. (l) Sheparovych, R.; Motornov, M.; Minko, S. *Langmuir* **2008**, *24*, 13828-13832. (m) Lin, Y. H.; Teng, J.; Zubarev, E. R.; Shulha, H.; Tsukruk, V. V. *Nano Lett.* **2005**, *5*, 491-495.

12. (a) Zhao, B. *Polymer* **2003,** *44*, 4079-4083. (b) Zhao, B. *Langmuir* **2004,** *20*, 11748-11755. (c) Zhao, B.; He, T. *Macromolecules* **2003,** *36*, 8599-8602. (d) Zhao, B.; Haasch, R. T.; MacLaren, S. *J. Am. Chem. Soc.* **2004,** *126*, 6124-6134. (e) Zhao, B.; Haasch, R. T.; MacLaren, S. *Polymer* **2004,** *45*, 7979-7988. (f) Li, D. J.; Sheng, X.; Zhao, B. *J. Am. Chem. Soc.***2005**, *127*, 6248−6256. (g) Santer, S.; Kopyshev, A.; Donges, J.; Rühe, J.; Jiang, X. G.; Zhao, B.; Müller, M. *Langmuir* **2007,** *23*, 279-285.
13. (a) Chiu, J. J.; Kim, B. J.; Kramer, E. J.; Pine, D. J. *J. Am. Chem. Soc.* **2005**, *127*, 5036-5037. (b) Shan, J.; Nuopponen, M.; Jiang, H.; Viitala, T.; Kauppinen, E.; Kontturi, K.; Tenhu, H. *Macromolecules* **2005**, *38*, 2918-2926. (c) Zubarev, E. R.; Xu, J.; Sayyad, A.; Gibson, J. D. *J. Am. Chem. Soc.* **2006**, *128*, 4958-4959. (d) Guo, Y.; Moffitt, M. G. *Macromolecules* **2007**, *40*, 5868-5878. (e) Cheng, J.; He, J.; Li, C.; Yang, Y. *Chem. Mater.* **2008**, *20*, 4224-4230.
14 Minko, S.; Luzinov, I.; Luchnikov, V.; Müller, M.; Patil, S.; Stamm, M.

Macromolecules **2003**, *36*,7268-7279.

15. Hamley, I. W. *The Physics of Block Copolymers*, Oxford University Press: Oxford, 1998.
16. Zhao, B.; Zhu, L. *J. Am. Chem. Soc.* **2006,** *128*, 4574-4575.
17. Zhu, L; Zhao, B. *J. Phys. Chem. B* **2008**, *112*, 11529-11536.
18. Hawker, C. J.; Bosman, A. W.; Harth, E. *Chem. Rev.* **2001**, *101*, 3661-3688.
19. (a) Motornov, M.; Sheparovych, R.; Lupitskyy, R.; MacWilliams, E.; Hoy, O.; Luzinov, I.; Minko, S. *Adv. Funct. Mater.* **2007**, *17*, 2307-2314; (b) Motornov, M.; Sheparovych, R.; Lupitskyy, R.; MacWilliams, E.; Minko, S. *J. Colloid & Interface Sci.* **2007**, *310*, 481-488.
20. Matyjaszewski, K.; Miller, P. J.; Shukla, N.; Immaraporn, B.; Gelman, A.; Luokala, B. B.; Siclovan, T. M.; Kickelbick, G.; Vallant, T.; Hoffmann, H.; Pakula, T. *Macromolecules* **1999**, *32*, 8716−8724.
21. (a) Dao, J.; Benoit, D.; Hawker, C. J. *J. Polym. Sci. Part A: Polym. Chem.***1998**, *36*, 2161−2167. (b) Zhao, B.; Jiang, X. M.; Li, D. J.; Jiang, X. G.; O'Lenick, T. G.; Li, B.; Li, C. Y. *J. Polym. Sci. Part A: Polym. Chem.* **2008**, *46*, 3438-3446.
22. (a) Philipse, A. P.; Vrij, A. *J. Colloid Interface Sci.* **1989**, *128*, 121−136. (b) Bogush, G. H.; Tracy, M. A.; Zukoski, C. F., IV. J. Noncryst. Solids **1988**, *104*, 95−106.
23. Husseman, M.; Malmstrom, E. E.; McNamara, M.; Mate, M.; Mecerreyes, D.; Benoit, D. G.; Hedrick, J. L.; Mansky, P.; Huang, E.; Russell, T. P.; Hawker, C. J. *Macromolecules* **1999**, *32*, 1424-1431.
24. (a) Tunca, U.; Karliga, B.; Ertekin, S.; Ugur, A. L.; Sirkecioglu, O.; Hizal, G.

Polymer **2001,** *42*, 8489-8493. (b) Tunca, U.; Erdogan, T.; Hizal, G. *J. Polym. Sci., Part A: Polym. Chem.* **2002,** *40*, 2025-2032.

25. Hiemenz, P. C.; Lodge, T. P. *Polymer Chemistry*, 2nd Ed., CRC Press: Boca Raton, 2007.
26. (a) Chen, W. Y.; Zheng, J. X.; Cheng, S. Z. D.; Li, C. Y.; Huang, P.; Zhu, L.; Xiong, H. M.; Ge, Q.; Guo, Y.; Quirk, R. P.; Lotz, B.; Deng, L. F.; Wu, C.; Thomas, E. L. *Phys. Rev. Lett.* **2004**, *93*, 028301. (b) Zheng, J. X.; Xiong, H. M.; Chen, W. Y.; Lee, K.; Van Horn, R. M.; Quirk, R. P.; Lotz, B.; Thomas, E. L.; Shi, A.-C.; Cheng, S. Z. D. *Macromolecules* **2006**, *39*, 641-650.
27. Savin, D. A.; Pyun, J.; Patterson, G. D.; Kowalewski, T.; Matyjaszewski, K. *J. Polym. Sci., Part B: Polym. Phys.***2002**, *40*, 2667−2676.
28. The density of P*t*BA was not found in the literature. We used the density of poly(*tert*-butyl methacrylate) (1.03 g/cm^3) in the calculation. The density of PS is 1.05 g/cm^3.
29. Bates, F. S. *Science* **1991**, *251*, 898-905.
30. Feng, C. L.; Vancso, G. J.; Schonherr, H. *Langmuir* **2005,** *21*, 2356-2363.
31. Mark, J. E., *Physical Properties of Polymers Handbook*. AIP Press: New York, 1996.

Chapter 4. Synthesis and Phase Morphology of High Grafting Density Asymmetric Mixed Poly(*t*-butyl acrylate)/Polystyrene Brushes on Silica Particles

Abstract

A set of high grafting density mixed poly(*tert*-butyl acrylate) (P*t*BA)/polystyrene (PS) brushes with P*t*BA number average molecular weight (M_n) fixed at 18.6 kDa and PS M_n ranging from 8.7 to 28.0 kDa was synthesized from 172 nm asymmetric difunctional initiator (Y-initiator)-functionalized silica particles by sequential surface-initiated atom transfer radical polymerization of *tert*-butyl acrylate and nitroxide-mediated radical polymerization (NMRP) of styrene. The Y-initiator-functionalized particles were prepared by the immobilization of a triethoxysilane-terminated Y-initiator onto the surface of bare silica particles via a hydrolysis/condensation process. The overall grafting densities of the obtained mixed brushes were 0.9 – 1.2 chains/nm^2, which were significantly higher than those of mixed brushes prepared from silica particles that were surface functionalized by a monochlorosilane-terminated Y-initiator (0.6 – 0.7 chains/nm^2). Differential scanning calorimetry analysis showed that all high density mixed brushes exhibited two distinct glass transitions, suggesting that the two grafted polymers were microphase separated in the brush layer. TEM showed that with the increase of PS M_n from 8.7 to 28.0 kDa, the morphology of the mixed brushes changed from mostly isolated PS nanodomains buried in the P*t*BA matrix, to a nearly cocontinuous nanostructure, and two-layered nanostructures composed of a laterally microphase-separated bottom layer and a thin PS top layer. These morphologies were similar to the asymmetric mixed brushes with grafting densities of 0.6 – 0.7 chains/nm^2, however, the feature sizes of the patterns formed from the microphase separation were much smaller. The observed grafting density effect on the pattern feature size was further confirmed from the study of a high grafting density mixed brush sample

with P*t*BA M_n of 23.7 kDa and PS M_n of 25.7 kDa. Our results are qualitatively consistent with the theoretical predictions of Zhulina and Balazs.

4.1 Introduction

Mixed brushes, composed of two chemically distinct homopolymers each end-grafted on a solid substrate in a random or alternate fashion, are an intriguing class of surface-responsive materials.[1-4] Driven by free energy minimization, the two grafted polymers in the brush layer can undergo spontaneous chain reorganization in response to environmental variations. Consequently, mixed brushes exhibit different nanostructures and surface properties under different conditions. These brushes have attracted tremendous interest in the past two decades because of their rich phase behaviors and potential in technological applications; their responsive properties have been intensively investigated, both theoretically and experimentally.[1-10]

Marko and Witten predicted that under equilibrium melt conditions binary symmetric mixed homopolymer brushes on a flat substrate would undergo lateral microphase separation, yielding a "rippled" nanostructure.[1a] They pointed out that transitions between different ordered states could be achieved by altering the component compositions and molecular weights. After this seminal work, the lateral microphase separation of symmetric mixed brushes under melt or near-melt conditions and in nonselective solvents were also observed in other theoretical or simulation studies.[1c,d,3-6] Moreover, the effects of various molecular parameters on the phase morphology of mixed brushes were investigated, and many interesting nanostructures have been predicted.

Of particular interest to the work described in this chapter are the effects of chain length disparity and grafting density on the self-assembled nanostructures of mixed brushes.[3,4a,5,6] The effect of chain length disparity on phase morphology of mixed brushes has been

theoretically investigated.[5,6] Using computer simulations, Roan studied the microphase separation of mixed brushes on spherical nanoparticles with a radius comparable to the $<R_{rms}>$ values of grafted polymers and observed a variety of ordered nanostructures.[5] For instance, the equilibrium morphology evolves from a rippled, to a 12-islanded, and then a layered structure with the increase of chain length difference under the condition that the grafting densities of two polymers are identical. Wang and Müller recently used single-chain-in-mean-field simulations to investigate the phase behavior of asymmetric mixed brushes on flat substrates.[6] At a large chain length asymmetry, mixed brushes were found to self-assemble into a two-layered nanostructure in a nearly nonselective solvent: a laterally structured bottom layer and a top layer containing only the longer polymer species.[6] The effect of grafting density on microphase separation of mixed brushes has also been studied theoretically. In general, decreasing the grafting density leads to the weakening of the demixing interactions between two grafted polymers in the brush layer.[3] In the limit where the two polymers are highly incompatible and their grafting densities are high, Zhulina and Balazs found, by scaling arguments, that in nonselective poor solvents the periodicity of the ripple pattern scales with the one sixth power of the area per chain,[3] i.e., the ripple wavelength decreases with increasing grafting density.

There have been a few experimental studies on asymmetric mixed brushes on flat substrates.[8c,9d] Minko et al. prepared a series of asymmetric mixed brushes by a "grafting to" method and investigated them by atomic force microscopy (AFM) and contact angle measurements.[8c] For a small chain length asymmetry, the brushes were found to exhibit lateral and vertical segregation, depending on the solvent quality. With the increase of

molecular weight asymmetry, a transition from a "rippled" to a layered structure was observed. Our group previously synthesized mixed brushes with various chain length asymmetries from asymmetric difunctional initiator (Y-initiator)-functionalized silicon wafers by sequential surface-initiated atom transfer radical polymerization (ATRP) and nitroxide-mediated radical polymerization (NMRP) and studied their responsive properties upon exposure to different solvents by AFM, X-ray photoelectron spectroscopy, and contact angle measurements.[9d] Although interesting results have been obtained from these studies, the phase morphologies of asymmetric mixed brushes had not been directly visualized in these two works.

Transmission electron microscopy (TEM) allows for direct observation of phase morphologies of mixed brushes, provided that the samples are suitable for TEM experiments and are properly stained, if needed.[11,12] We recently reported the synthesis of a series of asymmetric mixed poly(*t*-butyl acrylate) (P*t*BA)/polystyrene (PS) brushes by sequential ATRP of *t*BA and NMRP of styrene from 160 nm silica particles that were functionalized by a monochlorosilane-terminated Y-initiator.[13] The total grafting densities (σ_{total}) of these mixed brushes were 0.6 – 0.7 chains/nm^2 (these brushes are termed intermediate grafting density mixed brushes, IDMB). With the increase of PS M_n from below to above the M_n of P*t*BA, the morphology of mixed brushes evolved from isolated, nearly spherical PS nanodomains buried inside the P*t*BA matrix, to short PS cylinders, to nearly bicontinuous nanostructures, and a two-layered nanostructure composed of a laterally microphase-separated bottom layer and a thin PS top layer.

Although mixed brushes were intensively studied in recent years, few experimental

investigations were directed to the effect of grafting density on phase morphology of mixed brushes. In the present work, we prepared a set of high grafting density asymmetric mixed P*t*BA/PS brushes (HDMB, σ_{total} = 0.9 – 1.2 chains/nm^2) and studied their phase behavior by using differential scanning calorimetry (DSC) and TEM. A triethoxysilane-terminated Y-initiator was synthesized and immobilized onto silica particles via a hydrolysis/condensation process (Scheme 4.1). This initiator immobilization method was first used by Ohno et al. for the synthesis of high density homopolymer brushes on silica particles (σ_{total} = 0.65 – 0.9 chains/nm^2).[14] P*t*BA brushes were then grown first from Y-initiator particles by surface-initiated ATRP of *t*BA at 75 °C, followed by NMRP of styrene at 120 °C. The "living" nature[15] of NMRP allows for the synthesis of mixed brushes with various PS molecular weights in a one-pot reaction (Scheme 4.1). Their morphologies were compared with intermediate density mixed P*t*BA/PS brushes made from monochlorosilane-functionalized silica particles. We found that the feature sizes of the patterns formed from self-assembly of HDMB were significantly smaller than those from IDMB.

4.2 Experimental Section

4.2.1 Materials. Styrene (99%, Aldrich) and *tert*-butyl acrylate (*t*-BA, 99%, Aldrich) were dried with CaH_2, distilled under reduced pressure, and stored in a refrigerator prior to use. CuBr (98%, Aldrich) was purified according to the procedure described in the literature[16] and stored in a desiccator. *N*, *N*, *N*′, *N*′, *N*″-pentamethyldiethylenetriamine (PMDETA, 99 %, Aldrich) was dried with calcium hydride, distilled under a reduced pressure, and stored in a desiccator. Tetraethoxysilane (98%) and ammonium hydroxide (25% in water)

Scheme 4.1. Schematic Illustration for the Synthesis of High Grafting Density Mixed P*t*BA/PS Brushes with a Fixed P*t*BA M_n and Various PS Molecular Weights by Sequential Atom Transfer Radical Polymerization (ATRP) and Nitroxide-Mediated Radical Polymerization (NMRP) from Y-Initiator-Functionalized Silica Particles.

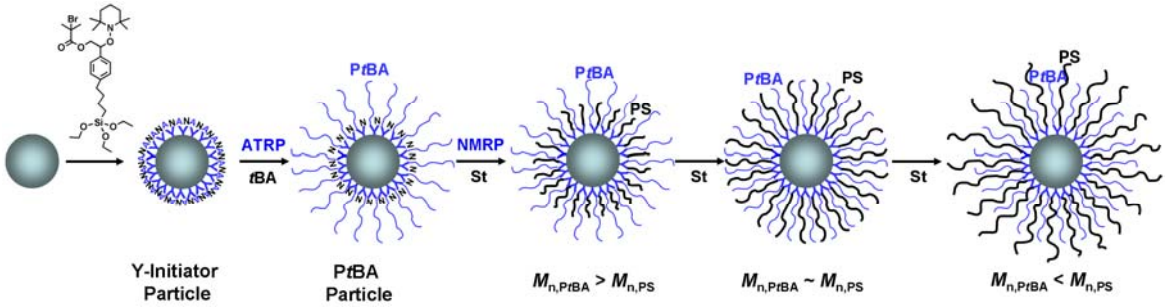

were purchased from Arcos and used as received. Triethoxysilane (95 %) was purchased from Aldrich. Platinum-divinyltetramethyldisiloxane complex in xylene (2.1~2.4% Pt concentration in xylene) was obtained from Gelest, Inc. and used as received. 2-[4-(But-3-enyl)phenyl]-2-(2',2',6',6'-tetramethyl-1'-piperidinyloxy)ethyl 2-bromo-2-methylpropanoate (Y-silane precursor) was synthesized according to the procedure described procedure described in reference 9f. 1-Phenyl-1-(2',2',6',6'-tetramethyl-1'-piperidinyloxy)ethane (STEMPO), an initiator for NMRP, was synthesized according to the procedure described in the literature.[17] All other chemical reagents were purchased from either Aldrich or Fisher and used without further purification.

4.2.2 Characterization. Size exclusion chromatography (SEC) was carried out at ambient temperature using PL-GPC 20 (an integrated SEC system from Polymer Laboratories, Inc.) with a refractive index detector, one PLgel 5 μm guard column (50 × 7.5 mm), and two PLgel 5 μm mixed-C columns (each 300 × 7.5 mm, linear range of molecular weight from 200 to 2,000,000 according to Polymer Laboratories, Inc.). The data were processed using Cirrus^{TM} GPC/SEC software (Polymer Laboratories, Inc.). THF was used as the carrier solvent at a flow rate of 1.0 mL/min. Polystyrene standards (Polymer Laboratories, Inc.) were used for calibration. The ^{1}H NMR spectra were recorded on a Varian Mercury 300 MHz NMR spectrometer and the residual solvent proton peak was used as the internal standard. Thermogravimetric analysis (TGA) was performed in air at a heating rate of 20 °C/min from room temperature to 800 °C using TA Q-series Q50. The particle samples for TGA were dried at 50 °C in vacuum for at least 5 h.

4.2.3 Synthesis of Bare Silica Particles. Bare silica particles were prepared using the

Stöber process.[18] Ammonium hydroxide (25 % in water, 13.953 g) and tetraethoxysilane (TEOS, 7.074 g) were each mixed with 5 mL of ethanol. The two solutions were then added into a 500 mL flask that contained 190 mL of ethanol. The concentrations of NH_3, TEOS, and water in the solution were 0.44 M, 0.15 M, 3.05 M, respectively. The mixture was stirred vigorously at room temperature for 4 h. The particles were isolated by centrifugation (Eppendorf 5804 Centrifuge, 6000 rpm), redispersed in ethanol, and centrifugated again. This washing process was repeated with ethanol one more time, water four times, and ethanol again. The particles were dried with a stream of air flow (1.807 g).

4.2.4 Synthesis of Triethoxysilane-Terminated Y-initiator. 2-[4-(But-3-enyl)phenyl]-2-(2',2',6',6'-tetramethyl-1'-piperidinyloxy)ethyl 2-bromo-2- methylpropanoate (Y-silane precursor, 0.655 g, 1.367 mmol) was added into a 25 mL two-necked flask and dried at room temperature in vacuum for 30 min. Triethoxysilane (3.0 mL, 16.3 mmol) was injected into the flask via a syringe under N_2 atmosphere, followed by addition of the Platinum-divinyltetramethyldisiloxane complex in xylene (60 μL). The mixture was stirred at 45 ºC under nitrogen atmosphere and the hydrosilylation reaction was monitored by ^1H NMR spectroscopy analysis. Once the reaction was complete, excess triethoxysilane was removed by vacuum at 45 ºC and the product was used directly without further purification in the next step for the preparation of Y-initiator-functionalized silica particles.

4.2.5 Synthesis of Y-Initiator-Functionalized Silica Particles. Bare silica particles (602 mg) were dispersed in ethanol (50 mL) by ultrasonication. A solution of ammonium hydroxide (25% in water, 5.18 g) in EtOH (20 mL) was added dropwise into the particle dispersion. After the mixture was stirred at 40 ºC for 2 h, a solution of

triethoxysilane-terminated Y-initiator freshly prepared from 0.655 g of Y-silane precursor in EtOH (5 mL) was added dropwise into the dispersion. After the mixture was stirred at 40 ºC for 18 h, the particles were isolated by centrifugation, redispersed in EtOH, and centrifugated again. This washing process was repeated with ethanol additional two times and then THF two times, followed by drying with a stream of air flow to yield dry particles (621 mg). The average size of Y-initiator-functionalized silica particles was 172 nm, determined from TEM micrographs.

4.2.6 Synthesis of High Grafting Density P*t*BA Brush-Grafted Silica Particles with P*t*BA M_n of 18.6 kDa. The Y-initiator-functionalized silica particles (Y-initiator particles, 297 mg) were dispersed in anisole (10.0 mL) in a 50 mL two-necked flask by ultrasonication. CuBr (49.8 mg, 0.346 mmol), *t*-BA (21.326 g, 166.6 mmol), *N*,*N*,*N*′,*N*′,*N*″-pentamethyldiethylenetriamine (60.3 mg, 0.349 mmol), and ethyl 2-bromoisobutyrate (54.4 mg, 0.279 mmol) were added into a separate 100 mL three-necked flask and stirred under N_2 atmosphere. The dispersion of Y-initiator particles was then quickly transferred into the three-necked flask via a syringe and the reaction mixture was degassed immediately by three freeze-pump-thaw cycles. The polymerization was started by placing the flask in a 75 °C oil bath and monitored by SEC and ^{1}H NMR spectroscopy analysis. After 64 h, the reaction was stopped by removing the flask from the oil bath and opening it to air. The polymerization mixture was diluted with THF (20 mL) and the particles were separated by centrifugation. The supernatant was passed through a column of neutral, activated aluminum oxide to remove the copper catalyst. The hairy particles were re-dispersed in THF, allowed to stand overnight (the green precipitate was

removed), and isolated again by centrifugation. This washing process was repeated with THF one more time and chloroform three times, followed by drying the particles with a stream of air flow, yielding P*t*BA brush-grafted silica particles (0.323 g). The $M_{n,SEC}$ and polydispersity index (PDI) of the free P*t*BA formed from the free initiator in the polymerization were 18.6 kDa and 1.09, respectively, determined from SEC analysis using polystyrene calibration.

4.2.7 Synthesis of High Grafting Density Mixed P*t*BA/PS Brush-Grafted Silica Particles with P*t*BA M_n of 18.6 kDa and Various PS Molecular Weights. The P*t*BA brush-grafted silica particles (P*t*BA M_n = 18.6 kDa, 0.262 g) were dispersed in anisole (12.959 g) in a 50 mL two-necked flask using an ultrasonic water bath. The particle dispersion was then transferred into a 100 mL three-necked flask that contained STEMPO (55.5 mg, 0.213 mmol), followed by the addition of styrene (17.688 g, 170.1 mmol). The mixture was degassed by three freeze-pump-thaw cycles. The polymerization was started by placing the flask in a 120 °C oil bath and monitored by ^{1}H NMR spectroscopy and SEC analysis. Samples were taken from the reaction mixture using a degassed syringe and diluted with THF when the molecular weight of the free polystyrene formed from free initiator STEMPO reached desired values. The mixed P*t*BA/PS brush-grafted particles were separated from the free polymer by centrifugation, re-dispersed in THF, and centrifugated again. For each sample, this washing process was repeated four times to remove the physically adsorbed polymer. The particles were then dried with a stream of air flow.

4.2.8 DSC Study of High Grafting Density P*t*BA Brush- and Mixed P*t*BA/PS Brush-Grafted Silica Particles. DSC analysis of polymer brush-grafted particles was

conducted on a TA Q-1000 DSC instrument that was calibrated with sapphire. The high density P*t*BA brush- and mixed P*t*BA/PS brush-grafted particles were thermally annealed at 120 °C in vacuum for 3 h and then cooled to room temperature. For each sample, approximately 10 – 15 mg of particles was used in the analysis. The heating and cooling rates were 10 °C/min; the second heating thermogram was used to determine the glass transitions.

4.2.9 TEM Study of High Grafting Density Mixed P*t*BA/PS Brush-Grafted Silica Particles. Chloroform, a good solvent for both P*t*BA and PS, was used to prepare the particle dispersions. For each sample, 1 – 2 mg of particles was dispersed in 2 mL of chloroform in a small vial by ultrasonication in a ultrasonic water bath for 5 min. The particle dispersion was drop cast onto a carbon-coated, copper TEM grid using a glass pipette and was allowed to dry at ambient conditions. The samples were annealed with $CHCl_3$ vapor at room temperature as detailed below. The sample-loaded TEM grids were placed in a small glass dish with a diameter of 2". The dish was then transferred into a glass jar that contained ~ 1 mL of $CHCl_3$. The jar was covered with a watch glass. After being annealed by $CHCl_3$ vapor at room temperature for > 3 h, the samples were removed from the jar, allowed to dry at ambient conditions for 30 min, and then stained with RuO_4 at room temperature for 20 min. TEM experiments were performed on a JEOL 1210 at an accelerating voltage of 100 kV.

4.3 Results and Discussion

4.3.1 Synthesis of High Grafting Density Asymmetric Mixed P*t*BA/PS Brushes on Silica Particles. We used a procedure similar to that reported by Ohno et al.[14] to

immobilize a triethoxysilane-containing Y-initiator (Scheme 4.1) onto bare silica particles. The key of this method is the ammonia-catalyzed hydrolysis and condensation of the Y-initiator-terminated triethoxysilane on the surface of bare silica particles in ethanol, yielding a high density initiator layer on silica particles. The bare silica particles were synthesized by the Stöber process, which is known to produce silica particles with a relatively uniform size distribution.[18] The triethoxysilane-containing Y-initiator was prepared by a platinum-catalyzed hydrosilylation reaction of 2-[4-(but-3-enyl)phenyl]-2-(2',2',6',6'-tetramethyl-1'-piperidinyloxy) ethyl 2-bromo-2-methylpropanoate (the Y-silane precursor) with triethoxysilane ($HSi(OC_2H_5)_3$). After the immobilization reaction proceeded at 40 °C for 18 h, the particles were isolated by centrifugation and repeatedly washed with THF. The average diameter of the Y-initiator-functionalized silica particles (Y-initiator particles) was 172 nm, measured from TEM micrographs. Thermogravimetric analysis (TGA) showed that the weight loss of Y-initiator particles relative to bare silica particles was 4.4 % when the weight retention difference at 100 °C between the two curves was taken into consideration (Figure 4.1).

The Y-initiator particles were then used for preparing mixed P*t*BA/PS brushes. P*t*BA was grown first by surface-initiated ATRP[19] of *t*-butyl acrylate carried out in anisole at 75 °C using CuBr/PMDETA as catalyst and ethyl 2-bromoisobutyrate (EBiB) as free initiator. The TEMPO group in the Y-initiator was previously confirmed to be stable under this ATRP condition.[9,20] The polymerization was stopped when the molecular weight of the free P*t*BA reached 18.6 kDa, determined by size exclusion chromatography (SEC). The polydispersity index (PDI) of this free polymer was 1.09, suggesting that the

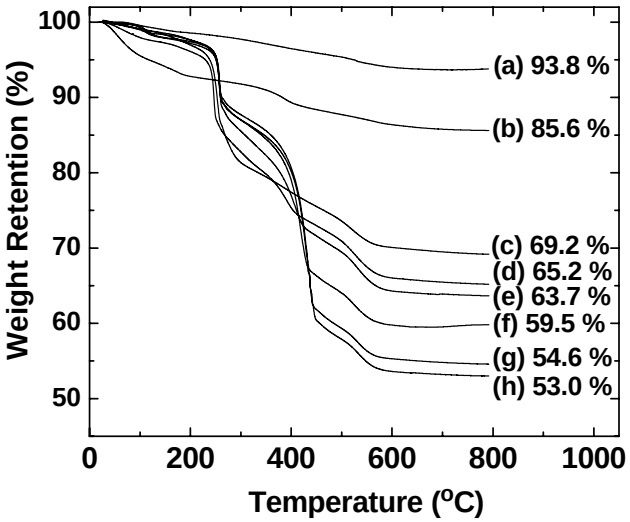

Figure 4.1. Thermogravimetric analysis (TGA) of (a) bare silica particles, (b) Y-initiator particles, (c) P*t*BA brush-grafted particles with P*t*BA M_n of 18.6 kDa, (d) mixed brush-grafted particles with P*t*BA M_n of 18.6 kDa and PS M_n of 8.7 kDa (particle-**I-1**), (e) mixed brush-grafted particles with P*t*BA M_n of 18.6 kDa and PS M_n of 13.4 kDa (particle-**I-2**), (f) mixed brush-grafted particles with P*t*BA M_n of 18.6 kDa and PS M_n of 19.4 kDa (particle-**I-3**), (g) mixed brush-grafted particles with P*t*BA M_n of 18.6 kDa and PS M_n of 25.3 kDa (particle-**I-4**), and (h) mixed brush-grafted particles with P*t*BA M_n of 18.6 kDa and PS M_n of 28.0 kDa (particle-**I-5**). TGA was performed in air at a heating rate of 20 ºC/min from room temperature to 800 ºC.

polymerization was controlled. The average degree of polymerization (DP) of the free polymer was 143, which was calculated from the monomer conversion and the initial monomer-to-initiator ratio. The monomer conversion was determined by ^{1}H NMR spectroscopy analysis. It has been established that the molecular weight and molecular weight distribution of polymer brushes synthesized by surface-initiated "living"/controlled radical polymerization, including high density homopolymer brushes (with grafting density of 0.65 – 0.90 chains/nm^2), are essentially identical to those of the free polymer formed from the free initiator.[9f,14,21] TGA showed that the weight retention of P*t*BA brush-grafted particles at ~ 800 °C was 69.2 % (Figure 4.1). By using the average size of Y-initiator particles (172 nm), TGA data, and the DP of free P*t*BA, and assuming that the density of silica particles was identical to bulk SiO_2 (2.07 g/cm^3),[9f,19] the grafting density of P*t*BA brushes on silica particles was calculated to be 0.63 chains/nm^2. This value was comparable to those of high density homopolymer brushes (σ= 0.65 – 0.90 chains/nm^2) on silica particles reported by Ohno et al.[14] and was significantly higher than that of P*t*BA brushes that were grown from monochlorosilane-terminated Y-initiator-functionalized silica particles (σ = 0.36 chains/nm^2).[13] By taking advantage of the "living" nature of NMRP, a set of mixed P*t*BA/PS brush-grafted particle samples with PS molecular weights ranging from below to above the P*t*BA M_n were synthesized from P*t*BA brush-grafted particles in a one-pot reaction via surface-initiated NMRP of styrene. The polymerization was carried out in anisole at 120 °C, and a free initiator, 1-phenyl-1-(2',2',6',6'-tetramethyl-1'-piperidinyloxy)ethane (STEMPO), was added into the reaction mixture to facilitate the control of surface-initiated polymerization. Five mixed brush samples with the same P*t*BA

M_n but different PS molecular weights were obtained at different polymerization times. The particles were isolated by centrifugation and repeatedly washed with THF. The free polymers were purified and analyzed by SEC.

SEC analysis of five free polymers showed that the molecular weight of PS increased smoothly with the increase of reaction time, while the PDI gradually decreased, indicating that the polymerization was controlled.[22] Specifically, the M_n of PS increased from 8.7 kDa (the corresponding hairy particles designated as particle-**I-1**), to 13.4 kDa (the particles designated as particle-**I-2**), to 19.4 kDa (the particles designated as particle-**I-3**), to 25.3 kDa (the particles designated as particle-**I-4**), and 28.0 kDa (the particles designated as particle-**I-5**). From Figure 4.1, the weight retention of mixed brush-grafted particles at 800 °C decreased with the increase of PS M_n, from 65.2 % for particle-**I-1**, to 63.7 % for particle-**I-2**, to 59.5 % for particle-**I-3**, 54.6 % for particle-**I-4**, and 53.0 % for particle-**I-5**. Using the silica residue at 800 °C as reference and taking into consideration the difference in weight retention at 100 °C between hairy particles and Y-initiator particles, we calculated the relative amount of the grafted polymers on silica particles in each sample and plotted it again the PS molecular weight (Figure 4.2). The amount of the grafted polymers increased with PS M_n, however the increase was slow in the beginning of the polymerization. This seemed to be inherent to the TEMPO-mediated radical polymerization, as our group previously also observed a slow period in the study of the kinetics of NMRP.[9f] On the basis of the average size of Y-initiator particles (172 nm), the TGA data in Figure 4.1, and the PS M_n, we calculated the grafting density of PS in each sample. The results are summarized in Table 4.1. The total grafting densities of two polymers ($\sigma_{total} = \sigma_{PtBA} + \sigma_{PS}$)

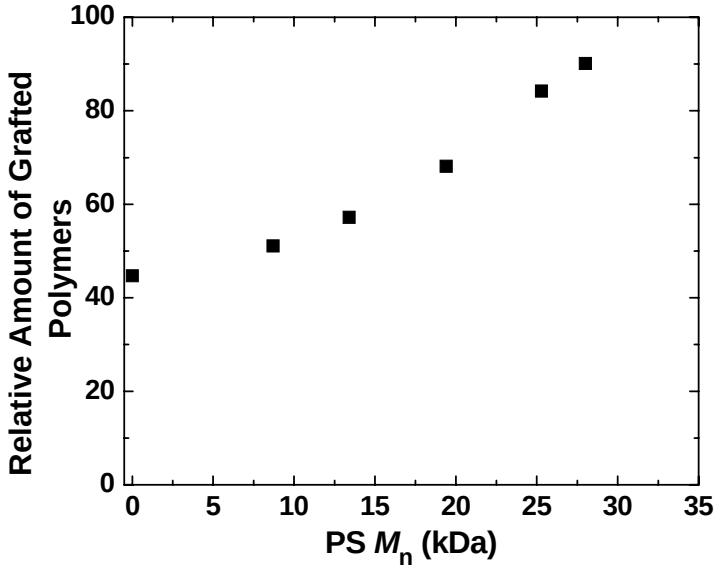

Figure 4.2. The amount of the grafted polymers in mixed P*t*BA/PS brush-grafted silica particles relative to the silica residue at 800 °C, calculated from TGA data, versus polystyrene molecular weight.

Table 4.1. Molecular Characteristics of Mixed P*t*BA/PS Brushes with Various P*t*BA and PS Molecular Weights on Silica Particles and the Corresponding Free Polymers

Sample No.	PS M_n (kDa), PDI, DP [b]	DP_{PS}/ DP_{PtBA} [c]	σ_{PS} and σ_{total} (chains/nm^2)[d]	Typical PS Domain Width & Periodicity (nm)[g]
Particle-**I-1** [a]	8.7, 1.28, 84	0.59	0.26, 0.89	8, NA
Particle-**I-2** [a]	13.4, 1.19, 129	0.90	0.33, 0.96	8, 12
Particle-**I-3** [a]	19.4, 1.14, 187	1.31	0.43, 1.06	8, 12
Particle-**I-4** [a]	25.3, 1.13, 243	1.70	0.56, 1.19	7, 11
Particle-**I-5** [a]	28.0, 1.11, 269	1.88	0.58, 1.21	6, 11
Particle-**II-1**	14.8, 1.24, 142	0.74	0.21, 0.57	13, NA
Particle-**II-2**	18.7, 1.20, 180	0.94	0.26, 0.62	13, NA
Particle-**II-3**	24.9, 1.17, 239	1.25	0.27, 0.63	15, 20
Particle-**II-4**	30.4, 1.14, 292	1.53	0.32, 0.68	17, 22
Particle-**III-1**	25.7, 1.14, 247	1.31	0.51, 0.99	8, 13

[a] Particle-**I-1**, **-2**, **-3**, **-4**, and **-5** were prepared from P*t*BA brush-grafted silica particles with P*t*BA M_n of 18.6 kDa and PDI of 1.09; DP_{PtBA} = 143; the grafting density of P*t*BA (σ_{PtBA}) was 0.63 chains/nm^2.

[b] The values of M_n and polydispersity index (PDI) of PS were determined by SEC; the DPs of polystyrenes were calculated from M_ns.

[c] The ratio of DPs of two polymers.

[d] The PS grafting density (σ_{PS}) in each sample was calculated using the size of Y-initiator particles, DP_{PS}, and TGA data. The total grafting density $\sigma_{total} = \sigma_{PtBA} + \sigma_{PS}$.

[e] Particles-**II-1**, **-2**, **-3**, and **-4** were prepared from P*t*BA brush-grafted silica particles with P*t*BA M_n of 24.5 kDa and PDI of 1.11, which were prepared from 160 nm monochlorosilane-terminated Y-initiator-functionalized silica particles.[13] DP_{PtBA} = 191. The σ_{PtBA} was 0.36 chains/nm^2.

[f] Particle-**III-1** was prepared from P*t*BA brush-grafted silica particles with P*t*BA M_n of 23.7 kDa and PDI of 1.09;[22] the DP_{PtBA} was 189 and the σ_{PtBA} was 0.48 chains/nm^2.

[g] The width of a typical PS nanodomain and the ripple wavelength were estimated from TEM micrographs.

in these samples were in the range of 0.9 – 1.2 chains/nm^2. Except the first two samples (particle-**I-1** and **-2**), the grafting densities of two polymers were reasonably close to each other. The lower PS grafting densities of particle-**I-1** and **-2** could be the result of the slow reaction period in the early stage of the polymerization.[9f] Calculations showed that the average distance between grafting sites in these mixed brush samples was 0.91 – 1.06 nm, indicating that the polymers were densely grafted and highly stretched. For comparison, we include in Table 4.1 four intermediate density mixed P*t*BA/PS brush samples with total grafting densities of 0.6 – 0.7 chains/nm^2 (particle-**II-1**, **-2**, **-3**, and **-4**). These IDMB samples were synthesized from 160 nm silica particles that were functionalized by a monochlorosilane-terminated Y-initiator. The detailed synthesis and characterization can be found in Chapter 3.[13] Clearly, the total grafting densities of mixed brushes in the particle-**I** series were substantially higher than those in the particle-**II** series. At a similar ratio of DP_{PS} to DP_{PtBA}, the σ_{total} for a sample in the particle-**I** series was 1.5 – 1.8 times that for the corresponding sample in the particle-**II** series.

4.3.2 Differential Scanning Calorimetry (DSC) Study of High Grafting Density Mixed P*t*BA/PS Brush-Grafted Silica Particles. DSC has been widely used to study the phase behavior of multicomponent polymeric systems. It was previously observed that there were two distinct glass transitions in the DSC thermogram for the microphase separated mixed brushes on silica particles, while miscible mixed brushes exhibited only one broad glass transition,[11] suggesting that DSC can be used to determine whether the two grafted polymers in the mixed brush layer are microphase separated or not. Figure 4.3 shows the DSC thermograms of five HDMB samples along with the corresponding high density P*t*BA

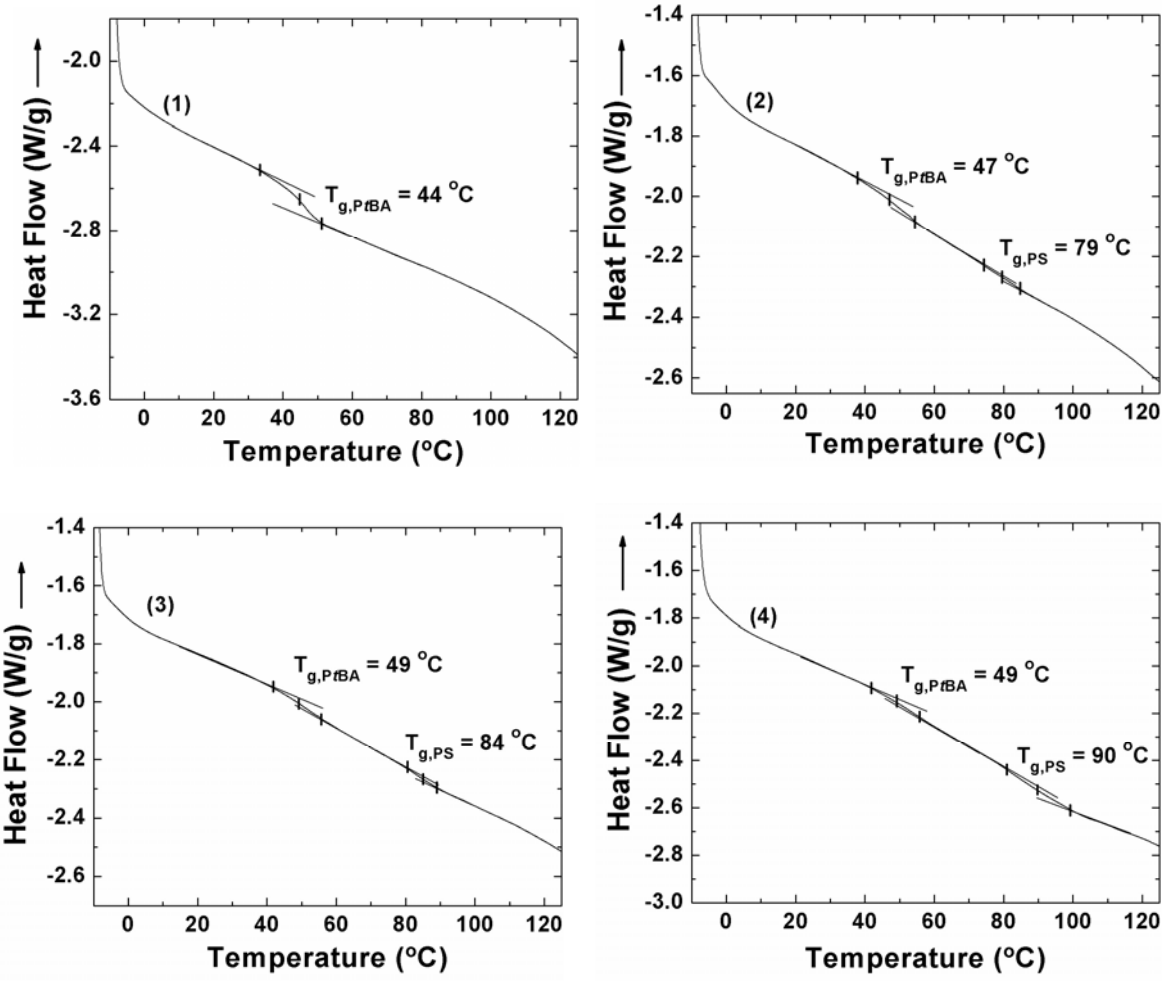
(1)
$T_{g,PtBA}$ = 44 °C
(2)
$T_{g,PtBA}$ = 47 °C
$T_{g,PS}$ = 79 °C
(3)
$T_{g,PtBA}$ = 49 °C
$T_{g,PS}$ = 84 °C
(4)
$T_{g,PtBA}$ = 49 °C
$T_{g,PS}$ = 90 °C
Heat Flow (W/g) ⟶
Temperature (°C)

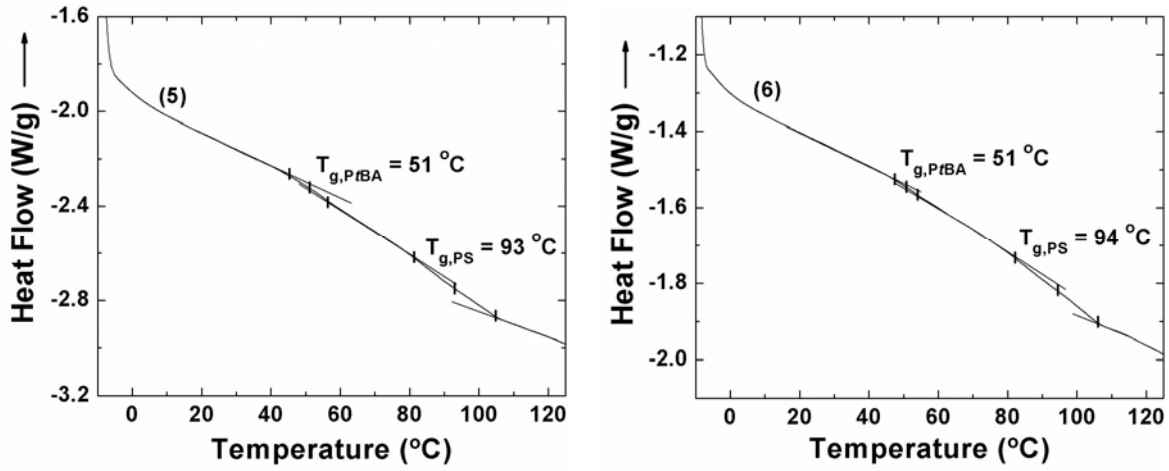

Figure 4.3. Differential scanning calorimetry (DSC) analysis of (1) P*t*BA brush-grafted silica particles (P*t*BA M_n = 18.6 kDa), (2) particle-**I-1** (P*t*BA M_n = 18.6 kDa and PS M_n = 8.7 kDa), (3) particle-**I-2** (P*t*BA M_n = 18.6 kDa and PS M_n = 13.4 kDa), (4) particle-**I-3** (P*t*BA M_n = 18.6 kDa and PS M_n = 19.4 kDa), (5) particle-**I-4** (P*t*BA M_n = 18.6 kDa and PS M_n = 25.3 kDa), and (5) particle-**I-5** (P*t*BA M_n = 18.6 kDa and PS M_n = 28.0 kDa). The heating and cooling rates in the DSC analysis were 10 °C/min.

hairy particles. All particles were thermally annealed at 120 °C in vacuum for 3 h prior to the DSC analysis. For P*t*BA hairy particles, the glass transition occurred in the temperature range of 33 to 51 °C with the middle point at 44 °C (thermogram **1**), which was essentially the same as that of P*t*BA brushes grafted on 160 nm silica particles with P*t*BA M_n of 24.5 kDa and grafting density of 0.36 chains/nm^2 (45 °C).[13] All five mixed brush samples exhibited two glass transitions with the middle points at 47 – 51 and 79 – 94 °C, which corresponded to the glass transitions of P*t*BA and PS, respectively, indicating that the two grafted polymers were phase separated. Note that the PS glass transition of particle-**I-1** was quite weak, but still discernable.

By carefully examining the DSC thermograms in Figure 4.3, we can find three trends for the two glass transitions. Firstly, with the increase of PS molecular weight from 8.7 kDa to 28.0 kDa, the T_g of PS increased from 79 °C (particle-**I-1**), to 84 °C (particle-**I-2**), to 90 °C (particle-**I-3**), to 93 °C (particle-**I-4**), and 94 °C (particle-**I-5**). This increase can be attributed to the molecular weight effect on T_g.[13,23] Secondly, the T_g of P*t*BA also increased with the increase of PS chain length, from 44 °C for homopolymer P*t*BA brushes, to 47 °C (particle-**I-1**), to 49 °C (particle-**I-2** and -**3**), and 51 °C (particle-**I-4** and -**5**). This is likely due to the confining effect of PS, a higher T_g polymer, on P*t*BA nanodomains. Thirdly, the temperature range of the P*t*BA glass transition in particle-**I-1** (16 °C) was almost the same as that of P*t*BA homopolymer brushes on silica particles (18 °C), while the transition zone became increasingly narrower with the increase of PS molecular weight from 13.4 to 28.0 kDa (Table 4.2). The temperature ranges of the P*t*BA glass transition for particle-**I-1**, -**2**, -**3**, -**4** and -**5** were ~ 16, 14, 14, 12 and 6 °C, respectively. On the other

Table 4.2. Glass Transitions of High Density Homopolymer P*t*BA Brushes and Mixed P*t*BA/PS Brushes on Silica Particles

Sample No.	DP_{PS}/DP_{PtBA} [b]	$T_{g,PtBA}$ (^oC)[c]	Temp. Range of P*t*BA Glass Transition (^oC) [c]	$T_{g,PS}$ (^oC)[c]	Temp. Range of PS Glass Transitions (^oC)[c]
P*t*BA Particles [a]	0	44	33 – 51	NA	NA
Particle-**I-1**	0.59	47	38 – 54	79	74 – 84
Particle-**I-2**	0.90	49	41 – 55	84	80 – 88
Particle-**I-3**	1.31	49	42 – 56	90	81 – 99
Particle-**I-4**	1.70	51	45 – 57	93	81 – 105
Particle-**I-5**	1.88	51	48 – 54	94	82 – 106

[a] P*t*BA brush-grafted silica particles with P*t*BA M_n of 18.6 kDa, the grafting density of P*t*BA (σ_{PtBA}) was 0.63 chains/nm^2. [b] The ratio of degree of polymerization (DP) of PS to that of P*t*BA. [c] The glass transition temperature (T_g) and the temperature range of glass transition were determined from DSC thermograms in Figure 4.3.

hand, the PS transition zone became increasingly wider, from 10 and 8 °C for particle-**I-1** and **-2**, respectively, to 18 °C for particle-**I-3**, and 24 °C for particle-**I-4** and **-5**. The glass transition ranges are related to the segmental mobilities of polymer chains; the variations observed in Figure 4.3 could result from the different nanostructures formed from microphase separation of two grafted polymers in the brush layer. For a large chain length disparity, as suggested by theoretical and simulation studies[5,6] and confirmed in our previous experimental work,[13] a two-layered nanostructure was formed, composed of a laterally microphase separated bottom layer and a thin top layer of the longer species. The longer polymer species thus had different segmental mobilities in the bottom and outer layers and consequently exhibited a broad glass transition. On the other hand, the chains of another polymer were completely wrapped by the longer species, which manifested in a narrower glass transition zone. Evidently, this is the case for particle-**I-1** in which DP_{PS}/DP_{PtBA} was 0.59 and for particle-**I-3**, **-4** and **-5** in which the ratios of DP_{PtBA} to DP_{PS} were 1.31, 1.70, and 1.88, respectively. Particle-**I-2** was in between these extremes (DP_{PS}/DP_{PtBA} = 0.90) and the two grafted polymers were likely to self-assemble into a "rippled" morphology.

4.3.3 Phase Morphologies of High Grafting Density Asymmetric Mixed P*t*BA/PS Brushes on Silica Particles. For TEM study of phase morphologies of mixed P*t*BA/PS brushes, the particles were dispersed in $CHCl_3$, a good solvent for both P*t*BA and PS, drop cast onto carbon-coated TEM grids, and then annealed with $CHCl_3$ vapor in a closed jar for at least 3 h. The samples were stained with RuO_4 at room temperature for 20 min and then examined under a transmission electron microscope. Note that RuO_4 stains PS

chains, making PS and P*t*BA nanodomains appear dark and bright, respectively, under the electron microscope.[11-13] Figure 4.4 shows the typical top-view TEM micrographs of five HDMB samples (particle-**I-1** to -**5**). For comparison, the representative TEM images of particle-**II-1** to -**4** are presented in Figure 4.5 (the TEM samples of particle-**II-1** to -**4** were prepared using the same procedure for HDMB samples). Clearly, all high density mixed brushes were microphase separated, consistent with the DSC results. Moreover, the morphology varied with the increase of PS molecular weight. By comparing the TEM micrographs in Figures 4.4 and 4.5, one can easily find out that the grafting density has a significant effect on the self-assembled nanostructures of mixed brushes, particularly, the feature size. For particle-**I-1** in which the PS M_n (8.7 kDa) was significantly lower than that of P*t*BA (18.6 kDa, DP_{PS}/DP_{PtBA} = 0.59), the PS chains self-assembled into irregular, mostly isolated nanodomains with a typical width of 8 nm (the nanodomain pointed by an arrow in Figure 4.4A; see the illustrated nanostructure in Scheme 4.2a). This is similar to the morphology of particle-**II-1** (DP_{PS}/DP_{PtBA} = 0.74) where PS segregated into isolated nanodomains with a typical width of 13 nm (the nanodomain pointed by an arrow in Figure 4.5A). Different from Figure 4.5A, the dark PS nanodomains in particle-**I-1** were denser and smaller. The smaller size is believed to mainly result from the higher overall grafting density (σ_{total} = 0.89 chains/nm^2 for particle-**I-1** and 0.57 chains/nm^2 for particle-**II-1**), though the difference in PS molecular weight may also contribute to it. The PS in particle-**II-2** was slightly longer than that in particle-**II-1**; short cylinders with a typical width of 13 nm were observed (the nandomain pointed by an arrow in Figure 4.5B). For

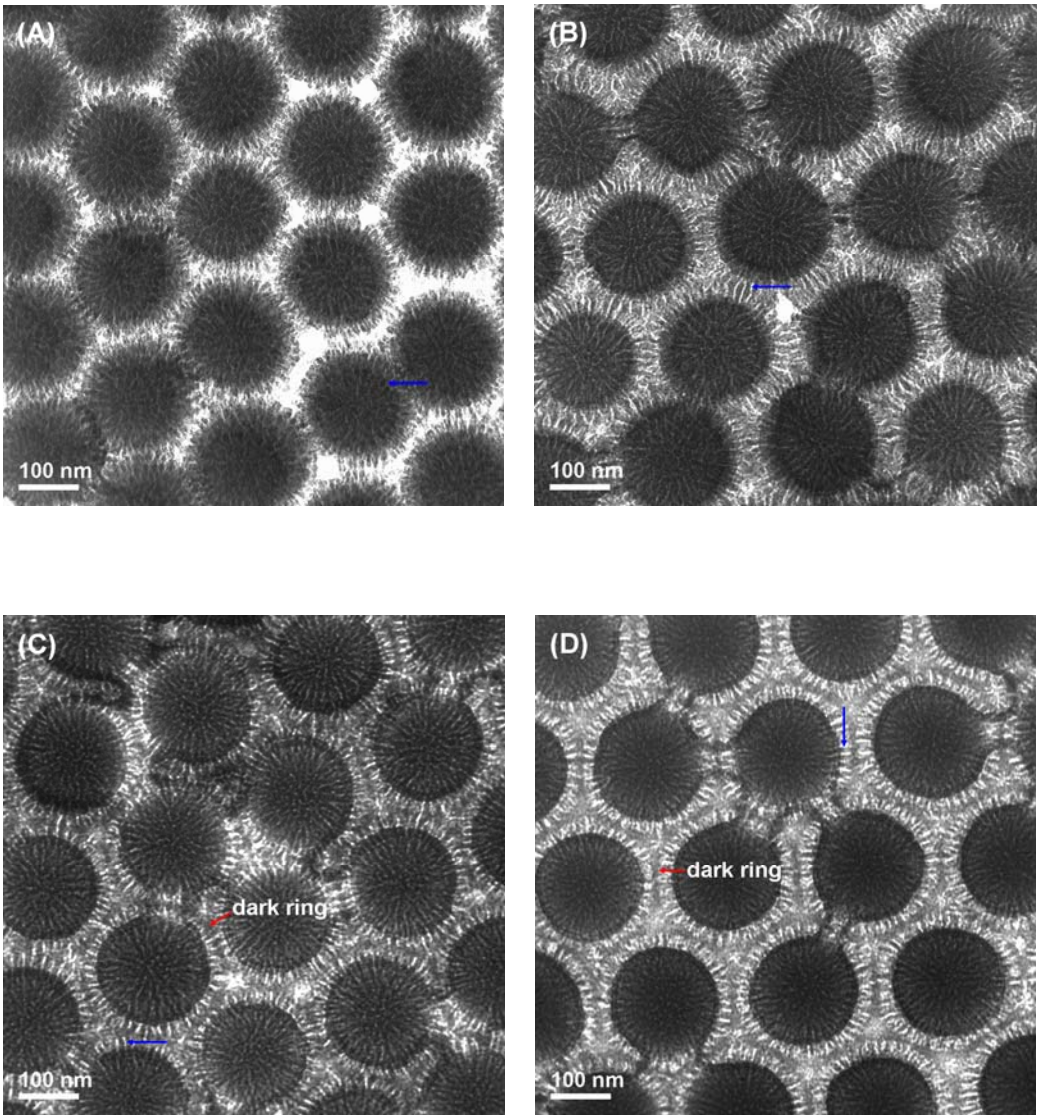
(A)
100 nm
(B)
100 nm
(C)
dark ring
100 nm
(D)
dark ring
100 nm

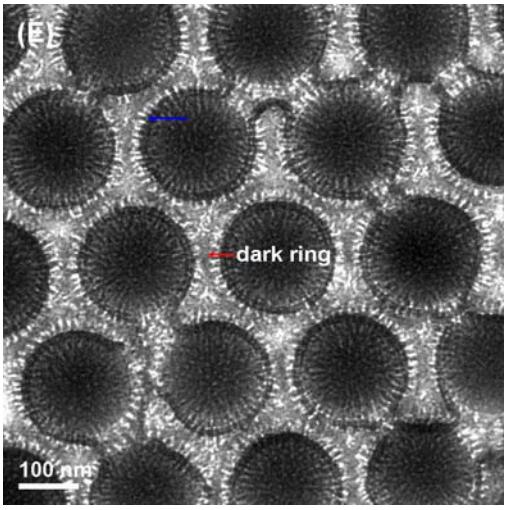

Figure 4.4. Top-view TEM micrographs of (**A**) particle-**I-1** (P*t*BA M_n = 18.6 kDa, σ_{PtBA} = 0.63 chains/nm^2; PS M_n = 8.7 kDa, σ_{PS} = 0.26 chains/nm^2; DP_{PS}/DP_{PtBA} = 0.59), (**B**) particle-**I-2** (P*t*BA M_n = 18.6 kDa, σ_{PtBA} = 0.63 chains/nm^2; PS M_n = 13.4 kDa, σ_{PS} = 0.33 chains/nm^2; DP_{PS}/DP_{PtBA} = 0.90), (**C**) particle-**I-3** (P*t*BA M_n = 18.6 kDa, σ_{PtBA} = 0.63 chains/nm^2; PS M_n = 19.4 kDa, σ_{PS} = 0.43 chains/nm^2; DP_{PS}/DP_{PtBA} = 1.31), (**D**) particle-**I-4** (P*t*BA M_n = 18.6 kDa, σ_{PtBA} = 0.63 chains/nm^2; PS M_n = 25.3 kDa, σ_{PS} = 0.56 chains/nm^2; DP_{PS}/DP_{PtBA} = 1.70), and (**E**) particle-**I-5** (P*t*BA M_n = 18.6 kDa, σ_{PtBA} = 0.63 chains/nm^2; PS M_n = 28.0 kDa, σ_{PS} = 0.58 chains/nm^2; DP_{PS}/DP_{PtBA} = 1.88) after being cast from and annealing with $CHCl_3$, a good solvent for both P*t*BA and PS. The samples were stained with RuO_4 vapor at room temperature for 20 min.

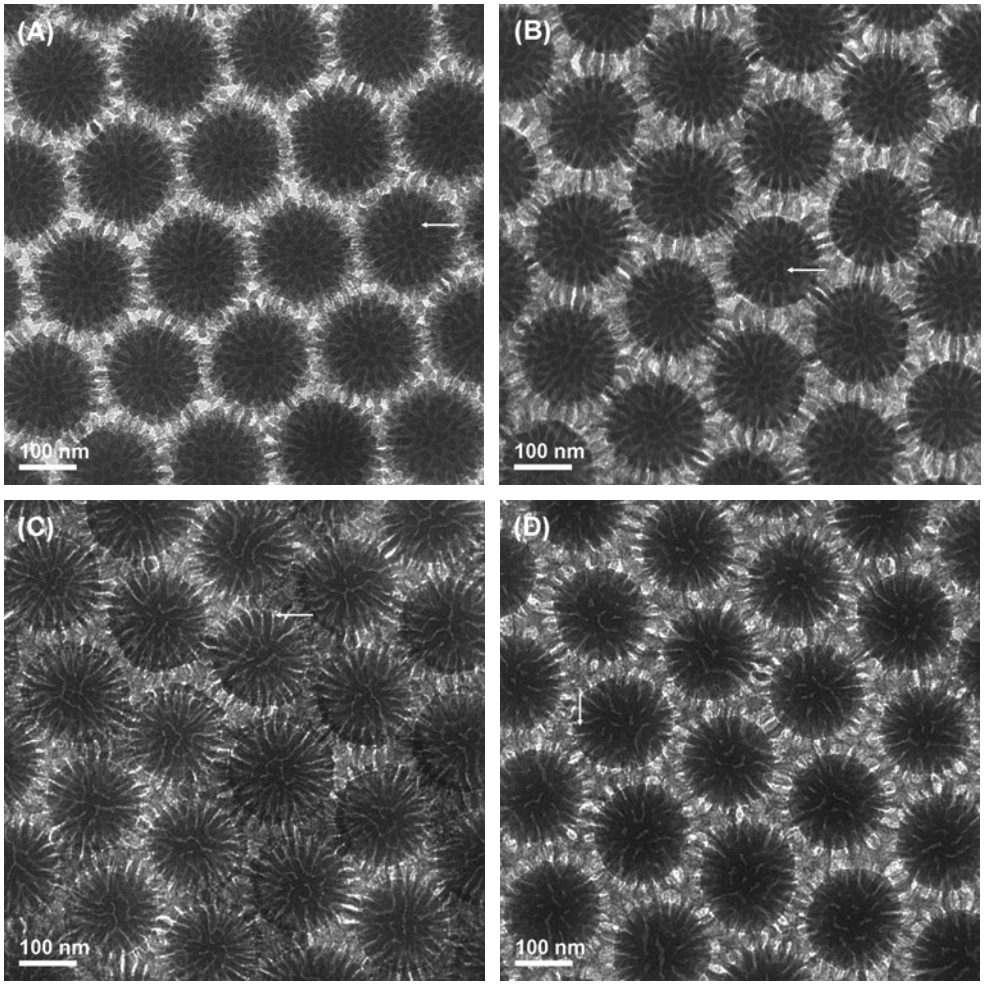

Figure 4.5. Top-view TEM micrographs of (**A**) particle-**II-1** (P*t*BA M_n = 24.5 kDa, σ_{PtBA} = 0.36 chains/nm^2; PS M_n = 14.8 kDa, σ_{PS} = 0.21 chains/nm^2; DP_{PS}/DP_{PtBA} = 0.74), (**B**) particle-**II-2** (P*t*BA M_n = 24.5 kDa, σ_{PtBA} = 0.36 chains/nm^2; PS M_n = 18.7 kDa, σ_{PS} = 0.26 chains/nm^2; DP_{PS}/DP_{PtBA} = 0.94), (**C**) particle-**II-3** (P*t*BA M_n = 24.5 kDa, σ_{PtBA} = 0.36 chains/nm^2; PS M_n = 24.9 kDa, σ_{PS} = 0.27 chains/nm^2; DP_{PS}/DP_{PtBA} = 1.25), and (**D**) particle-**II-4** (P*t*BA M_n = 24.5 kDa, σ_{PtBA} = 0.36 chains/nm^2; PS M_n = 30.4 kDa, σ_{PS} = 0.32 chains/nm^2; DP_{PS}/DP_{PtBA} = 1.53) after being cast from and annealing with $CHCl_3$, a good solvent for both P*t*BA and PS. The samples were stained with RuO_4 vapor at room temperature for 20 min.

Scheme 4.2. Schematic Illustration of Microphase Separation of High Grafting Density Mixed P*t*BA/PS Brushes with P*t*BA M_n (a) lower than, (b) comparable to, and (c) higher than that of PS M_n.

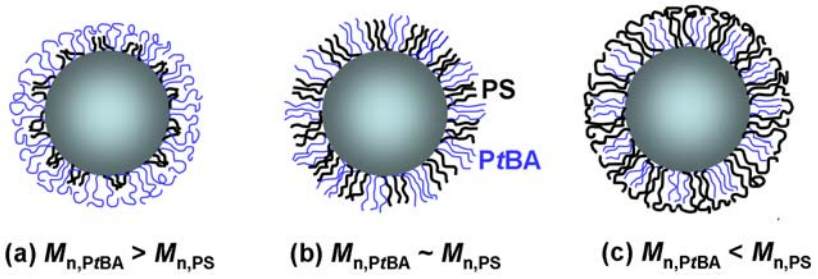

particle-**I-2** where the chain lengths of two polymers were very close to each other (DP_{PtBA} = 143 and DP_{PS} = 129), the two grafted polymers underwent lateral microphase separation, producing a "rippled" nanostructure (Figure 4.4B), though there was a difference in the grafting densities of two polymers (σ_{PtBA} = 0.63 chains/nm^2; σ_{PS} = 0.33 chains/nm^2). Note that simulations studies have suggested that the co-continuous "rippled" morphology can tolerate small chain length and grafting density asymmetries.[5,6] The polymer chains spread out and covered the interstitial space among the particles. Interestingly, the dark and bright stripes from one particle were connected to those from neighboring particles, forming alternating bridging nanostructures (marked by a blue arrow in Figure 4.4B). No dark or bright thin layer was observed at the boundary of neighboring hairy particles, suggesting that the nanostructure was simply a "rippled" phase with no thin layer of a pure species on the top (Scheme 4.2b). This is consistent with the DSC result for this sample, where relatively narrow glass transitions were observed for both polymers. The width of a typical PS stripe and the ripple wavelength on the particles were estimated to be 8 nm and 12 nm, respectively. This sample resembles particle-**II-3** in which the two grafted polymers self-assembled into a "rippled" nanostructure (Figure 4.5C). However, the feature size of particle-II-3 is significantly larger with the PS stripe width of 15 nm and the ripple wavelength of 20 nm (the PS and P*t*BA stripes pointed by the arrow in Figure 4.5C).

For particle-**I-3** in which the chain length of PS (DP = 187) was slightly longer than that of P*t*BA (DP = 143) and the grafting densities of two polymers were comparable (σ_{PtBA}= 0.63 chains/nm^2; σ_{PS} = 0.43 chains/nm^2), the morphology (Figure 4.4C) is quite similar to that of particle-**I-2** (Figure 4.4B), but there is a difference. A dark layer appeared

in the interstitial area between the particles and each particle was surrounded by a nearly continuous "ring" of such a dark layer (marked by a red arrow in Figure 4.4C). This suggests that the two grafted polymers microphase separated into a two-layered nanostructure in which the bottom layer was laterally microphase separated and covered by a thin PS top layer because the PS chains were slightly longer than that of P*t*BA (Scheme 4.2c). The typical width of dark PS nanodomains and the typical periodicity in the bottom layer as marked by a blue arrow were 8 nm and 12 nm, respectively, which were significantly smaller than those of particle-**II-3** (15 and 20 nm, respectively). From Figure 4.4C, the PS and P*t*BA nanodomains that were underneath the thin PS layer appeared to be mostly cylindrical. Note that the ratios of DP_{PS} to DP_{PtBA} and σ_{PS} to σ_{PtBA} in particle-**II-3** were almost the same as those in particle-**I-3**, but dark rings in Figure 4.5C were not as visible and defined as in Figure 4.4C. We speculate that at lower grafting densities, the PS nanodomains formed from lateral microphase separation can accommodate more PS segments, while at higher grafting densities, the polymer chains are more stretched, resulting in the formation of a thin PS top layer. The distribution of PS segments in two layers is presumably the origin of the broader PS glass transition of particle-**I-3** compared with those of particle-**I-1** and -**2** (Figure 4.3).

For particle-**I-4** and -**5** where the grafting densities of two polymers were very close to one another and the PS chain length was significantly longer than that of P*t*BA, two-layered nanostructures were formed as in particle-**I-3** and composed of a microphase separated bottom layer and a dark PS top layer. The dark rings became thicker with the increase of PS molecular weight (Figure 4.4D and E). Moreover, compared with the bottom layer in

particle-**I-3**, the P*t*BA nanodomains became increasingly isolated. The typical width of PS nanodomains and the periodicity were 7 and 11 nm, respectively, in particle-**I-4**, and 6 and 11 nm, respectively in particle-**I-5** (marked by blue arrows). These values are significantly smaller than those observed in particle-**II-4** (17 and 23 nm, respectively). Note that the ratios of DP_{PS} to DP_{PtBA} and σ_{PS} to σ_{PtBA} were all similar for particle-**I-4**, **-5**, and -**II-4** (Table 4.1) and the dark rings can also be seen in the TEM image of particle-**II-4** (Figure 4.5D). The difference in the overall grafting density appears to be responsible for the observed feature sizes.

We previously reported self-assembled nanostructures of particle-**II-1** to **-4** after thermal annealing at 120 °C, which was above the glass transition temperatures of PS and P*t*BA.[13] The phase morphology evolution was the same as observed here for the particles after being cast and annealed with $CHCl_3$ vapor. However, compared with the morphology of the same sample after thermal annealing, the width of PS nanodomains here was slightly larger; the PS nanodomains look slightly "swollen", especially for particle-**II-4** (Figure 4.5D). This observation could be due to the following reasons. (i) $CHCl_3$ is a good solvent for both PS and P*t*BA. Theoretical studies have suggested that the microphase separation of mixed brushes in a nonselective solvent may be delayed with improving the solvent quality.[4b] We speculate that the interfacial layer between PS and P*t*BA nanodomains was thicker and RuO_4 also stained the interfacial layer. (ii) The solubility parameter of $CHCl_3$ is 9.3 $(cal/cm^3)^{0.5}$.[23] Using the group molar attraction constants and molar volume constants from a textbook,[24] we calculated the solubility parameters of PS and P*t*BA and they were 9.5 and 8.5 $(cal/cm^3)^{0.5}$, respectively. Thus, $CHCl_3$ is a slightly better solvent for PS than

for P*t*BA; it could slightly preferentially swell PS during the solvent casting and annealing processes, making PS width slightly larger.

The DP of P*t*BA in HDMB was 143, lower than that of P*t*BA in IDMB (DP = 191). To further confirm that the observed much smaller feature sizes in Figure 4.4 were mainly due to the high total grafting density, not the molecular weight differences in HDMB and IDMB, we synthesized another high density mixed P*t*BA/PS brush sample (Particle-**III-1** in Table 4.1).[25] The values of P*t*BA M_n, DP, and PDI were 23.7 kDa, 189, 1.09, respectively, while the M_n, DP, and PDI of PS were 25.7 kDa, 247, 1.14, respectively. The calculated grafting density of P*t*BA was 0.48 chains/nm^2 and the PS grafting density was 0.51 chains/nm^2. DSC analysis showed that the two grafted polymers were microphase separated.[25] A morphology similar to those in Figure 4.4C, D and E was observed, i.e., a two-layered nanostructure composed of a laterally microphase separated bottom layer and a thin PS top layer (Figure 4.6). The width of a typical PS nanodomain and the periodicity in the bottom layer marked by a blue arrow were 8 and 13 nm, respectively, which were similar to those in Figure 4.4C. This confirmed that the observed much smaller feature sizes in Figure 4.4 resulted from the higher grafting densities. Our results are qualitatively consistent with the theoretical predictions of Zhulina and Balazs.[3] It can be imagined that at high grafting densities, polymer chains are highly stretched, which means that the entropy of polymer chains is considerably lower compared with that in IDMB. Consequently, the lateral microphase separation is restricted to a smaller lateral dimension as any further stretching of polymer chains in the lateral direction would further decrease the entropy, which may not be compensated by the energy gain from lateral microphase separation.

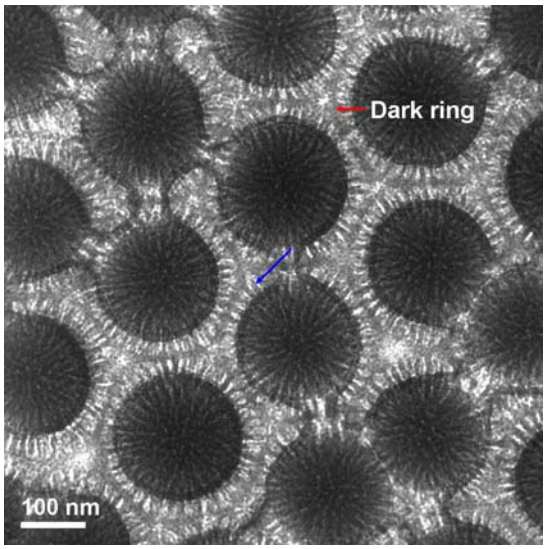

Figure 4.6. Top-view TEM micrograph of particle-**III-1** (P*t*BA M_n = 23.7 kDa, σ_{PtBA} = 0.48 chains/nm^2; PS M_n = 25.7 kDa, σ_{PS} = 0.51 chains/nm^2; DP_{PS}/DP_{PtBA} = 1.31) after being cast from and annealing with $CHCl_3$, a good solvent for both P*t*BA and PS. The sample was stained with RuO_4 vapor at room temperature for 20 min.

4.4 Conclusions

We synthesized a series of high grafting density asymmetric mixed P*t*BA/PS brushes with a fixed P*t*BA M_n of 18.6 kDa and PS molecular weight ranging from 8.7 to 28.0 kDa from 172 nm Y-initiator-functionalized silica particles by sequential ATRP and NMRP. The Y-initiator particles were prepared from bare silica particles by using a triethoxysilane-terminated Y-initiator via a hydrolysis/condensation process in the presence of ammonia. The total grafting densities of the obtained mixed P*t*BA/PS brushes were in the range of 0.9 – 1.2 chains/nm^2, which were significantly larger than those of IDMB synthesized from monochlorosilane-terminated Y-initiator functionalized silica particles (0.6 – 0.7 chains/nm^2). DSC analysis suggested that all high grafting density mixed brushes were microphase separated. TEM studies showed that the phase morphology of high grafting density mixed brushes on silica particles evolved from mostly isolated PS nanodomains in the P*t*BA matrix, to nearly co-continuous, wormlike nanostructures, and a two-layered nanostructure composed of a laterally microphase separated bottom layer and a thin top layer of the longer polymer chains with the increase of PS molecular weight from below to above that of P*t*BA. This observation is similar to that of intermediate density mixed brushes with total grafting densities of 0.6 – 0.7 chains/nm^2. However, the feature sizes of the patterns formed from microphase separation of HDMB were appreciably smaller than those of IDMB, which was attributed to the difference in total grafting density. These results are consistent with theoretical predictions. In HDMB, polymer chains are much more stretched than those in IDMB. As a result, the lateral microphase separation occurred in a smaller lateral dimension because splaying of polymer chains to any larger

extent in the lateral direction would further decrease the entropy, which is not compensated by the energy gain from lateral microphase separation. This is the first time that the effect of grafting density on phase morphology of mixed brushes was directly observed by TEM. The results could allow us to better use mixed brushes in the design and fabrication of novel nanostructured materials for future technological uses.

References:

1. (a) Marko, J. F.; Witten, T. A. *Phys. Rev. Lett.* **1991,** *66*, 1541-1544. (b) Marko, J. F.; Witten, T. A. *Macromolecules* **1992,** *25*, 296-307. (c) Dong, H. *J. Phys. II Fr.* **1993,** *3*, 999-1020. (d) Brown, G.; Chakrabarti, A.; Marko, J. F. *Europhys. Lett.* **1994,** *25*, 239-244. (e) Luzinov, I.; Minko, S.; Tsukruk, V. V. *Prog. Polym. Sci.* **2004**, *29*, 635-698. (f) Luzinov, I.; Minko, S.; Tsukruk, V. V. *Soft Matter* **2008**, *4*, 714-725. (g) Zhao, B.; Brittain, W. J. *Prog. Polym. Sci.* **2000**, *25*, 677-710.
2. Zhao, B.; Zhu, L. *Macromolecules* **2009**, *42*, 9369-9383.
3. Zhulina, E.; Balazs, A. C. *Macromolecules* **1996,** *29*, 2667-2673.
4. (a) Lai, P. Y. *J. Chem. Phys.* **1994,** *100*, 3351-3357. (b) Soga, K. G.; Zuckermann, M. J.; Guo, H. *Macromolecules* **1996,** *29*, 1998-2005. (c) Singh, C.; Pickett, G. T.; Balazs, A. C. *Macromolecules* **1996,** *29*, 7559-7570. (d) Müller, M. *Phys. Rev. E* **2002,** *65*, 030802. (e) Minko, S.; Müller, M.; Usov, D.; Scholl, A.; Froeck, C.; Stamm, M. *Phys. Rev. Lett.* **2002,** *88*, 035502. (f) Wenning, L.; Müller, M.; Binder, K. *Europhys. Lett.* **2005**, *71*, 639-645. (g) Merlitz, H.; He, G. L.; Sommer, J. U.; Wu, C. X. *Macromolecules* **2009**, *42*, 445-451.
5. Roan, J.-R. *Phys. Rev. Lett.* **2006**, *96*, 248301.
6. Wang, J.; Müller, M. *J. Phys. Chem. B.* **2009**, *113*, 11384-11402.
7. (a) Sidorenko, A.; Minko, S.; Schenk-Meuser, K.; Duschner, H.; Stamm, M. *Langmuir* **1999,** *15*, 8349-8355. (b) Minko, S.; Usov, D.; Goreshnik, E.; Stamm, M. *Macromol. Rapid Commun.* **2001,** *22*, 206-211. (c) Motornov, M.; Minko, S.; Eichhorn, K. J.; Nitschke, M.; Simon, F.; Stamm, M. *Langmuir* **2003,** *19*, 8077-8085.

(d) Lemieux, M.; Usov, D.; Minko, S.; Stamm, M.; Shulha, H.; Tsukruk, V. V. *Macromolecules* **2003,** *36*, 7244-7255. (e) Usov, D.; Gruzdev, V.; Nitschke, M.; Stamm, M.; Hoy, O.; Luzinov, I.; Tokarev, I.; Minko, S. *Macromolecules* **2007**, *40*, 8774-8783. (f) Santer, S.; Kopyshev, A.; Yang, H. K.; Rühe, J. *Macromolecules* **2006,** *39*, 3056-3064.

8. (a) Minko, S.; Patil, S.; Datsyuk, V.; Simon, F.; Eichhorn, K. J.; Motornov, M.; Usov, D.; Tokarev, I.; Stamm, M. *Langmuir* **2002,** *18*, 289-296. (b) Minko, S.; Müller, M.; Motornov, M.; Nitschke, M.; Grundke, K.; Stamm, M. *J. Am. Chem. Soc.* **2003,** *125*, 3896-3900. (c) Minko, S.; Luzinov, I.; Luchnikov, V.; Müller, M.; Patil, S.; Stamm, M. *Macromolecules* **2003**, *36*,7268-7279. (d) Ionov, L.; Minko, S.; Stamm, M.; Gohy, J. F.; Jerome, R.; Scholl, A. *J. Am. Chem. Soc.* **2003,** *125*, 8302-8306. (d) Ionov, L.; Sidorenko, A.; Stamm, M.; Minko, S.; Zdyrko, B.; Klep, V.; Luzinov, I. *Macromolecules* **2004**, *37*, 7421-7423. (e) LeMieux, M. C.; Julthongpiput, D.; Bergman, K. N.; Cuong, P. D.; Ahn, H. S.; Lin, Y. H.; Tsukruk, V. V. *Langmuir* **2004,** *20*, 10046-10054. (f) Wang, J.; Kara, S.; Long, T. E.; Ward, T. C. *J. Polym. Sci., Polym. Chem.* **2000**, *38*, 3742-3750. (g) Julthongpiput, D.; Lin, Y. H.; Teng, J.; Zubarev, E. R.; Tsukruk, V. V. *Langmuir* **2003,** *19*, 7832-7836. (h) Tsujii, Y.; Ohno, K.; Yamamoto, S.; Goto, A.; Fukuda, T. *Adv. Polym. Sci.* **2006**, *197*, 1-45. (i)Ionov, L.; Houbenov, N.; Sidorenko, A.; Stamm, M.; Luzinov, I.; Minko, S. *Langmuir* **2004,** *20*, 9916-9919. (j) Ionov, L.; Sidorenko, A.; Stamm, M.; Minko, S.; Zdyrko, B.; Klep, V.; Luzinov, I. *Macromolecules* **2004**, *37*, 7421-7423. (k) Motornov, M.; Sheparovych, R.; Tokarev, I.; Roiter, Y.; Minko, S. *Langmuir* **2007**, *23*, 13-19.

9. (a) Zhao, B. *Polymer* **2003,** *44*, 4079-4083. (b) Zhao, B. *Langmuir* **2004,** *20*, 11748-11755. (c) Zhao, B.; He, T. *Macromolecules* **2003,** *36*, 8599-8602. (d) Zhao, B.; Haasch, R. T.; MacLaren, S. *J. Am. Chem. Soc.* **2004,** *126*, 6124-6134. (e) Zhao, B.; Haasch, R. T.; MacLaren, S. *Polymer* **2004,** *45*, 7979-7988. (f) Li, D. J.; Sheng, X.; Zhao, B. *J. Am. Chem. Soc.***2005**, *127*, 6248−6256. (g) Santer, S.; Kopyshev, A.; Donges, J.; Rühe, J.; Jiang, X. G.; Zhao, B.; Müller, M. *Langmuir* **2007,** *23*, 279-285.

10. (a) Chiu, J. J.; Kim, B. J.; Kramer, E. J.; Pine, D. J. *J. Am. Chem. Soc.* **2005**, *127*, 5036-5037. (b) Shan, J.; Nuopponen, M.; Jiang, H.; Viitala, T.; Kauppinen, E.; Kontturi, K.; Tenhu, H. *Macromolecules* **2005**, *38*, 2918-2926. (c) Zubarev, E. R.; Xu, J.; Sayyad, A.; Gibson, J. D. *J. Am. Chem. Soc.* **2006**, *128*, 4958-4959. (d) Guo, Y.; Moffitt, M. G. *Macromolecules* **2007**, *40*, 5868-5878. (e) Cheng, J.; He, J.; Li, C.; Yang, Y. *Chem. Mater.* **2008**, *20*, 4224-4230. (f) Motornov, M.; Sheparovych, R.; Lupitskyy, R.; MacWilliams, E.; Hoy, O.; Luzinov, I.; Minko, S. *Adv. Funct. Mater.* **2007**, *17*, 2307-2314; (g) Motornov, M.; Sheparovych, R.; Lupitskyy, R.; MacWilliams, E.; Minko, S. *J. Colloid & Interface Sci.* **2007**, *310*, 481-488.

11. Zhao, B.; Zhu, L. *J. Am. Chem. Soc.* **2006,** *128*, 4574-4575.

12. Zhu, L; Zhao, B. *J. Phys. Chem. B* **2008**, *112*, 11529-11536.

13. Jiang, X. M.; Zhong, G. J.; Horton, J. M.; Jin, N. X.; Zhu, L.; Zhao, B. *Macromolecules* **2010**, *43*, 5387-5395.

14. Ohno, K.; Morinaga, T.; Koh, K.; Tsujii, Y.; Fukuda, T. *Macromolecules* **2005**, *38*, 2137-2142.

15. Hawker, C. J.; Bosman, A. W.; Harth, E. *Chem. Rev.* **2001**, *101*, 3661-3688.

16. (a) Matyjaszewski, K.; Miller, P. J.; Shukla, N.; Immaraporn, B.; Gelman, A.; Luokala, B. B.; Siclovan, T. M.; Kickelbick, G.; Vallant, T.; Hoffmann, H.; Pakula, T. *Macromolecules* **1999**, *32*, 8716−8724. (b) Jiang, X. G., Lavender, C. A.; Woodcock, J. W.; Zhao, B. *Macromolecules* **2008**, *41*, 2632-2643.

17. (a) Dao, J.; Benoit, D.; Hawker, C. J. *J. Polym. Sci. Part A: Polym. Chem.***1998**, *36*, 2161−2167. (b) Zhao, B.; Jiang, X. M.; Li, D. J.; Jiang, X. G.; O'Lenick, T. G.; Li, B.; Li, C. Y. *J. Polym. Sci. Part A: Polym. Chem.* **2008**, *46*, 3438-3446.

18. (a) Philipse, A. P.; Vrij, A. *J. Colloid Interface Sci.* **1989**, *128*, 121−136. (b) Bogush, G. H.; Tracy, M. A.; Zukoski, C. F., IV. *J. Noncryst. Solids* **1988**, *104*, 95−106.

19. (a) Li, D. J.; Jones, G. L.; Dunlap, J. R.; Hua, F. J.; Zhao, B. *Langmuir* **2006**, *22*, 3344-3351. (b) Li, D. J.; Zhao, B. *Langmuir* **2007**, *23*, 2208-2217. (c) Li, D. J.; Dunlap, J. R.; Zhao, B. *Langmuir* **2008**, *24*, 5911-5918. (d) Jiang, X. M.; Wang, B. B.; Li, C. Y.; Zhao, B. *J. Polym. Sci. Part A: Polym. Chem.*, **2009**, *47*, 2853-2870.

20. He, T.; Li, D. J.; Sheng, X.; Zhao, B. *Macromolecules* **2004**, *37*, 3128-3135.

21. Husseman, M.; Malmstrom, E. E.; McNamara, M.; Mate, M.; Mecerreyes, D.; Benoit, D. G.; Hedrick, J. L.; Mansky, P.; Huang, E.; Russell, T. P.; Hawker, C. J. *Macromolecules* **1999**, *32*, 1424-1431.

22. The data can be found in Appendix.

23. Hiemenz, P. C.; Lodge, T. P. *Polymer Chemistry*, 2nd Ed., CRC Press: Boca Raton, 2007.

24. Coleman, M. M.; Painter, P.C. *Fundamentals of Polymer Science: An Introductory Textbook*, 2nd Ed., CRC Press: Boca Raton, 1998.

25. The synthesis and characterization of particle-**III-1** can be found in Appendix.

Appendix

A.1. Synthesis of High Grafting Density P*t*BA Brush-Grafted Silica Particles with P*t*BA M_n of 23.7 kDa. The Y-initiator particles (238 mg) were dispersed in anisole (14.4 g) in a 50 mL two-necked flask using an ultrasonic water bath. CuBr (52.6 mg, 0.365 mmol), *t*-BA (28.165 g, 220.0 mmol), *N*, *N*, *N*′, *N*′, *N*″-pentamethyldiethylenetriamine (61.4 mg, 0.355 mmol), and ethyl 2-bromoisobutyrate (51.1 mg, 0.262 mmol) were added into a separate 100 mL three-necked flask and stirred under N_2 atmosphere. The particle dispersion was then transferred into the three-necked flask via a syringe and the reaction mixture was degassed by three freeze-pump-thaw cycles. The flask was then placed in a 75 °C oil bath and the polymerization was monitored by SEC and ^{1}H NMR spectroscopy analysis. After the reaction proceeded for 143 h, the flask was removed from the oil bath and opened to air. THF (20 mL) was added into the flask to dilute the mixture. The particles were separated by centrifugation and the supernatant was passed through a column of neutral, activated aluminum oxide to remove the copper catalyst. The particles were re-dispersed in THF, allowed to stand overnight (the green precipitate was removed), and centrifugated again. This washing process was repeated with THF one more time and chloroform three times, followed by drying the particles with a stream of air flow, yielding P*t*BA brush-grafted silica particles (0.077 g). The $M_{n,SEC}$ and PDI of the free P*t*BA formed from the free initiator in the polymerization were 23.7 kDa and 1.09, respectively, determined from SEC analysis using polystyrene calibration.

A.2 Synthesis of High Grafting Density Mixed P*t*BA/PS Brush-Grafted Silica Particles with P*t*BA M_n of 23.7 kDa and PS M_n of 25.7 kDa. The P*t*BA brush-grafted silica

particles (M_n = 23.7 kDa, 0.057 g) were dispersed in anisole (8.613 g) in a 50 mL two-necked flask using an ultrasonic water bath. The particle dispersion was then transferred into a 100 mL three-necked flask that contained the free NMRP initiator STEMPO (40.6 mg, 0.156 mmol), followed by the addition of styrene (12.647 g, 121.6 mmol). The polymerization mixture was degassed by three freeze-pump-thaw cycles. The flask was then placed in a 120 °C oil bath and the polymerization was monitored by ^{1}H NMR spectroscopy and SEC analysis. The polymerization was stopped when the molecular weight of the free polymer formed from the free initiator STEMPO reached 25.7 kDa. The mixture was diluted with THF. The particles were separated from the free polymer by centrifugation, re-dispersed in THF, and centrifugated again. The particles were then dried with a stream of air flow.

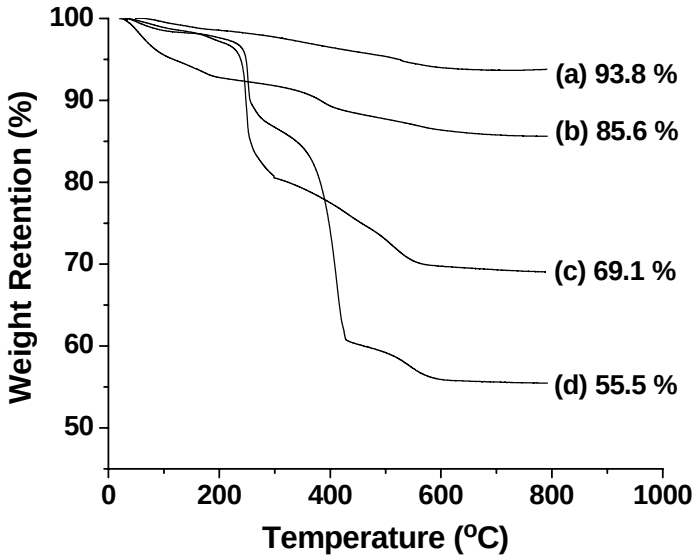

Figure A.1. Thermogravimetric analysis (TGA) of (a) bare silica particles, (b) Y-initiator particles, (c) P*t*BA brush-grafted particles with P*t*BA M_n of 23.7 kDa, (d) mixed brush-grafted particles with P*t*BA $M_{n,SEC}$ of 23.7 kDa and PS M_n of 25.7 kDa (particle-**III-1**). TGA was performed in air at a heating rate of 20 ºC/min from room temperature to 800 ºC.

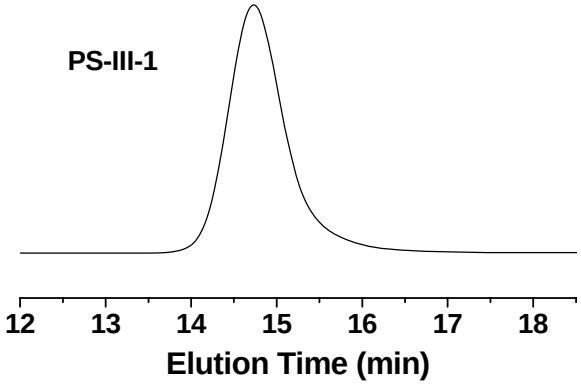

Figure A.2. Size exclusion chromatography trace of free polymer formed (corresponding to particles-**III-1**) from free initiator STEMPO in the synthesis of mixed P*t*BA/PS brush-grafted silica particles by NMRP of styrene at 120 °C from P*t*BA brush-grafted particles with P*t*BA M_n of 23.7 kDa. PS M_n = 25.7 kDa, PDI = 1.14.

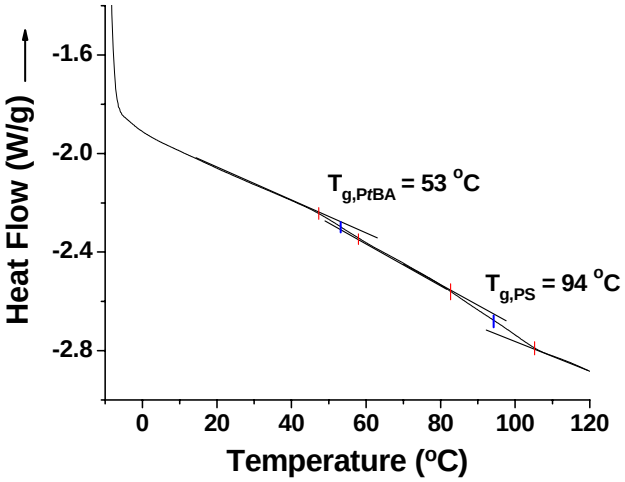

Figure A.3. Differential scanning calorimetry (DSC) analysis of particle-**III-1** (P*t*BA M_n = 23.7 kDa, σ_{PtBA} = 0.48 chains/nm^2; PS M_n = 25.7 kDa, σ_{PS} = 0.51 chains/nm^2; DP_{PS}/DP_{PtBA} = 1.31). The heating and cooling rates in the DSC analysis were 10 °C/min.

Vita

Xiaoming Jiang was born in Jiangsu, China. He attended Nanjing University of Technology from 1993 to 1997, where he received a B.E. degree in Polymer Engineering. Then he worked on chemical analysis for two years in Jiangyin Power Plant as an assistant engineer. In August, 1999, he started his master program in the Department of Polymer Science and Engineering at the Nanjing University of Technology. He joined Dr. Xianyi Chen's group and worked on polymer composites. He received a M.E. degree in Material Science in 2002. In August, 2002, he enrolled as a graduate student in the Department of Chemistry at the Oklahoma State University, Stillwater. He joined Dr. Warren Ford's group and worked on polymer functionalization of carbon nanotubes. He received a M.S. degree in Polymer Chemistry in 2005. In August, 2005, he started his Ph.D. program in the Department of Chemistry at the University of Tennessee, Knoxville. He joined Dr. Bin Zhao's group working in the field of polymer brush-grafted particles. Xiaoming Jiang received a Doctor of Philosophy Degree in Chemistry from the University of Tennessee in 2010.